Synthesis and characterization of polythiophene functionalized with electron-poor moieties for applications in organic electronics

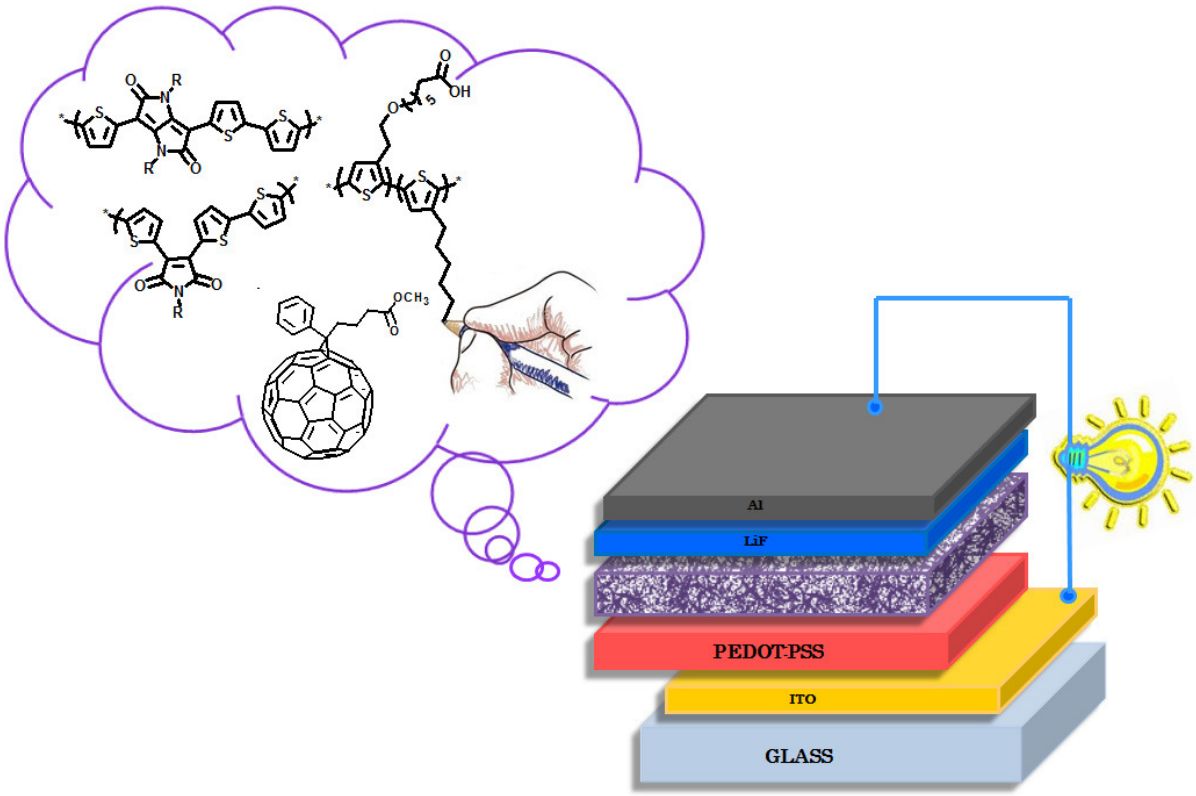

Ramona Gironda

Ph.D. School in Material Science, XXV cycle
Thesis presented for the degree of Doctor Europaeus

Supervisor: Prof. A. Papagni, Dr. A. Yassar
Dean of the Doctorate: Prof. Gian Paolo Brivio

January 2013

To Tommaso and
my family

Contents

List of Abbreviations

AFM	Atomic Force Microscopy
BCP	Block copolymer
BHJ	Bulk Heterojunction
BLA	Bond length alternation
C_{60}	Buckminsterfullerene-60
C_{70}	Buckminsterfullerene-70
CV	Cyclic Voltammetry
D-A	donor-acceptor
DCB	o-dichlorobenzene
DMF	*N,N*-Dimethylformamide
DPV	Differential Pulse Voltammetry
EDOT	ethylenedioxythiophene
EQE	External quantum Efficiency
FET	Field-effect transistors
FF	Fill Factor
GPC	Gel Permeation Chromatography
GRIM	Grignard metathesis
H-H	Head-to-head
HOMO	Highest occupied molecular orbital
HRMS	High resolution Mass
HT	Head to-tail
ICT	Intra-molecular charge transfer
Iso-DPP	1,4-dibutyl-3,6-di(thiophene-2-yl)pyrrolo[3,2-b]pyrrole-2,5-dione
ITO	Indium Thin Oxide
Jsc	Short Circuit Current
LBG	Low band gap
LDA	Lithium diisopropylamide

LUMO	Lowest unoccupied molecular orbital
$Ni(dppp)Cl_2$	[1,3-bis(diphenylphosphino)-propane]dichloronickel(II)
NMR	Nuclear Magnetic Resonance
OPV	Organic Photovoltaic
OSC	Organic Solar Cell
P(o-tolyl)3	Tri(*o*-tolyl)phosphine
P1	Poly (3-(2,2'-bithien-5-yl)-4-(thien-2-yl)-1-octyl-pyrrole-2,5-dione)
P2	Poly(3,4-di(2,2'-bithien-5-yl)-1-octyl-pyrrole-2,5-dione)
P3HT	Poly(3-hexylthiophene)
PCBM	[6,6]-phenyl-C61-butyric acid methylester
PCE	Photovoltaic efficiency
Pd_2dba_3	Tris(dibenzylideneacetone)dipalladium(0)
PDI	Polydispersity index
PhBT12	Poly(N-(dodecyl)-3,6-bis(4-dodecyloxythiophen-2-yl)phthalimide)
PV	Photovoltaic
PVC	Photovoltaic Solar Cells
SEC	Size Exclusion Chromatography
THF	Tetrahydrofuran
TPD	Thieno[3,4-*c*]pyrrole-4,6-dione
T-T	Tail-to-tail
Voc	Open Circuit Voltage

Abstract

Harvesting the unlimited and renewable energy from sunlight to produce electricity is one of the major scientific and technological challenges of the 21st century.

Among the available techniques, photovoltaic solar cells (PVCs) are very attractive because they can convert solar energy directly into electricity in a reasonable and economic appealing efficiency.

The development of PVCs is therefore an attractive alternative to address global environmental issues. However, the current high cost for the devices based on inorganic semiconductors has limited their widespread application.

Organic solar cells offer a compelling option for tomorrow's PV devices, since they can be easily prepared using low-cost and efficient roll-to-roll manufacturing processes.

During the last decade, Organic Photovoltaic (OPV) research has progressed remarkably both in terms of new materials and device performances. Particular interest have been devoted to bulk heterojunction (BHJ) devices in which the active layer consists of a blend of DONOR (p-type semiconductor) and ACCEPTOR (n-type semiconductor) materials. The active layer can be easily deposed through put techniques, facilitating the formation of large area, light weight, and potentially flexible devices.

Fullerenes C_{60}, C_{70} and in particular their soluble derivates (PCBM) are at the moment the most popular ACCEPTORS and only marginal research is devoted to the development of viable substitutes. On the other hand, the research has been focused on conjugated polymers, as DONOR material, due to their tunable properties by a structural design and the possibility to produce them at low costs.

Over the past decade, research has focused on regioregular poly(3-hexylthiophene) (P3HT) as the standard electron-donating material in polymer BHJ solar cells, with important progresses having been made in understanding the device science and the associated improvements in device efficiency. However, P3HT is not the ideal

polymer as it has a relatively large band gap (1.85 eV, and this means that it is not able to harvest the maximum of exploitable solar radiation) and its high-lying highest occupied molecular orbital (HOMO) (-5.1 eV) limits the open circuit voltage (V_{oc}) of P3HT/$PC_{61}BM$ devices to 0.6 V, consequently limiting the efficiency to about 5%. To overcome these limitations, low band gap materials with broad absorption spectra, to enhance sunlight harvest for higher short circuit current (J_{sc}); appropriately lower HOMO energy levels, to maximize the open circuit voltage (V_{oc}); higher hole mobilities, for higher J_{sc}; and higher fill factor (FF), have been proven to be an efficient strategy to improve device performance. Typically, a low band gap polymer is designed, via donor-acceptor (D-A) approach, by incorporating both electron-rich and electron-deficient moieties in the same conjugated backbone.

Among a wide variety of donor material, new low band gap polymers based on thiophene, as the donor unit, and iso-DPP (iso-diketopyrrolo-pyrrole) or maleimide, as the acceptor moieties, were designed. These latter electron-withdrawing units combine a low HOMO level and a rigid planar core that permit π-conjugation length and charge transfer into the polymer backbone. The polymers and the molecules obtained by Stille condensations were characterized into the device as DONOR material or third compound to blend with the classical mix P3HT/PCBM.

More into the detail, the Chapter 3 reports on the synthesis of a novel electron-deficient derivative, 1,4-dibutyl-3,6-di(thiophene-2-yl)pyrrolo[3,2-b]pyrrole-2,5-dione (iso-DPP). This new building block was copolymerized with bistannanes of thiophene and bithiophene by Stille polycondensation, affording the corresponding polymers (**PDPPT** and **PDPPTT**, respectively). These compounds exhibit small energy band gaps combined with low-lying HOMO energy levels. Energy band gaps of **PPDPT** and **PPDPTT**, calculated from absorption spectra, are 1.63 and 1.73 eV, respectively. The HOMO and LUMO energy levels of **PDPPT** and **PDPPTT** are -5.12, -3.50, -5.09 and -3.50 eV respectively, as determined by cyclic voltammetry. The power conversion efficiency of **PDPPT**:$PC_{60}BM$-based photovoltaic cells illuminated by AM 1.5G was 1.24%, without optimization of materials, significantly higher than for **PDPPTT**:$PC_{60}BM$, 0.33%. The results demonstrate that iso-DPP

based polymers are promising materials for bulk heterojunction solar cell applications.

A series of D-A polymers and oligomers based on N-alkyl-maleimide has been synthesized by a simple and efficient route explained in Chapter 4. The obtained low band-gap materials were applied into polymeric photovoltaic cells, to improve their efficiency by tuning their electronic properties. The introduction of small quantities (< 20% w/w) of polymers or oligomers containing N-alkyl-maleimide within active layer of P3HT/ $PC_{61}BM$ blends allowed to dramatically increase the efficiencies of BHJ solar cells (up to 80% of increase). This beneficial effect is attributed to improved charge photogeneration and transport. Poor photovoltaic results were obtained if the maleimide based polymer was employed alone as DONOR material, blended with $PC_{61}BM$.

In order to obtain good results in terms of device performances, not only a good chemical design of the DONOR polymer must be achieved, but also other parameters at the molecular and supramolecular levels should be carefully controlled. The full potential of any conjugated polymer for solar cells can only be realized with an optimized morphology. For this purpose the synthesis of random and diblock copolymers of poly(3-alkylthiophene)s bearing polar substituents was successfully developed by GRIM polymerization and the details are reported in Chapter 5.

3-Hexyl-thiophene was successfully copolymerised with a new derivative, 3-functionalised-thiophene (propyl 5-(2-(thiophen-3-yl)ethoxy) pentanoate), bearing an ester function. Under optimized conditions, this ester proved to be fully compatible with the Grignard metathesis polymerization. Saponification of the copolymer esters provided the corresponding polyacids. Photovoltaic properties of copolymers were investigated in bulk heterojunction devices with $PC_{61}BM$ as acceptor. Among all the amphiphilic copolymers, P3HT-*b*-P3AcidHT showed the best performance with a PCE of 4.2%, an open-circuit voltage (Voc) of 0.60 V, a short-circuit current density (Jsc) of 13.0 $mAcm^{-2}$, and a fill factor (FF) of 0.60.

All conjugated D-A molecule and polymers were characterized by chemical investigation and their optical, electrochemical, morphological and photovoltaic properties were investigated.

Abstract (French version)

Convertir l'énergie illimitée et renouvelable du soleil pour produire de l'électricité est l'un des plus grands défis scientifiques et technologiques du 21e siècle. Parmi les techniques disponibles, les cellules solaires photovoltaïques (cellules PV) sont très intéressantes car elles peuvent convertir directement l'énergie solaire en électricité avec un rendement assez élevé. Le développement des cellules PV est donc une alternative intéressante pour aborder les problèmes environnementaux mondiaux. Cependant, le coût élevé pour les dispositifs à base de semi-conducteurs inorganiques a limité leur application à grande échelle.

Les cellules solaires organiques offrent une option convaincante pour les dispositifs photovoltaïques de demain, car ils peuvent être facilement mis en œuvre à faible coût et bénéficier de procédés de fabrication rouleaux à rouleaux (roll-to-roll) ou feuilles à feuilles (sheet-to-sheet).

Au cours de la dernière décennie, la recherche sur le photovoltaïque organique (OPV) a progressé de manière remarquable à la fois en ce qui concerne de nouveaux matériaux et aussi les performances des dispositifs. Un intérêt particulier a été consacré aux composants à hétérojonction en volume (BHJ), dans lesquels la couche active est constituée d'un mélange intime de matériaux : un DONNEUR (semi-conducteur de type p) et un accepteur (semi-conducteur de type n). La couche active peut être facilement déposée par des techniques en voie liquide, et ainsi faciliter la fabrication sur de grandes surfaces, avec un poids léger, et donc sur des substrats potentiellement flexibles.

Les fullerènes C_{60} ou C_{70} et en particulier leurs dérivés solubles (PCBM) sont pour le moment les ACCEPTEURS les plus populaires, et seulement une recherche marginale est consacrée à la mise au point de matériaux de remplacement viables. La recherche s'est concentrée sur des polymères conjugués, comme matériau de donneur, en raison de leurs propriétés accordables par conception structurale et une potentielle production à faible coût.

Au cours de la dernière décennie, les études se sont intéressées au poly (3-hexylthiophène) (P3HT) régio-régulier comme principal matériau donneur d'électrons dans les cellules solaires polymères en volume (BHJ). D'importants progrès ayant été réalisés dans la compréhension des dispositifs améliorant ainsi l'efficacité de ceux ci. Toutefois, le P3HT n'est pas le polymère idéal car il possède une bande interdite relativement large (1,85 eV) et sa plus haute orbitale moléculaire occupée (HOMO) (-5,1 eV) restant trop grande, elle limite la tension de circuit ouvert (Voc) des dispositifs P3HT/PC_{61}BM à 0,6 V. Ceci à pour conséquence de limiter l'efficacité des cellules aux alentours de 5%. Pour résoudre ce problème et augmenter la conversion solaire, une stratégie efficace est d'utiliser des matériaux à faible bande interdite avec des spectres d'absorption larges. Il en résulte une augmentation du courant de court-circuit (Jsc). En choisissant de manière appropriée le niveau HOMO, on peut maximiser la tension en circuit ouvert (Voc). Enfin des mobilités de trous supérieures et une meilleure Jsc engendreront un meilleur facteur de forme (FF). Typiquement, un polymère de faible largeur de bande interdite est réalisé par l'intermédiaire d'une approche donneur-accepteur (D-A), en incorporant les deux fractions celle riche en électrons et celle pauvre en électrons sur le même squelette conjugué.

Parmi un large éventail de nouveaux matériaux donneurs à faible bande interdite, des polymères où l'unité du donneur est à base de thiophène ont été fabriqués; ces composés conçus ont comme groupement accepteur : l'iso-DPP (iso-dicétopyrrolopyrrole) ou maléimide. Ces structures électro-attractrices combinent un niveau HOMO bas et un noyau rigide plan qui permet une longueur de conjugaison π et un transfert de charges dans le squelette du polymère. Les polymères et les

molécules obtenues par condensation de Stille ont été caractérisés dans des dispositifs comme matériau donneur ou comme additif dans le mélange classique P3HT/PCBM.

Il sera détaillé dans le chapitre 3, la synthèse d'un nouveau dérivé déficient en électrons, le 1,4-dibutyl-3,6-di-(thiophène-2-yl)-pyrrolo-[3,2-b]-pyrrole-2,5-dione (iso-DPP). Cette nouvelle brique moléculaire a été co-polymérisée avec des bistannanes de thiophène et des bithiophènes par polycondensation de Stille, pour obtenir les polymères correspondants (respectivement PDPPT et PDPPTT). Ces composés présentent une faible bande d'énergie interdite combinée à des niveaux d'énergie HOMO bas. Les bandes d'énergie interdites de PPDPT et PPDPTT, calculées à partir des spectres d'absorption, sont respectivement de 1,63 et 1,73 eV. Les niveaux HOMO et LUMO déterminés par voltampérométrie cyclique sont de -5,12 et -3,50 eV pour le PDPPT, et de -5,09 et -3,50 eV pour le PDPPTT. L'efficacité, sous éclairement AM 1.5G, des cellules photovoltaïques à base de PDPPT: $PC_{60}BM$ est de 1,24%, sans optimisation des matériaux, nettement plus élevée que pour celle des dispositifs à base de PDPPTT: $PC_{60}BM$ qui est de 0,33%. Les résultats démontrent que les polymères à base d'iso-DPP sont des matériaux prometteurs pour l'utilisation en cellules solaires à hétérojonction en volume.

Une série de polymères donneur-accepteur et d'oligomères donneur-accepteur conçs sur des structures à base de N-alkyl-maléimide ont été synthétisés par une voie simple et efficace expliquée dans le chapitre 4. Les matériaux à faible gap obtenus ont été utilisés dans des cellules photovoltaïques polymères, afin d'en améliorer leur efficacité en optimisant leurs propriétés électroniques. L'introduction de petites quantités (<20% en rapport en masse) de polymères ou d'oligomères contenant des N-alkyl-maléimide à l'intérieur des couches actives de mélanges P3HT / $PC_{61}BM$ a permis d'augmenter considérablement l'efficacité de ces cellules solaires à hétérojonction en volume (jusqu'à 80% d'augmentation). Cet effet bénéfique est attribué à une amélioration de la photo-génération des charges et du transport dans la couche. Quand le maléimide est utilisé seul comme matériau donneur mélangé au $PC_{61}BM$, les résultats sont en revanches mauvais.

Afin d'obtenir de bons résultats en performances de dispositifs, il faut non seulement réaliser un bon design chimique du polymère donneur, mais contrôler soigneusement d'autres paramètres au niveau moléculaire et supramoléculaire. Le meilleur potentiel d'un polymère conjugué ne peut être obtenu qu'avec une optimisation maitrisée de la morphologie de celui-ci. A cet effet, la synthèse de copolymères aléatoires et di-bloc à base de poly-(3-alkylthiophène) portant des substituants polaires a été développée avec succès par polymérisation GRIM. Ces détails sont présentés dans le chapitre 5.

La co-polymérisation du 3-hexyl-thiophène avec un nouveau dérivé, 3-thiophène-fonctionnalisé (propyl-5-(2-(thiophén-3-yl)-éthoxy)-pentanoate), porteur d'une fonction ester a été réalisée avec succès. Dans des conditions optimales, cet ester s'est avéré être pleinement compatible avec la polymérisation par métathèse de Grignard. La saponification des copolymères esters a conduit aux polyacides correspondants. Les propriétés photovoltaïques de ces copolymères ont été étudiées dans des dispositifs à hétérojonctions en volume avec $PC_{61}BM$ comme accepteur. Parmi tous les copolymères amphiphiles, le P3HT-*b*-P3AcidHT a montré les meilleurs résultats avec un rendement de conversion de 4,2%, une tension de circuit ouvert (Voc) de 0,60 V, une densité de courant de court-circuit (Jsc) de 13,0 $mAcm^{-2}$, et un facteur de forme (FF) de 0,60.

Toutes les molécules conjuguées Donneur-Accepteur et les polymères ont été caractérisés par des méthodes chimiques et leurs propriétés optiques, électrochimiques, ainsi que les propriétés morphologiques et photovoltaïque ont été étudiés.

1. Introduction

Harvesting energy directly from sunlight using photovoltaic devices is considered one of the most important ways to address growing global energy needs using a renewable resource.

The interest in solar cells has risen strongly in recent years, due to the increasing energy demands and shortage of fossil fuels. Today, the dominant photovoltaic (PV) technology is based on crystalline silicon but on the other hand there has been a continuous interest in searching for new types of low-cost solar cells to integrate inorganic devices.

Three factors must to keep in mind when one compares systems for photovoltaic applications: efficiency, lifetime and cost.

Photovoltaic efficiency (PCE), explained in detail in the next Chapter, is defined by the ratio of power output to power input.

For silicon-based PVs the efficiency is about 25%,[1] with commercial modules that show efficiencies in the range of 15–18%[2]; while organic photovoltaics (OPVs) show a maximum so far reported efficiency of about 8%[3]. However, this value has been estimated to improve if the right conditions are chosen.[4]

The lifetime of a device is defined as the time to reach half of initial efficiency or half of the circuit current value[5]. In the case of inorganic PVs is more than 35 years, whereas for the OPV is a crucial factor, because relevant literature reports lifetime of few hours in air. Consequently, OPV devices need to be encapsulated.

The cost of silicon PV production is very high due to some operative parameters, such as temperature and high purity, while the production cost of OPVs is smaller of orders of magnitude.

Therefore, there has been a continuous interest in searching for new types of low-cost solar cells to integrate inorganic silicon thanks to their advantage to produce flexible very large area devices in a fast and cheap printing production. Organic

solar cells offer a compelling option for tomorrow's PV devices since they can be easily prepared using low-cost and efficient roll-to-roll manufacturing processes.

The basis for organic solar cells was born in the 1954 from the dark conductivity in halogen doped organic compounds, although many of them were not stable[6]. In the following years, a lot of systematic research was done to understand the basis of the charge transport properties in the low molecular systems[7].

The first generation of organic photovoltaic solar cells, based on single organic layer sandwiched between two metal electrodes of different work functions[8], only led to very low power conversion efficiency due to poor charge carrier generation and unbalanced charge transport.

The next breakthrough was achieved by introducing the bilayer heterojunction concept. This configuration, containing a p-type layer for hole transport and an n-type layer for electron transport, has been implemented by Tang to improve the photocurrent of the solar cell device. He reported in 1986 about 1% power conversion efficiency for two organic materials (a phtalocyanine derivative as p-type semiconductor and a perylene derivative as n-type semiconductor) sandwiched between a transparent conducting oxide (ITO) and a metal electrode.[9]

Figure 1.1 shows schematically the working mechanism of bilayer organic solar cells. In contrast to inorganic photovoltaic devices, the active layer produces a neutral mobile excited state (exciton) after the absorption of light instead of free charge carriers. This Coulomb correlated electron-hole pair, the exciton, diffuses to the donor-acceptor (D-A) interface where the exciton dissociation occurs via an electron-transfer process. The fully separated free charge carriers go to the respective electrodes in the opposite direction with the aid of the internal electric field, which in turn generates the photocurrent and photovoltage. In such devices, only excitons created within the distance of about 10 nm[10] from the interface can reach the heterojunction interface. This leads to the loss of absorbed photons further away from the interface and results in low quantum efficiencies.

Consequently, the performance of bilayer heterojunction devices is greatly limited by the small area of charge-generating interface between the donor and acceptor.[11,12,13,14]

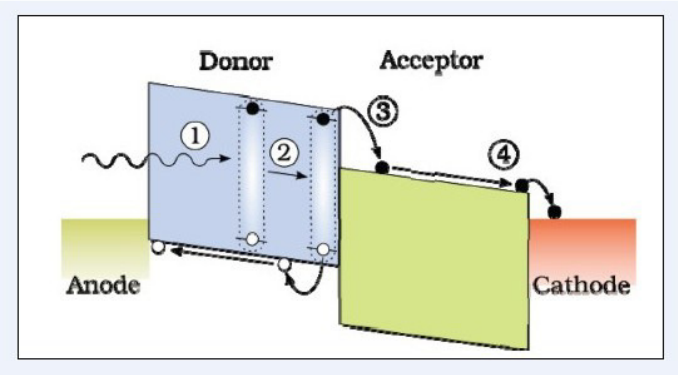

Figure 1.1 Working mechanism for donor-acceptor heterojunction solar cells.

In 1995, a major breakthrough was realized by Sariciftci et al., who introduced a novel concept accounting for the low exciton diffusion length in disordered organic semiconductors, so-called bulk heterojunction[15] (BHJ). Tremendous research effort arose from this discovery of efficient photoinduced electron transfer in conjugated polymer-fullerene (poly[2-methoxy-5-(2'-ethyl-hexyloxy)-*p*-phenylenevinylene] (MEH-PPV) blend and a drastic increase in the generated photocurrent can be achieved by employing an interpenetrating network of donor and acceptor materials. Solution-processed bulk-heterojunction photovoltaic cells were first reported in 1995[16] by Yu and co-workers, who introduced a novel concept of active layer by blending donor and acceptor materials. As reported in Figure 1.2, an interpenetrating network with a large D-A interfacial area can be achieved through controlling the phase separation between the two components. In this ideal situation any absorbing site in the blend is within few nanometers of the D-A interface, leading to much enhanced quantum efficiency of charge separation. The formation of a bicontinuous and interpenetrating network creates two channels which transport holes, in the donor domain, and electrons in the acceptor one, resulting in efficient charge collection.

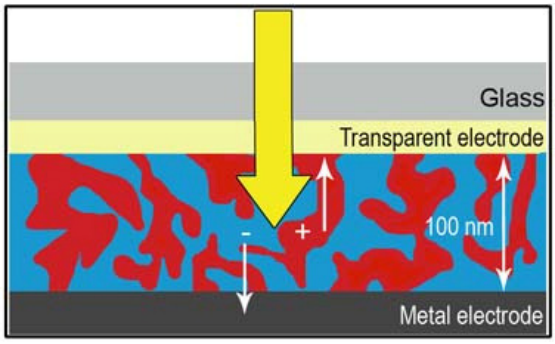

Figure 1.2 Architecture of a bulk heterojunction photovoltaic.
First a photon is absorbed by the donor material, and an exciton is created. It can diffuses towards a donor/acceptor interface, where the electron is transferred to the acceptor material. Even though the hole and electron are now on different materials they are still strongly bound by Coulomb interaction and need to be dissociated into free carriers, after which they are transported through the two respective phases and can be collected at the electrodes.

Because the BHJ configuration only requires a single active layer to create an internal D-A heterojunction, the fabrication of the device can be greatly simplified by spincoating a polymer–acceptor composite, or by coevaporation of conjugated small molecules.

From the standpoint of state of the art active materials, the research has been focused on two distinct classes of p-type semiconductors: polymeric materials (mostly) and monodisperse, molecular materials. As for the n-type materials, fullerene derivative has proved to be an ideal n-type material thanks to its various intrinsic advantages: it possesses a relatively low LUMO level, that means thermodynamically favorable to accepting electrons from an excited p-type material; it has unique stabilization of negative charge, due to the triply degenerate LUMO level, and the photoinduced electron transfer from donor polymer to a C_{60} derivative can be on a time scale of 45 fs, that is several orders of magnitude faster than the radiative decay of photoexcitation. Finally, C_{60} derivatives also exhibit very high electron mobility in field effect transistors (FETs).

Despite these advantages, the poor solubility of C_{60} in most of the common organic solvents and its ability to crystallize led to functionalize C_{60} structures with solubilizing moieties.[17,18,19,20]

To date, the particularly soluble [6,6]-phenyl-C61-butyric acid methyl ester (well known as PCBM), synthetized by Wudl and Hummelen in 1995,[21] is the most used acceptor in the BHJ technology. This particular derivative has one apparent drawback coming from its structural symmetry that leads to an insufficient absorption in the visible spectrum. To overcome the problem another functionalized fullerene was synthetized, C_{70} PCBM, which has lower structural symmetry and shows more transitions.[22]

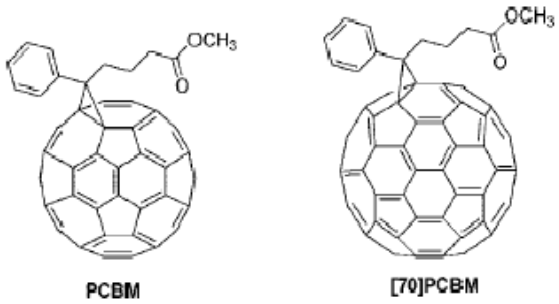

Figure 1.3. Structure of PCBM and C_{70}PCBM

If C_{60} derivatives are now the best class of compounds obtained so far as n-type material there is still need to research the ideal p-type counterpart. Conjugated structures offer optical and electronic properties of semiconductors but also many advantages in term of cost and processability. In the last decade several new polymers have been reported showing very promising properties in polymer solar cell application. Record efficiencies close to 10% have been recently reported for BHJSCs, making organic photovoltaic (OPV) competitive with amorphous silicon technologies.[23]

Some guides lines, detailed in the next section, must to be respected in terms of molecular structure and physical properties in order to obtain good efficiencies.

Regioregular poly(3-hexylthiophene) (P3HT) is the most important conjugated polymer used for this purpose and it achieves an efficiency of 6.5%.[24] This polymer, with a medium band gap and high crystallinity compared to MEH-PPV, was introduced to decrease the mismatch between the solar spectrum and the absorption spectrum of polymer used by Sariciftci. Even though P3HT is still the standard

materials for BHJSC, the bandgap of P3HT is around 1.9 eV, absorbing only up to 650 nm, that limits the harvest of solar light to 22.4% (see Figure 1.4). To harvest more photons in the near infra red region it is necessary to develop new polymers with a lower band gap.

Low-bandgap polymers, based on the internal D–A interactions, are the most promising choice to develop new semiconducting polymers for BHJSCs, thanks to the possibility to tune their optical and electronic properties by proper combinations of D and A units.

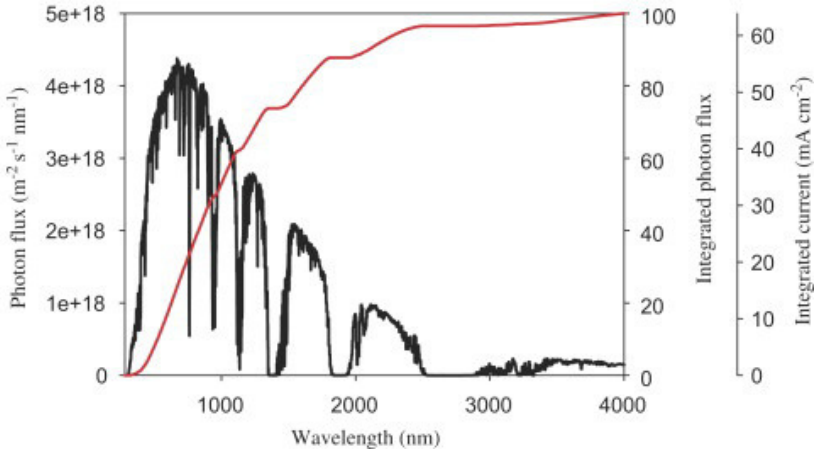

Figure 1.4 Photon flux as function of wavelength.
The percentage of the total photon flux and the corresponding maximum current is displayed at the x-axis.

A record PCE of over 8% has been achieved with these new developed D-A low band gap polymers[25].

The recent increase in power efficiency of OPV cells has been obtained mainly by the design of new semiconducting polymers and materials and even higher efficiencies (15-20%) are envisaged for the next 5-10 years.[26] This indicates that the development of novel conjugated polymers will certainly play a crucial role in driving this research.

This thesis work is structured as follows: the manuscript begins with an introduction of the basic concept of the OPV. The principle of molecular design with optimal

band gap, the relationship between structure and properties and the device performances will be discussed in Chapter 2. In Chapters 3 and 4 are presented the results in terms of synthesis, chemical characterization and device performance of the new low band gap polymers based on iso-diketopyrrolopyrrole and maleimide, respectively. Chapter 5 describes the role of morphology of the active layer and how the new block copolymers (BCPs) can be a solution in this context. A report on the synthesis and the characterization of amphiphilic BCP with fixed hydrophobic block length, obtained by GRIM polymerization, is described in detail. The photovoltaic properties, as a function of block composition, related to the morphology of the blend are also presented.

---

[1] J. H. Zhao; A. H. Wang; M. A. Green; F. Ferrazza, *Appl. Phys. Lett*., **1998**, 73, 1991.

[2] Y. F. Zhou; M. Eckab; M. Kruger, *Energy Environ. Sci*., **2010**, 1851.

[3] M. A. Green; K. Emery; Y. Hishikawa; W. Warta, *Prog. Photovolt Res. Appl*. **2011**, 19, 84.

[4] M. C. Scharber; D. Mühlbacher; M. Koppe; P. Denk; C. Waldauf; A. J. Heeger; C. J. Brabec, *Adv. Mater*. **2006**, 18, 789.

[5] J. Alstrup; K. Norrman; M. Jørgensen; F. C. Krebs, *Sol. Ener. Mater. Sol. Cells* **2006**, 90, 2777.

[6] H. Akamatsu; H. Inokuchi; Y. Matsunaga, Nature, **1954**, 173, 168.

[7] M. Pope; C. E. Swenberg, *Electronic Processes in Organic Crystals and Polymers, 2nd edition*, **1999**.

[8] G.A. Chamberlain, *Organic Solar Cells*, **1983**, 8, 47.

[9] C. Tang, *Appl. Phys. Lett*. **1986**, 48, 183.

[10] C. Deibel; V. Dyakonov, *Rep. Prog. Phys*.**2010**, 73, 096401.

[11] J.J. M. Halls; K. Pichler; R.H. Friend; S.C. Moratti; A.B. Holmes, *Appl. Phys. Lett*. **1996**, 68, 3120.

[12] M. Theander; A. Yartsev; D. Zigmantas; V. Sundstròm; W. Mammo; M.R. Andersson; O. Inganàs, *Phys. ReV. B* **2000**, 61, 12957.

[13] A. Haugeneder; M. Neges; C. Kallinger; W. Spirkl; U. Lemmer; J. Feldmann; U. Scherf; E. Harth; G**ü**gel, A.; M**ü**llen, K. *Phys. ReV. B* **1999**, 59, 15346.

[14] D.E. Markov; E. Amsterdam; P.W.M. Blom; A.B. Sieval; J.C. Hummelen, *J. Phys. Chem*. A **2005**, 109, 5266.

[15] N.S. Sariciftci; L. Smilowitz; A.J. Heeger; F. Wudl, *Science* **1992**, 258, 1474.

[16] G. Yu, J. Gao, J. C. Hummelen, F. Wudl, A. J. Heeger, *Science* **1995**, 270,1789.

[17] S.A. Becker; K. Sivula; D.F. Kavulak; J.M. Fréchet, *J. Chem.Mater*. **2007**, 19, 2927.

[18] I. Riedel; E. von Hauff; J. Parisi; N. Martìn; F. Giacalone; V. Dyakonov, *AdV. Funct. Mater*. **2005**, 15, 1979.

[19] L.M. Popescu; P. van't Hof; A.B. Sieval; H.T. Jonkman; J.C. Hummelen, *Appl. Phys. Lett*. **2006**, 89, 213507.

[20] Z. Xu; L.M. Chen; G. Yang; C.H. Huang; J. Hou; Y. Wu; G. Li; C.S. Hsu; Y. Yang, *AdV. Funct. Mater*. **2009**, 19, 1.

[21] J.C. Hummelen; B. W. Knight; F. LePeg; F. Wudl, *J. Org. Chem*. 1995, 60, 532.

[22] J.W. Arbogast; C.S. Foote, *J. Am. Chem. Soc*. **1991**, 113, 8886.

[23] G. Li; R. Zhu; Y. Yang, *Nature Photonics* **2012**, 6, 153.

[24] Z. Guangjin; H. Youjun; Li Yongfang, *Advanced materials*, **2010**, 22, 39, 4355.

[25] H. Zhou; L. Yang; W. You, *Macromolecules*, **2012**, 45, 2, 607.

[26] L.J.A. Koster; S.E. Shaheen; J.C. Hummelen, *Advanced Energy Materials* **2012**, 2, 10, 1246.

2. Low Band Gap Polymers

2.1 Sun Spectrum: reason for aiming at Low Band Gap Polymers

The sun is the most important source of renewable energy and its core releases 3.86 x 10^{26} J of energy every second. Just outside the atmosphere of the earth the power density is 1366 Wm^{-2} but part of the visible light is lost, by absorption and reflection, when the light energy passes the atmosphere according to the air mass present in the light way. The power density depends on latitude, time, day and year. The solar spectrum under AM 1.5 conditions is depicted in Fig. 1.4 of the previous chapter. The air mass is abbreviated as AM, followed by a number that describes its mass. For istance, just outside the atmosphere, in space, the spectrum is AM0.

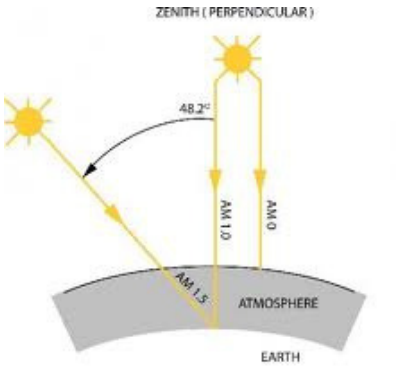

Figure 2.1: "AM1.5", 1.5 atmosphere thickness, corresponds to a solar zenith angle of $\angle z$ =48.2°. While the summertime AM number for mid-latitudes during the middle parts of the day is less than 1.5, higher figures apply in the morning and evening and at other times of the year. Therefore AM1.5 is useful to represent the overall yearly average for mid-latitudes. Consequently, the solar industry uses AM1.5 for all standardized testing of terrestrial solar panels.

At the surface of the earth at equator, under ideal conditions with a spectrum according to the air mass (AM1) part of energy is lost and at the latitudes of northern Europe and northern America the absorption loss is higher resulting in the AM1.5 spectrum.

[1] The solar spectrum under AM 1.5 conditions corresponds to the sun being at 45º above the horizon.

The photon flux (*f(λ)*) plotted as a function of the wavelength gives a good picture of how many photons can be harvested and is calculated by equation 2.1:

$$f(\lambda) = \frac{I_s(\lambda)}{E_\lambda(\lambda)} \qquad (eq.\,2.1)$$

where the photon energy $E_\lambda(\lambda)$ is a function of λ (eq. 2.2)

$$E_\lambda(\lambda) = h\nu = h\frac{c}{\lambda} \qquad (eq.\,2.2)$$

where h is Planck constant (6.626×10^{-34} Js), c is the speed of light (2.998×10^{8} ms^{-1}), λ is the wavelength in nm and $I_S(\lambda)$ is the sun irradiance in W $m^{-2}nm^{-1}$.

The integrated photon flux (F(λ) evaluated by eq. 2.3

$$\mathrm{F}(\lambda) = \frac{\int_{\lambda=280}^{\lambda} f(\lambda)d\lambda}{A} = \frac{\Delta\lambda\sum_{\lambda=280}^{\lambda} f(\lambda)}{A} \qquad (eq.\,2.3)$$

is obtained by dividing the value of the integration of photon flux *f(λ)* for the area under the sun irradiance curve, which, in turn, is determined by eq. 2.4

$$A_s = \int_{\lambda=280}^{\lambda=4000} f(\lambda)d\lambda = \Delta\lambda \sum_{\lambda=280}^{\lambda=4000} f(\lambda) \qquad (eq.\,2.4)$$

The integration range from 280 to 4000 nm has been chosen, because the sun irradiance is practically zero beyond these limits.[2]

Assuming that every photon is converted to one electron in OPV device the F(λ) is transformed into the maximum theoretical current (integrated current I_t, eq.2.5)

$$I_t = \mathrm{F}(\lambda) \cdot e \qquad (eq.\,2.5)$$

where e is the elementary charge (1.602×10^{-19} C).

In Figure 2.2a-b the photon flux, the integrated photon flux and the integrated current are plotted as a function of wavelength and show why there is a great interest

to harvest photons at longer wavelengths. The ideal optimum band gap of the polymers is currently subject to discussion, but in general polymer that absorbs light at longer wavelengths should be used in order to obtain higher maximal theoretical current.

a)

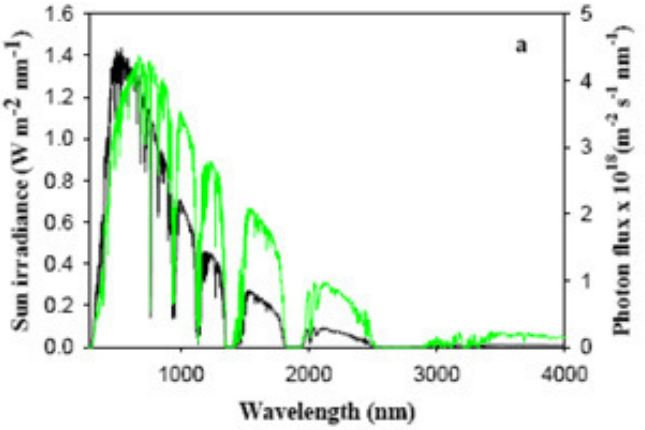

b)

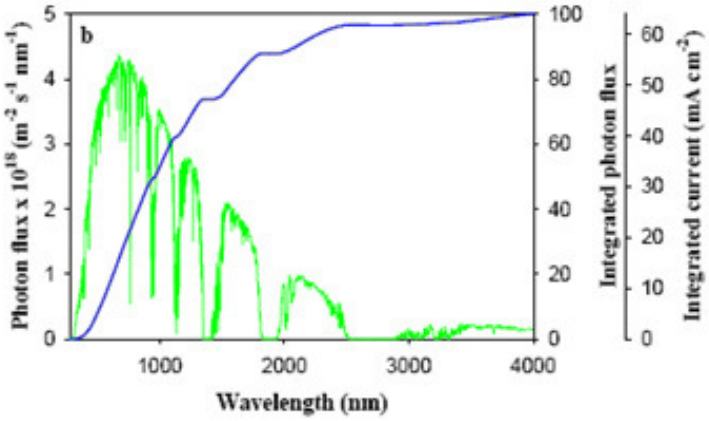

Figure 2.2: a) Sun irradiance (black) and photons flux (green) as a function of wavelength. The sun intensity spectrum is based on data from NREL[3]
b) Photon flux as a function of wavelength (green) and the integral (blue) is shown with two axes, one showing the integrated photons and one the theoretical current.

The experimental efficiencies obtained from low band gap materials do not coincide with the theoretically predicted value for the optimum band gap, since factors like morphology and charge carrier mobility play a role.

However, it is important to extend the absorption of the photoactive layer beyond 600 nm in order to obtain a better overlap with the solar spectrum and improve the efficiency of the device. This requires rational design of low band gap (LBG) materials.

2.2 Parameters Governing the Overall Performance of Solar Cells

In the previous paragraph we have shown how photoactive layer with red and near infra-red absorption allows harvesting more photons and resulting in higher currents. Now will explain how the current can lead to higher performance of the device. The increase in the current is not assured, because others parameters have to be taken into account. In fact, the power conversion efficiency (PCE) of the solar cells is defined as the ratio between P_{out} and P_{in} (eq.2.6), where the output power is expressed as product of Voc, Jsc and FF.[4,5,6] Open circuit voltage (Voc) is defined as the voltage between the terminals when no current is drawn (infinite load resistance), and short-circuit current density (Jsc) is the current when the terminals are connected to each other (zero load resistance).

$$PCE = \frac{P_{out}}{P_{in}} = \frac{V_{oc} \times J_{sc} \times FF}{P_{in}} \qquad (eq.2.6)$$

Figure 2.3 depicts a J–V curve under dark and incident-light illumination: Voc, Jsc, and FF are illustrated. In BHJScs a suitable polymer for attaining a high value of P_{out}, has to be designed paying attention to the following issues:

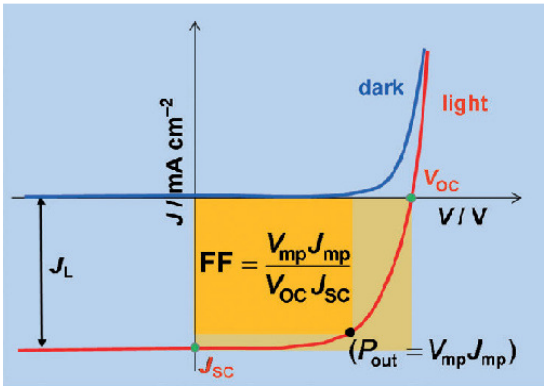

Fig 2.3: Current–voltage (J–V) characteristics of a typical solar cell

a) **Open Circuit Voltage**: the $\mathbf{V_{oc}}$ is defined in the models proposed by Scharber [7] et al. and Koster[8] et al. as the difference between HOMO level of the polymer and the LUMO of the acceptor, and represents the maximum photovoltage measured in a solar cell, which depends on the organic material and energetic level of their frontier orbitals. Figure 2.4 illustrates how the Voc can be increased by tuning the energy levels in a BHJ device. Starting from polymer with a Voc(1) and lowering its LUMO energy level from red straight line to the dotted red line, the value of the Voc doesn't change, but the value of its band gap changes. Nevertheless, combining the low band gap with an acceptor having a higher LUMO (from blue straight line to the dotted line) the result is an increase of Voc(2). When $PC_{61}BM$ is employed as acceptor, its LUMO level is -4.2 eV and the lowest possible LUMO level of the polymer would be around -3.9 eV, because an offset of ~0.3 eV between the LUMO energy levels of the polymer and acceptor is required to facilitate efficient exciton dissociation. Lowering more the HOMO level of the polymer produce a larger band gap, thus diminishing the light absorbing ability of the polymer (thereby a lower Jsc).

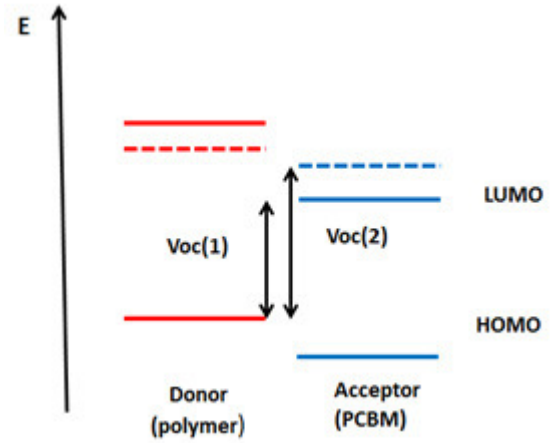

Fig 2.4: Increased PCE by tuning the DONOR-ACCEPTOR energy levels.

b) **Short-Circuit Current**: **Jsc** depends on the photon absorption of the active layer and represents the maximum photocurrent that could be obtained in a given solar cell. In order to maximize the number of excitons generated, the absorption of the donor-acceptor blend during the solar illumination should match the solar spectrum. Roughly 70% of the sunlight energy is distributed in the visible and near-IR region and, since $PC_{61}BM$ has a poor absorption in this part of spectrum, the polymer has to serve as the main light absorber. Most of the solar flux is distributed in the wavelength region from 380 (3.26eV) to 900 nm (1.38eV)[9]; hence, an ideal polymer should have a broad and strong absorption in the same range, from 3.26 down to 1.4−1.5eV. It is found that measured Voc matches closely to the theoretical value, which is the energetic difference between the donor HOMO and the acceptor LUMO; conversely, the short-circuit current results lower than the predict value. This is due to a series of loss mechanism, like molecular recombination, that could occur during the charge generation or transport. Consequently, the domain size of donor and acceptor plays a very important role in the actual short-circuits current. When domain sizes are too large, excitons will be lost due to exciton decay, nonetheless, too small domain sizes can induce an enhanced recombination of the charge carriers.[10] Also, the donor and acceptor domains need to have a percolated pathway towards anode and

cathode, respectively, in order for charges to be collected. A large range of solvents, polymer/fullerene ratios, annealing treatments and additives are typically required to induce the correct morphology.[11,12,13]

c) **Fill Factor**: **FF** describes the quality of the solar cell and is determined by the photogenerated charge carriers and the fraction that thereof reaches the electrodes. The maximum area within the J–V curve determines the FF. In fact, the FF depends on the competition between charge carrier recombination and transport processes. Additionally, the series resistances significantly influence the FF and should be minimized. The molar absorption coefficient of the molecule should be high to obtain a high external quantum efficiency (EQE) and the HOMO/LUMO energy levels should be properly adjusted to give increased Voc and FF.

The external quantum efficiency (EQE) is defined by the number of photogenerated charge carriers over the number of incident monochromatic photons. Besides the high value of PCE, solution processability and long-term stability of both materials, used into the polymer solar cells, are of equal importance for future application and commercialization.

In summary, to attain high performance efficiency, the polymers should have a good solubility; high molecular weight; proper energy levels, that means HOMO level around −5.4 eV and LUMO level around −3.9 eV if PCBM is used as acceptor material; high hole mobility and optimal morphology and long-term stability.

Furthermore, the overall solar cell performance can largely depend on the active area of the tested cell. Most of the laboratories use small-area devices to reduce loss of material. This leads to overestimation of the device efficiency due to edge effects.[14] Illumination of the nominal area can overcome this problem but even then extremely small cell areas should be avoided.

2.3 Design Consideration for Low Band Gap Polymers

The most critical factor for a rational design of materials and their combinations suited to obtain efficient OSCs is that a multiparameter problem should be mastered.

It is not only the proper combination of DONOR[1]* and ACCEPTOR[2]* materials, but as well optimization of Jsc, Voc, and FF by the control of absorption properties, HOMO–LUMO energy levels, material composition, solid-state packing, transport, and processing conditions.

A typical configuration of the polymers used as DONOR in BHJ devices is depicted in the Figure 2.5. In most cases the general structure of the polymer is constituted of two parts: a conjugated backbone and side chains. The conjugated backbone is the most important component because all physical properties, such as energy levels, band gap and inter/intra molecular interactions are due to its part, while the side chains play a crucial role in terms of molecular weight, crystallinity, solubility and intermolecular interaction with PCBM, in order to create a proper mixing with an ACCEPTOR and form the desired morphology.

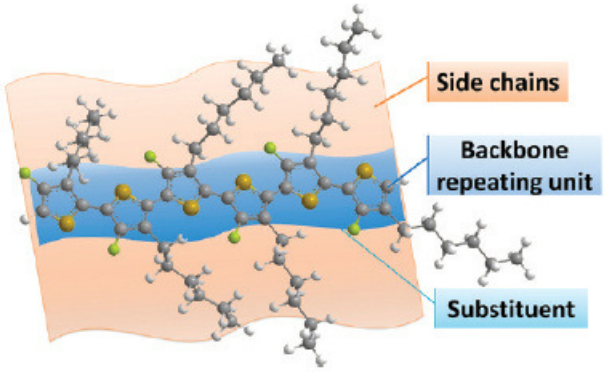

Fig 2.5: Typical configuration of DONOR polymer used in BHJ device

The choice of the side chain is also important to avoid the steric hindrance and twist of the conjugated backbone, which could mean low charge mobility or enhanced band gap. At last, substituents on the polymeric backbone are generally introduced in order to finely tune the electronic properties of the polymer.

[1]* In this paragraph "DONOR" indicates the polymer used in BHJ solar cells as hole transport while "donor" indicates the electron rich moiety contained into the LBG polymers.

[2]* in this paragraph "ACCEPTOR" indicates PCBM used in BHJ solar cells as electron transport while "acceptor" indicates the electron poor moiety contained into the LBG polymers.

There are different factors, that affect the band gap and one should be taken into account when designing new low band gap polymers:

(1) intra-chain charge transfer;

(2) bond-length alternation;

(3) aromaticity;

(4) substituents effects;

(5) intermolecular interactions;

(6) π-conjugation length

Most of the low band gap polymers reported in literature are based on thiophene derivates as homopolymer, copolymer or as part of fused ring system, but electron rich aromatic units, such as p-phenylenevinylene, are also presented.[57] A common strategy based on alternation of D-A alternating copolymers is a promising approach to develop semiconducting polymers with broader and stronger absorption with respect to P3HT, the best donor material for OPV.

The design of proper backbone, composed of an electron-rich (donor)[1]* unit and an electron-deficient (acceptor)[2]* moiety, allows obtaining a low band gap polymer with tunable energy levels.

The internal charge transfer between the donor and the acceptor moieties leads to more absorption.[15] π-electrons delocalization is facilitated thanks to the planar configuration adopted by the conjugated backbone and a delocalization along the structure leading to a smaller band gap.

This strategy was first proposed in 1993 by Havinga et al.[16] and in 2011 Chocos et al. reviewed the results reported so far on donor-acceptor copolymers based on thiophene, bithiophene or phenyl-derivate as donor [57].

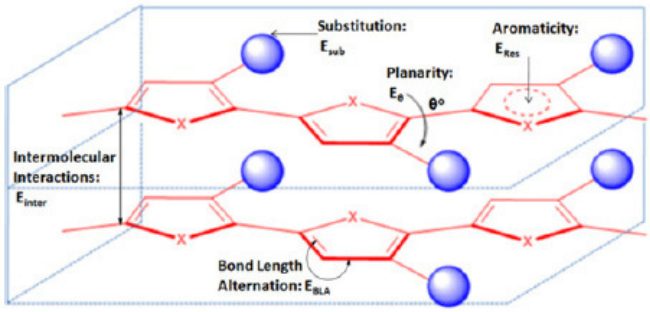

Fig 2.6: Structural factors affecting the band gap of π-conjugated polymers

Bredas et al. conducted a theoretical study where the bandgap of polythiophene and its derivatives have been calculated.[17] For the aromatic resonance contributor of a poly(thiophene), a bandgap of 2 eV was calculated while quinoid form shows a bandgap of 0.47 eV.

Planarity along the aromatic backbone also promotes a more delocalized HOMO distribution along the backbone, which enhances intermolecular charge-carrier mobility. Aromatic resonance energy, E_{res} (Fig. 2.6), is related to the band gap; hence, if this value is low the result is a low band gap polymer while higher value leads to a broader band gap, since a high Resonance Energy per Electron value prevents delocalization.[18,19]

In conclusion, if the HOMO level of the donor and the LUMO level of the acceptor are close in energy it results in a low band gap. Substituents on the DONOR play a fundamental role because they influence the energy levels and thereby the bandgap of a material. To achieve a lower band gap the strength of the donor and the acceptor must be tuned.

If an electron donating group is used, i.e. alkoxy or amine group, its electron density is pushed into the π-orbitals, raising the HOMO energy. In this way it is easier to remove an electron from the HOMO energy level. An accepting group, such as cyano, quinoxalines, pyrazines, thiadiazole or trifluoromethyl, lowers the LUMO due to the lowered reduction potential, making it easier to push an electron into the LUMO. This is efficiently achieved by using electron withdrawing groups (EWG)

on the acceptor moiety and electron donating groups such as thiophene or pyrrole on the donor one.

On the other hand alkyl chains are introduced to improve the molecular weight, solubility, and processability of conjugated polymers, because they are not well soluble due to their rigid backbone and their tendency to crystallize. Furthermore, to increase the intermolecular interactions, supramolecular ordening by alkyl side chains is introduced to enhance the solid-state packing. It has been found that some polymers show a lowered band gap in the solid state compared to the solution due to more order in the solid state.

If the conjugation length increases [20] the band gap is lowered, and the torsion angle can be reduced enhancing the backbone planarity and, consequently, further reducing the bandgap of the polymer.[21]

The design and synthesis of most small bandgap polymers reported in literature, is rationally based on these parameters in order to obtain the best material in terms of energy level and also to control the morphology of the active layer.

In BHJ solar cells, morphology and phase separation of the active layer also play a vital role in determining the overall performance. The dissociation of excitons and the creation of charges in the active bulk layer in OSCs is significantly influenced by its morphology.

The active layer morphology should reach a balance between the DONOR and ACCEPTOR domains and the intermolecular interactions between the donor and acceptor fragments.

2.3.1 Low Band Gap Polymer from Quinoid stabilization and Donor-Acceptor approach

All reported conjugated backbones can be arbitrarily classified into a few categories based on the constitution of the repeating unit, where the repeating unit of the homopolymer usually consists of a single aromatic unit or fused aromatics. The skeleton of a polyaromatic conjugated polymer can be simply explained as “a series

of consecutive carbon-carbon double bonds linked together by a carbon-carbon single bond".

The alternation of single and double bonds lowers the band gap, because of the two possible resonance structures for the ground state with nondegenerate energy. The first is called the aromatic form, where each aromatic unit (benzene or thiophene) maintains its aromaticity, confining π-electrons. The resonance structure, the quinoid form, arises from the delocalization of the π-electrons along the conjugated chain, which converts double bonds into single bonds and at the same time transforms single bonds into double bonds. Compared to the aromatic form, the quinoid form is energetically less stable and hence has a smaller band gap because adopting a quinoid structure requires destruction of the aromaticity and a loss in the stabilization energy. As reported in Fig 2.7, a reduction of the benzene-based aromatic units, in the conjugated main chain, allows a greater tendency to adopt the quinoid form through π-electron delocalization.[22]

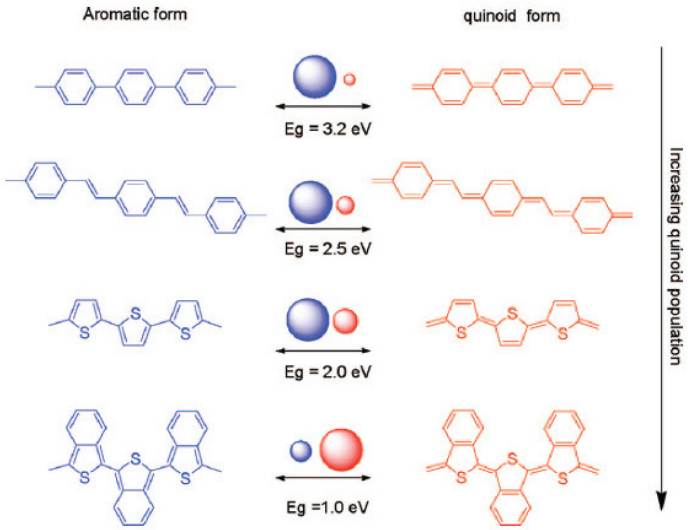

Fig 2.7: Aromatic and Quinoid form of poly(*p*phenylene), poly(*p*-phenylenevinylene), polythiophene, and polyisothianaphthene.

A geometrical parameter, i.e., bond length alternation (BLA), defined as the average of the difference in length between adjacent C-C bond in polyene chain, represents the ratio of the aromatic to quinoid population in a polyaromatic conjugated system.

If the aromatic form prevails in the ground state, a larger BLA value will be obtained.

For example, by inserting a double bond between two benzene in the backbone of poly(phenylenevinylene) the aromaticity is reduced and the value of the band gap decreases to ca. 2.4 eV starting from ca. 3.2 eV for the polyphenylene with a higher degree of aromaticity. Furthermore, thiophene has a lower aromaticity compared to benzene, so polythiophene is even more likely to adopt a quinoid form, and consequently, it has a lower band gap than 2.0 eV.

Various useful strategies to reduce the band gap are based on the molecular modification to impose steric or electronic effects on conjugated main chains. Planarity along the aromatic backbone results in a low band gap, due to a high degree of delocalization of the π-electron, thanks to p-orbital interaction; this in turn leads to a reduction of the band gap.

In general an increased conjugation length produces a decreased energy difference between HOMO and LUMO levels, but after a certain number of monomers the value of the band gap reaches a plateau, when the effective conjugation length is saturated.

A powerful strategy in designing low band gap conjugated polymers is based on a polymer where a conjugated electron-rich donor (D) unit and a conjugated electron-deficient acceptor (A) unit are employed in the same conjugated main chain. In this way, a low band gap is achieved by reduction of the difference in bond length along the polymer chain. In essence this concept suppressed the Peierls effect. [23,24] The donor–acceptor alternation gives two resonance forms D-A or $D^+ = A^-$ and through the introduction of this push-pull driving forces, in order to promote the formation of the quinoid mesomeric structure over the conjugated polymer chain, the value of BLA can be significantly reduced.

The polymers based on an electron acceptor unit coupled with an electron donor unit are low band gap polymers, for three main reasons. First, the alternation of donor and acceptor units can stabilize the quinoid form of the polymer since it increases

the double bond character between repeating units, stabilizing the quinoid form and reducing the bandgap.

Second, the band gap of the polymer is determined by the value of HOMO of the donor and the LUMO of the acceptor. A low band gap polymer is the result of a high energy level of the HOMO coupled with a low energy level of the LUMO of the acceptor. [25,26] As show in Fig 2.8 and according to the rules of perturbation theory, the HOMO of the donor unit interacts with the HOMO of the acceptor unit allowing the formation of two new HOMO levels for the D-A system. On the other hand, two new LUMO levels are produced by the interaction of the LUMO donor level with the acceptor one. A higher lying HOMO and lower lying LUMO levels are formed after the electrons redistribution from their original non-interacting orbitals to the new hybridized orbitals of the D-A polymer system. This leads to a narrowing of the optical band gap, which is experimentally evident in solvent with different polarity due the fact that an internal charge transfer is sensitive to the environment. In general, the energy required for absorption decreases as the solvent polarity increases.

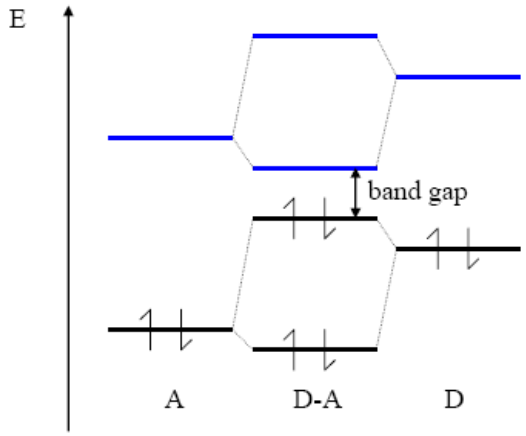

Fig 2.8: Orbital interactions of donor and acceptor units leading to a smaller band gap in a D-A conjugated polymer

Also, the degree of band gap reduction is strongly dependent on the strength of donor and acceptor segments bonded in the conjugated polymer.

Finally, the intermolecular interactions affect the band gap. As demonstrated for P3HT, the order of the solid state produces a red shift of the absorption spectrum and a lower band gap is achieved. [27]

A prerequisite to obtain a closely packed and ordered crystalline domain is a high stereoregular structure with an extended coplanar conjugated conformation.

After photon absorption and exciton dissociation, the most critical factor to obtain high photovoltaic performance is the charge-transport mobility. The molecular engineering strategies are also closely related to the charge-transporting properties of conjugated polymers. Physical and chemical properties such as π-electron delocalization, ordered and planar intermolecular channels, excellent electrochemical stability and reversibility will all facilitate the hole-transporting mobility.[28]

The donor molecules, most of the time thiophene-based or ethylenedioxythiophene-based (EDOT), are alternated to a wide variety of acceptors, the most common ones being based on the cyano group, the benzothiadiazole and the thienopyrazine moiety. The structure and the properties of the most important thiophene-based polymers will be reviewed in the next section.

2.4 Low Band Gap Polymers based on Thiophene unit

The PCE of the organic solar cells has now exceeded the 10% mark, with a significant improvement in the last decade. This has been made possible due to the development of low band-gap polymers with tunable electron affinity, ionization potential, solubility, miscibility with the fullerene acceptor and the improved understanding the factors affecting on the critical device parameters such as the V_{OC} and the J_{SC}.

The common design strategy for high performance polymers involve (a) synthesis from electron-rich (donor) and electron-deficient (acceptor) monomers via cross-coupling reaction; (b) highly conjugated, planar backbone structures via fused rings or otherwise, to promote the interchain π-π stacking and mobility; (c) straight or branched chain with alkyl or alkoxy groups to impart the solubility in common

organic solvents to enhance processability; and (d) the presence of electron withdrawing moieties into the monomer units to tune the HOMO and LUMO energy levels of the donor polymer.

The alternating incorporation of donor and acceptor units into the polymer backbone is one of the most promising approaches to achieve a low band-gap polymer due the intramolecular charge transfer interactions between the moieties. This strategy allows different values of the HOMO and LUMO energy levels of the polymer by varying the HOMO and LUMO energy levels of its donor and acceptor units. In this context, the most commonly used building blocks for this purpose are the thiophene derivatives because of the electron-rich sulfur atom and the rigid five-membered ring, which facilitates the extension of conjugation and increases the π–π intermolecular stacking.

Examples of low band gap polymers based on thiophene units and their properties are summarized below.

2.4.1 Poly(3-Alkyl)thiophenes and their analogues

Polythiophene represents the most important conjugated polymer utilized in a broad spectrum of applications in organic electronics, such as light-emitting diodes, field-effect transistors and plastic solar cells due to its excellent optical and electrical properties as well as good thermal and chemical stability. To date, a combination of poly(3-hexylthiophene) (P3HT) as the electron donor and PCBM as the electron acceptor in the active layer represents the most efficient BHJ solar cell with power conversion efficiency approaching 6% (8.3% certified, cell size 1 cm^2, Konarka, Lowell MA, USA/Nuernberg, Germany)[29], obtained by optimization and careful design of the polymer.

To improve the solubility of polythiophene, different substituents as side groups, R, have been explored, such as alkyl, alkoxy, acid, ester and phenyl groups, etc. Because 3-alkylthiophene is an asymmetrical molecule, three orientations are possible when the two thiophene rings are coupled between the 2- and 5-positions.

The first one is the 2-5′ coupling or head-to-tail (HT), the second one is 2-2′ or head-to-head coupling (HH), and the third is 5-5′ or tail-to-tail coupling (TT).

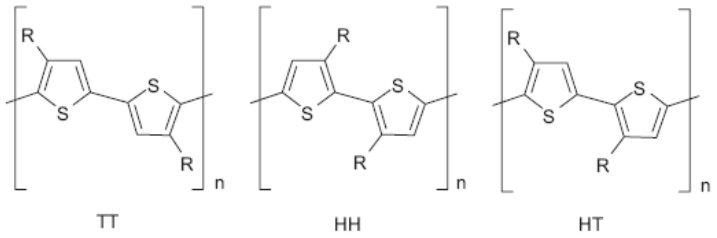

Chart 2.1: Structure of polythiophene in HH, HT and TT couplings

This gives the possibility to obtain a random structure with HT, HH or TT coupling; on the other hand, the coupling of each thiophene unit in a consecutive head-to-tail manner during the polymerization affords a regioregular poly(3-alkylthiophene) (P3AT) which is capable of adopting a coplanar conformation, resulting in a lower band gap polymer.

The first synthesis of regioregular HT coupled P3AT was reported by Mc Cullough in 1992 [30,31] in which regioregular polymerization of 3-alkylthiophene was controlled by selective lithiation of 2-bromo-3-alkylthiophene, using lithium diisopropylamide (LDA), followed by transmetalation with magnesium bromide to yield the organomagnesium intermediate. The use of a Ni(dppp)Cl_2 catalyst for the polymerization of this intermediate gives the corresponding poly(3-alkylthiophene) with over 90% head-to-tail regioselectivity.

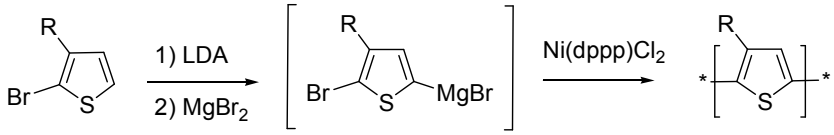

Scheme 2.1: Synthesis of Regioregular Poly(3-alkylthiophene) by the McCullough Route

Later on, McCullough reported another method for the synthesis of regioregular P3ATs by Grignard metathesis (GRIM).[32] Treatment of 2,5-dibromo-3-hexylthiophene with a variety of alkyl Grignard reagents resulted in two metalated regioisomers in an 85:15 ratio (independent of reaction time, temperature and Grignard reagent employed) via a magnesium exchange reaction. The authors

demonstrated that the GRIM polymerization of P3HT proceeds by a living chain growth mechanism, in respect to the traditionally step growth polycondensation.[33,34] As a result, low polydispersities (ca.1.2-1.3) and well-defined molecular weights can be controlled by the feed ratio of monomer to the Ni catalyst. The mechanism proposed from McCullough and Yokozawa is reported in the Scheme 2.2.[35,36]

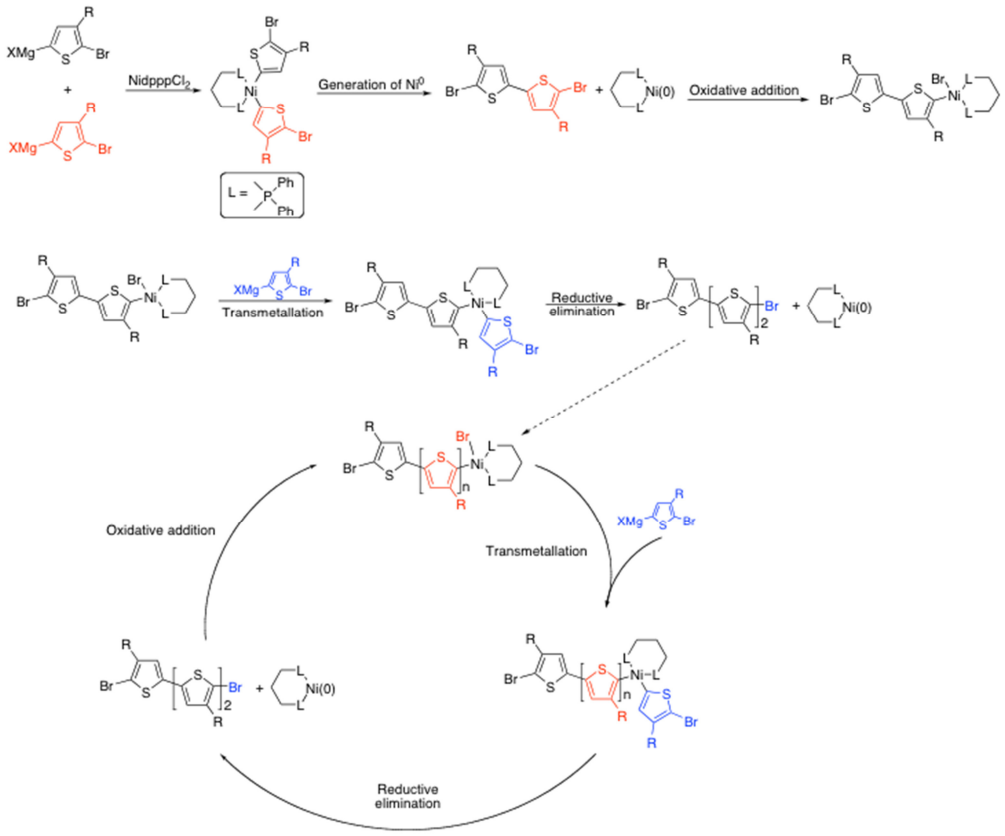

Scheme 2.2: Mechanism of GRIM polymerization proposed by Yokozawa[36]

GRIM coupling has become the most widely used method for producing P3ATs with predetermined high molecular weights. The molecular weight and the regioregularity of rrP3AT have been determined to play a crucial role on the light absorption and hole mobility within the blend and as a consequence to the overall OPV efficiency. Moreover, the optical band gap of rrP3HT is ~2.0 eV, while the

energy levels are situated at 2.8–3.0 eV for the LUMO level and ~5.0 eV for the HOMO level.

Between 2002 and 2010, more than 1000 publications can be found reporting the BHJ based on P3HT:PCBM (Source SciFinder). Half of these papers, that report photovoltaic performance with their respective PCE, have been successfully collected and analyzed.[37] Most PCE values have been found as being between 3,5% and 4%. The PCE distribution histogram and the maximum value for each of all papers taken into account are displayed in Fig 2.9.

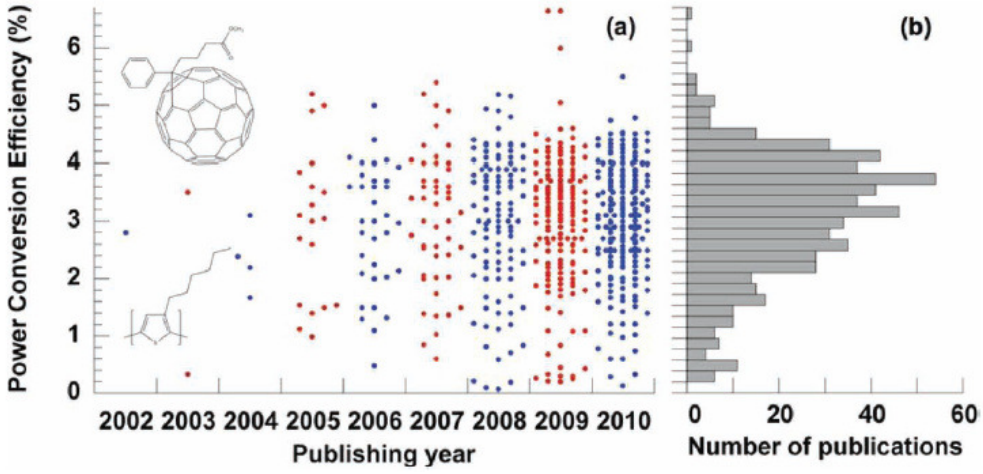

Fig 2.9: a) PCE of the P3HT:PCBM-based solar cells reported in each of the 579 publications screened reported in *Adv. Mater.* **2011**, *23*, 3597–3602. b) The overall distribution of PCE values from 2002 to 2010.

Due to the complexity of the polymer chemistry, materials science, device engineering, and device physics involved, extended studies on P3HT: PCBM blend will be continued in the coming years in order to explore these model materials until the next generation ones will take place. About device engineering and in order to compare the homogeneous data, not only the light source but also the surface area of the photovoltaic cells is a critical factor. Only a few papers have reported a large active area of more than 1 cm^2, because large-area devices require appropriate deposition techniques (Doctor Blade, screen-printing, roll to roll or inject-printing). The irradiance methodology is of importance too. [38]

In the case of standardized PV-cell characterization, in terms of light source and device area, the huge variability in reported efficiencies should be due to the material properties and the process reproducibility. In particular the purity of the organic materials and solvents are an issue, as the metal residues coming from catalysts. All of these impurities affect the charge-carrier transport and recombination rates. [39]

Numerous investigations relate that the higher the regioregularity, the better the crystallinity and the higher the charge-carrier mobility.

It was shown that the favorable morphology, for balanced hole and electron mobilities resulting, is based on a fibrilla structure, in which rrP3HT crystals is embedded in a matrix that is probably contain $PC_{61}BM$ nanocrystals and amorphous regions of rrP3HT.[40]

For a higher degree of P3HT crystallinity it has been demonstrated that the choice of the spin-coating solvent[41] and thermal annealing[42,42] are crucial parameters to obtain a good charge transport and maximum interfacial area for efficient charge generation. Thermal annealing of the P3HT:PCBM composite provides an external force to reorganize the polymer chains, with a result of a bicontinuous interpenetrating D-A layer.[43] However, prolonged thermal annealing produces more crystallization of regioregular P3HT and thereby tends to destroy the optimal morphology as a result of phase segregation between P3HT and PCBM. Therefore, a prolonged annealing forms macroscale domains larger than the exciton diffusion length.

Probably, the high driving force for crystallization of the rrP3HT initiates the phase segregation of the PCBM by exclusion from the ordered P3HT domains.

It has been shown that a too-high regioregularity may be an issue. Authors have demonstrated that decreasing the regioregularity leads to polymer-fullerene composites with superior thermal stability by lowering the driving force for the P3HT crystallization.[21,44]

In the first case of Chart 2.2, a random polythiophene (**P1**) bearing side chains at both 3 and 4 positions, synthetized by GRIM method[45], was employed with the aim

to reduce the regioregularity of P3HT, since the high regioregularity is responsible for the high degree of crystallinity, without changing its superior optoelectronic properties. On the other hand a rrP3HT has been synthesized using the same parameters and obtaining polymers with similar weights.

Whereas the devices containing a random polymer, as donor material, showed better thermal stability, with the appearance of a slightly lowering performance, the device based on rrP3HT had a decreased in performance upon annealing after 30 min at 150°C. These results indicate that the annealing time and the degree of regioregularity are critical to achieve stable photovoltaics.

P1 **P2**

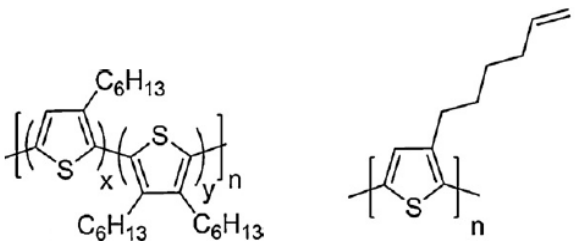

Chart 2.2: Chemical structures of the random and cross-linkable polythiophene derivatives

The second approach in based on a cross-linkable regioregular polythiophene (**P2**).[46] The presence of a vinyl group at the end of the side chain maintains the high crystallinity of the polymer, because is a small functionality and permits to crystallize in a manner similar to rrP3HT, due to their structural similarity; but simultaneously the thermal treatment can induce a cross-linking reaction of the vinyl group at the side chains. The devices have been fabricated using the same protocol for the new polymer and the control rrP3HT, both synthesized using the GRIM polymerization. BHJ devices were annealed at 150°C. At this temperature various spectroscopic results and the lower solubility in the common solvent confirmed the presence of cross-linked structure. The device based on new derivate showed, after annealing, photovoltaic parameters better than the control device. The higher value of PCE found in the case of cross-linkable polymer was attributed to the suppression of the formation of large PCBM aggregations.

Also other methods to control the morphology have been investigated, such as the slow drying of solvent[47], the use of additives or selective solvents and slow cooling[48] of the rrP3HT solution and various deposition techniques. [49,50,51]

Very recently, a series of rrP3ATs with different alkyl side chains were synthesized and their optoelectronic and morphological properties were compared with those of rrP3HT.[52]

The length of the solubilising group in the conjugated thiophene unit also plays an important role in determining the balance between crystallinity and miscibility and the solvent used for spin coating[53,54] have been shown to be of great importance to achieve optimal morphology.

It was found that chain lengths longer than eight carbons facilitate diffusion rates of PCBM from the polymer matrix during the thermal annealing.[53] This leads to a larger scale of phase separation, reduced interfacial area, and thereby lower device performance. The hexyl group in P3HT demonstrated an optimal balance with the best device performance in the poly(3-alkylthiophene) family.[54]

Addition of disorder alterates the driving force for crystallization leading to thermally stable bulk heterojunctions,[21] the P3HT with the lower regioregularity possessed superior thermal stability over those with higher regioregularities. This was ascribed to the suppression of the crystallization-driven phase separation through introduction of a controlled amount of disorder into the polymer backbone. Note that this result is consistent with previous observations.

The major function of the aliphatic chain substituent is to provide adequate solubility of polythiophenes imposing weak electronic interactions with the backbone.[55] Despite this, the introduction of alkoxy chains into the 3-position of polythiophenes is not only convenient as solubilizing groups but also greatly perturbs the molecular orbitals involved in tuning the band gap. In fact, poly(3-alkoxy-thiophene)s, synthesized by GRIM method, showed a lower band gap due to electron-donating effects that increase the HOMO level, but the poor properties in solution and the air instability of the film restricted its performance in solar cell devices.

In order to improve the PCE of the BHJ based on rrP3HT two drawbacks need major adjustments: the high optical band gap, which prevents devices for obtaining higher Jsc, and its value of the HOMO level at 5.0 eV, which leads to rather low Voc. Many LBG donor polymers were synthesized to overcome the first needs but for the relatively high-lying HOMO level only few examples have been presented with the aim to increase the Voc value through a lower HOMO level.

These examples include a series of terthiophene,[56, 57] quaterthiophene[58] and randomly bithiophene[59] polymers bearing various 3-alkyl side chains combined with unsubstituted thiophene rings in the polymer backbone (**P3, P4, P5**). The crystallinity and the PCE in polythiophene derivatives:PCBM based BHJ OPVs was examined as a function of substituent sequence distribution as well as the influence of the type and length of various alkyl side chains. The difference in the result are due basically on the twist of the backbone plane for the introduction of unsubstituted thiophene units, that perturb the planarity of the backbone and lowering the HOMO level if compared with rrP3HT.

P3 **P4**

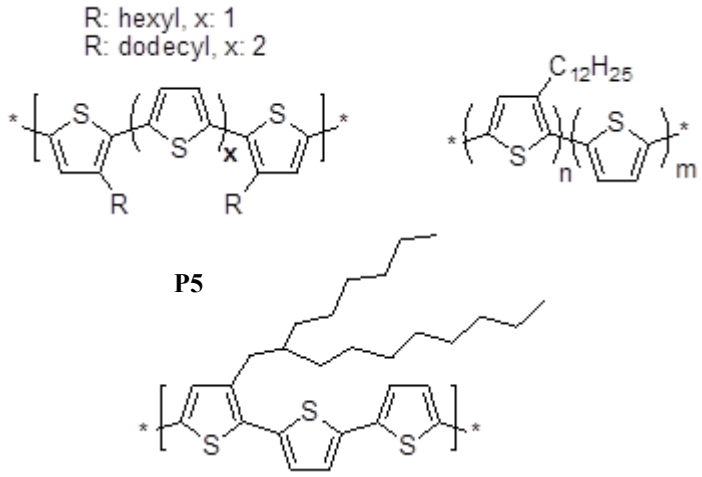

Chart 2.3: Chemical structures of different polythiophene derivatives

It was observed that all the HOMO levels are lying deeper than rrP3HT proving that the above approaches efficiently lower the HOMO level but the photovoltaic

performance of BHJs were very different, dependending on the placement and the choice of the alkyl side chain, which induces different crystallinity and miscibility with PCBM. In particular two polymers, which differ only in the sequence distribution of the alkyl side chain but with the same composition and electrochemically equivalent, showed different solar cell performance and the polymer with the random structure is superior to the polymer with defined structure.

2.4.2 Polythiophene derivatives with thiophene and thiophenevinylene as side chain

In an attempt to obtain broad absorption and desirable hole mobility, two-dimensional regioregular polythiophenes with alkylthiophenes as side chain pendants was copolymerized with an electron rich thiophene ring (**P6** with x=1; **P7** with x=2). Unlike the bi(thienylene–vinylene) system,[56] the alkyl-thiophenes in this study were directly attached onto the polythiophene backbones without vinylene linkers.

The coplanar conjugated structures render strong intermolecular π–π interaction, which would extend the degree of π-conjugation and this means remarkable hole mobility. X-ray crystallography reveals a nearly planar conformation of 2-D monomer.

The optical band gap of **P7** is lower than **P6** because of the longer length of its conjugated side chains.

Also, the polythiophene bearing the thiophen-alkyl side chain was copolymerized with either an electron withdrawing unit (**P8**)[60] or various donor-acceptor segments (**P9, P10, P11**) in which the thiophene rings plays the donor rule linked to different acceptor moieties (see Chart 2.4).

All this polymers have been synthetized using Stille cross-coupling polymerization.

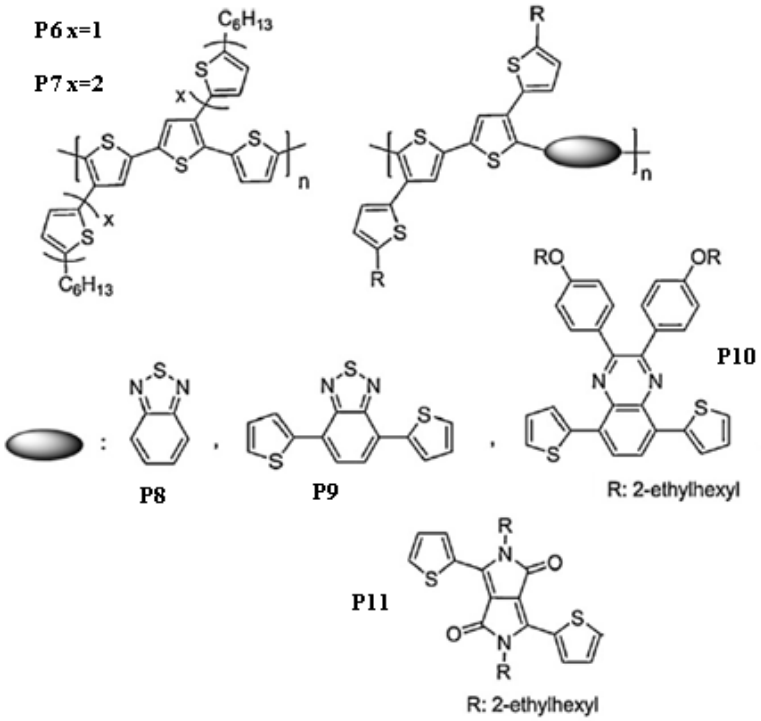

Chart 2.4: Chemical structures of different polythiophene derivatives with thiophene ring as pendant

The optical band gaps, the energy levels and the PCEs of the polythiophene derivates **P6**–**P11** are presented in Table 2.1 [61].

Polymers	E_g^{opt} (eV)	LUMO (eV)	HOMO (eV)	PCE (%)
P6	1,98	-	5,46	2,5
P7	1,77	-	5,62	1,3
P8	1,88	3,24	5,52	1,39
P9	1,6	3,38	5,04	1,28
P10	1,83	3,22	5,28	1,29
P11	1,29	3,62	5,17	1,67

Tab. 2.1: Optical band gap, electorchemical properties and photovoltaic efficiency of P6-P11

The results reveal that the electronic structures were readily tuned by copolymerizing with different conjugated electron-accepting units.

The synthesized copolymers were incorporated into donor-acceptor blends, with $PC_{71}BM$ using different composition ratios, in order to evaluate the photovoltaic performances. The highest PCE (2.5%) was obtained from **P6**:$PC_{71}BM$ system in 1:3 (w/w) with Jsc = 6.4 mA/cm^2, Voc = 0.91 V and FF = 0.43 upon annealing at 140 °C for 20 min. Comparing the photovoltaic characteristics of **P6** with those of **P7** it can be clearly noticed that the PCE of **P7** is significant lower than that of **P6** despite its higher HOMO level. Furthermore, the PCEs of the D–A polythiophene derivatives **P8-P11** in blends with $PC_{71}BM$ in 1:3 (w/w) ratio are between 1.28 and 1.67%. The above results indicate that these two-dimensional 4T-acceptor conjugated copolymers could enhance the charge-transport characteristics and are good materials for organic optoelectronic devices.

It is well known that extension of conjugation degree leads to enhancement and red-shift of the absorption spectra of conjugated polymers. Based on this consideration, a broad absorption was realized by attaching conjugated side chains containing thienylenevinylene on polythiophene backbone in different ratio. [62,63]

The absorption spectra, the energy levels and the photovoltaic properties are influenced by the content of the conjugated vinylene side chains, but the trends are different, depending on the structure of the side chain.

P12 **P13**

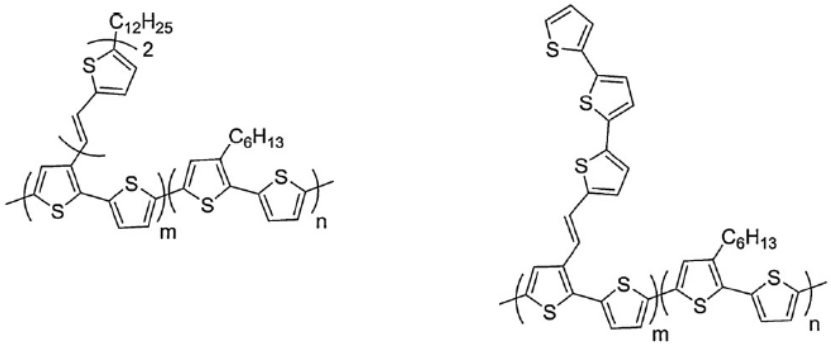

Chart 2.5: Chemical structures of different polythiophene derivatives with thienylevinylene as side chain.

The optical band gap in copolymer **P12** increases by decreasing the content of the conjugated side chains while in increase on the content of the conjugated side chains in the series of copolymer **P13** gives a blue-shift absorption caused from the optical band gap decreasing.

Polymers	n	m	E_g^{opt} (eV)	LUMO (eV)	HOMO (eV)	PCE (%)
P12a	0	1	1.80	2.97	4.96	1.71
P12b	0.01	0.99	1.81	2.95	4.94	2.57
P12c	0.41	0.59	1.82	2.96	4.93	3.18
P13a	1	0	-	-	-	0.87
P13b	0.9	0.1	-	2.72	5.07	1.47
P13c	0.8	0.2	-	2.75	5.07	1.91
P13d	0.7	0.3	-	2.79	5.09	1.65
P13e	0.6	0.4	-	2.84	5.09	1.47

Tab. 2.2: Optical band gap, electorchemical properties and photovoltaic efficiency of P12-P13.

Comparing the energy levels between the two copolymers **P12** and **P13** it is observed that the LUMO levels of **P12** derivatives are lower than the LUMO energy of the copolymer **P13**. On the other hand the electrochemical band gaps in the second case are higher than that of the **P12** polythiophene derivatives. This is an indication that bithienylenevinylene side chains can be used to decrease more effectively the band gap of the side chain conjugated polythiophenes than terthiophenevinylene side chains.

The photovoltaic properties of copolymers **P12** and **P13** were investigated when blended with $PC_{61}BM$, using different composition ratio, in BHJ architecture.

In comparison with the device based on P3HT, the Voc of the devices based on the bithienylenevinylene increased by ca. 0.1 V. The higher Voc is expected from the lower HOMO energy levels of the derivate but the photovoltaic parameters are different for the two polymer. In general it can be summarized that in the first case the PCE increases as the content of the conjugated side chain decreases, while the

PCE of the **P13** derivatives increases as the content of the bithienylenevinylene side chain reach up to 20% and then the PCE subsequent decreases for contents above 20%.

2.4.3 Polythiophene derivatives with imidazole as side chain

Conjugated polymers that contain side-chain-tethered conjugated acceptor moieties not only absorb light more effectively (multiple absorption), but also exhibit enhanced charge-transfer ability. These two desirable properties for photovoltaics applications can be reached by the introduction of an electron-acceptor unit onto the side chain of a conjugated polymer, that can increase the breadth of wavelengths of light absorbed and can also lower the band-gap to some extent.

Multiple absorptions is an approach that can be used to expand polymer absorption spectrum. The generated excitons can be readily dissociated into electrons and holes in this type of conjugated polymers, because of the internal field produced by the dipole moment built on its D–A molecular structure and subsequent charge transfer to nearby PCBM.

The GRIM method was employed for the synthesis of the homopolymer **P14**,[64] containing the electron-withdrawing and conjugated phenanthrenyl-imidazole group and the copolymers **P15/P16**, containing different contents of phenanthrenyl-imidazole moieties along with 3-alkyl substituted thiophene monomers.[65,66]

The optical, electrochemical and photovoltaic properties are summarized in Table 2.3. The band gap of **P15** and **P16** is reduced upon increasing the content of incorporated phenanthrenyl-imidazole moieties in the copolymers, due to the alteration of the HOMO and LUMO levels by the presence of the phenanthrenyl-imidazole moieties.

P14 **P15** **P16**

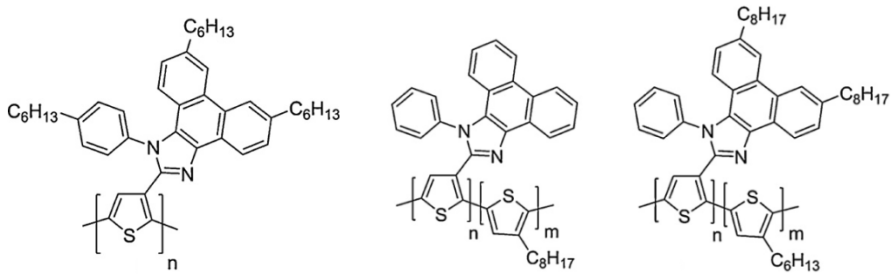

Chart 2.6: Chemical structures of different polythiophene derivatives with imidazole as side chain

Polymer	n	m	E_g^{opt} (eV)	LUMO (eV)	HOMO (eV)	PCE (%)
P14	/	/	1,85	2,9	4,7	4,1
P15a	10	90	/	3,57	5,35	/
P15b	20	80	/	3,6	5,3	/
P15c	30	70	/	3,64	5,25	/
P15d	50	50	1,82	3,66	5,21	1,68
P15e	70	30	1,81	3,7	5,2	2,15
P15f	80	20	1,77	3,75	5,15	2,8
P16a	20	80	1,88	2,8	4,7	/
P16b	40	60	1,86	2,87	4,7	2,42
P16c	60	40	1,85	2,95	4,65	2,63
P16d	80	20	1,83	3,02	4,65	2,85
P16e	90	10	1,8	3,05	4,65	3,45

Tab. 2.3: Energy levels and the optical band gap value Vs. the molecular composition of P14-P16.

The polymer band gap decreases increasing the content of phenanthrenyl-imidazole, which confirms that the presence of the octylphenanthrenyl-imidazole moieties increases to some extent the effective conjugation length of the polythiophene main chain. The polymers containing the unsubstituted withdrawing unit have a lower optical band gap compared to the structure bearing the alkyl chain on the

phenanthrenyl-imidazole, most probably because of the better π-π stacking between the polymer chains.

BHJ solar cells were fabricated with **P14-P16** derivatives blended with $PC_{61}BM$ and the PCE of the device was maximized by annealing the **P14**/PCBM blend at 120 °C for 30 min.

The more-balanced electron and hole mobility and the enhanced visible absorptions in the devices subject to annealing both contributed to a much higher short-circuit current density, which in turn led to a PCE as high as 4.1%.[60]

2.4.4 Cross-linked polythiophene derivatives

One of the approaches to overcome the problems associated with interchain charge transfer between individual macromolecules is the use of a network structure, like a cross-linked conjugated polymer, thanks to their ability to promote the carrier interchain hopping than amorphous films of the linear parent polymers.[67,68]

Extending the scope of this general approach, several crosslinked polythiophene derivatives, bearing various percentages of conjugated bridges, were synthesized through Stille polymerization and tested for OPV application.

Chart 2.7 reports the structure of crosslinked polythiophene derivatives with vinylene-phenylene-vinylene[69] (**P17**, VPV) and vinylene-terthiophene-vinylene[70] (**P18**,VTV) conjugated bridge. The corresponding energy and photovoltaic properties, as a function of the percentage of the conjugated bridge, are summarized in Table 2.4.

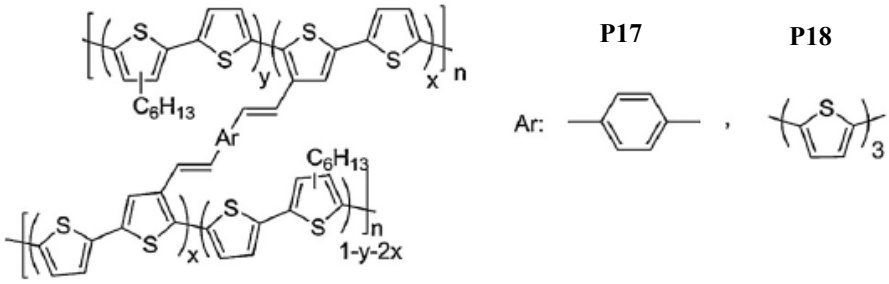

Chart 2.7: Chemical structures of cross-linked polythiophene derivates

It was found for both polymers that the conjugated bridges between the backbones improved the charge transportation of the polymers, but made the absorption spectrum blue-shifted. The increase of conjugated bridges, might result to a more pronounced distortion of the polymer backbone that effectively reduce the conjugation length of the polymer, also the twist of the backbone should be lower for the derivatives with VTV bridge compared to that bearing VPV bridge.[65,66]

Polymer	x	LUMO (eV)	HOMO (eV)	PCE (%)
P17a	0	2,77	5,06	0,37
P17b	0,02	2,76	5,07	1,05
P17c	0,05	2,74	5,13	1,26
P17d	0,1	2,73	5,23	0,78
P18a	0	2,77	5,06	0,87
P18b	0,02	2,77	5,06	1,72
P18c	0,04	2,75	5,06	1,47
P18d	0,08	2,74	5,11	1,21

Tab. 2.4: Energy levels and the photovoltaic performance of P17 and P18

Regarding the energy levels, an interesting point is the similar HOMO/LUMO values for both polymers, independently of the type of conjugated bonded chain.
BHJ solar cells based on polymers **P17** and **P18** mixed with $PC_{61}BM$ in 1:1 (w/w) ratio, were fabricated and the photovoltaic data were compared to those of poly(3-hexylthiophene-*co*-thiophene) without the conjugated bridges. As reported in Table 2.4 the derivates **P17b** and **P17c** showed an improved PCE compared to that of **P17a**. One possible explanation could be higher hole mobilities, measured by SLC method[65] but when the number of the conjugated bridge is too high, sa for **P17d**, the worsen photovoltaic properties reflect the poor solubility of the derivate. The similar trend was registered for the polymers **P18a-c**.

2.4.5 Oligothiophene copolymers with 2,1,3-benzothiadiazole unit into the main chain

In an attempt to obtain polythiophene derivatives with broad absorption and high hole mobility, various research groups synthesized a series of LBG (**P19-29**) based on thiophene as donor and 2,1,3-benzothiadiazole as acceptor.[71,72,73]

The structures (showed in Chart 2.8) may differ with respect to the number of thiophene units, position, type (linear or branched) and length of the alkyl chains bonded to thiophene ring.

Table 2.5 reported the optical band gap of the derivatives **P19-P29**. Polymer **P20** presents one thiophene more than **P19,** but the band gap is exactly the same; on the contrary the derivate **P21** shows a value lower than **P20** even if it contains the same amount of donor units into the backbone. This is most likely due to the introduction of the alkyl side chain on the thiophene unit in the β-position in relation to the 2,1,3-benzothiadiazole that gives steric hindrance. Also, the position of the alkyl chain on the thiophene ring plays a crucial role.

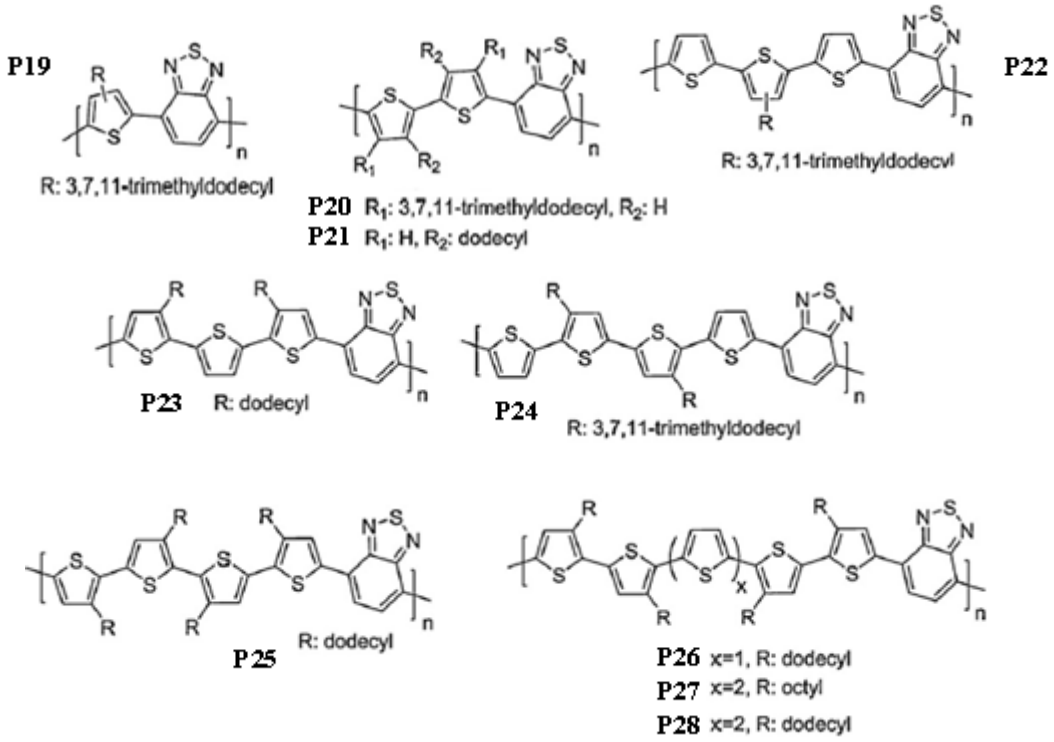

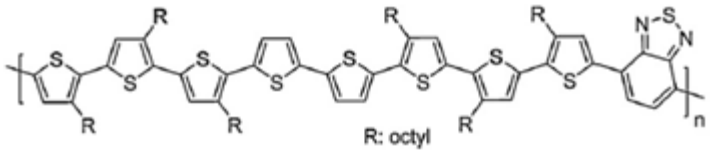

P29

Chart 2.8: Chemical structures of oligothiophene copolymers with 2,1,3-benzothiadiazole.

It is different if there are no alkyl side chains on the thiophene rings, next to the 2,1,3-benzothiadiazole and a branched dodecyl side chain on the thiophene unit between the two thiophenes (**P22**), or if the structure consists of two dodecyl side chains on the thiophene units in the β-position regarding to the 2,1,3-benzothiadiazole and no alkyl chain on the thiophene between the other two β-alkyl-thiophenes (**P23**). This is due to the planar geometry and closely packing at the solid state that the structure can adopts.

Polymer	E_g^{opt} (eV)	LUMO (eV)	HOMO (eV)
P19	2,10	3,30	5,40
P20	2,10	2,82	4,92
P21	1,97	3,23	5,59
P22	1,82	4,02	5,84
P23	1,59	3,17	5,03
P24	1,65	3,02	4,67
P25	1,72	3,18	5,20
P26	1,56	3,10	4,88
P27	1,78	3,37	5,26
P28	1,52	3,18	4,94
P29	1,82	3,30	5,23

Tab. 2.5: Optical band gaps and electrochemical data of P19-P29.

In conclusion the band gap is a function of the number of the thiophene rings around the withdrawing core and also of the density and the relative position of the alkyl side chains attached on the thiophene rings.

Concerning the electrochemical data, direct comparison between the polymers cannot be provided since different experimental techniques have been used to obtain the HOMO–LUMO energy level.[67,68,69]

The PCE of these polymers in blends with $PC_{61}BM$ are positioned in the range between 0.93% and 2.23%. The highest PCE (2.23%) is observed for the **P28** when is blended with $PC_{61}BM$ in 1:3 (w/w) ratio.[68] It should be noted that no difference on the PCE values is observed when thermal treatment is applied.

It was also tried the polymerization of substituted 2,1,3-benzothiadizole with alkoxy-group with one (**P30**), two (**P31**) or three (**P32**) thiophene units using Stille or Yamamoto cross-copuling polymerization[74].

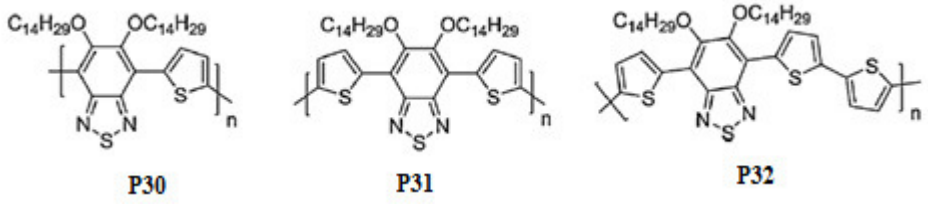

Chart 2.9: Chemical structures of the alkoxy-substituted 2,1,3-benzothiadizole copolymers.

The optical band gap and the PCE of the devices obtained from the blend with $PC_{61}BM$ (1:2 w/w) are summarized in Table 2.6. As reported from Helgesen[70] et al. a possible explanation for the lower PCE value of **P31** compared to **P30** and **P32** is the different route to obtain the polymer, Yamamoto in the first case and Stille coupling in the other ones, where excess of Ni(0) was used instead of Pd(II).

Polymer	E_g^{opt} (eV)	PCE(%)
P30	1,74	2,22
P31	1,73	0,62
P32	1,75	1,78

Tab. 2.6: Optical band gaps and photovoltaic efficiency of P30-P32.

Another class of polymers containing 2,1,3-benzothiadiazole, as electron-poor moiety, and 3,4,dioxythiophene, as electron-rich, have been synthetized by Ni-

catalized Yamamoto[75] polymerization or by oxidative polycondensation, using $FeCl_3$[76](**P33**).

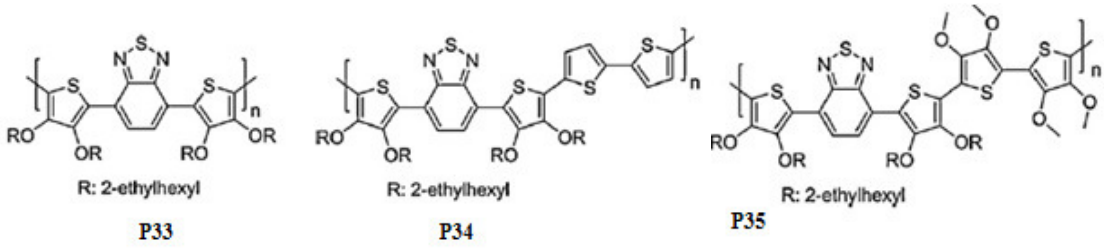

The electrochemical properties, determined by cyclic voltammetry (CV) or differential pulse voltammetry (DPV), are presented in Table 2.7. The electrochemical band gaps obtained using the DPV method are closer to the optically estimated values than that obtained using the CV method [71].

As reported in Table 2.7 the photovoltaic performance of the derivative containing unsubstituted bithiophene (**P34**) is two time higher that of the other two, probably due to their low hole mobilities and unfavorable thin film morphologies, confirmed by AFM results in blend with $PC_{61}BM$[71]. For the blend **P34**:$PC_{61}BM$ (1:8 w/w) the AFM images show a more heterogeneous morphology with dispersed large $PC_{61}BM$ domains in the active layer than in the case in which **P33**:$PC_{61}BM$ (1:4, w/w) was employed, giving a formation of very large PC61BM clusters and without the appearance of any interpenetrating network.

Polymer	CV		DPV			
	LUMO (eV)	HOMO (eV)	LUMO (eV)	HOMO (eV)	E_g^{opt} (eV)	PCE (%)
P33	3,53	5,35	3,59	5,35	1,6	0.88
P34	3,5	5,6	3,63	5,53	1,65	1.90
P35	3,47	5,28	3,62	5,24	1,55	0,7

Tab. 2.7: Optical band gaps,electrochemical data and PCE of P33-P35

2.4.6 Polythiophene derivates with other various electron-deficient moieties

According to the proposed approach of "weak donor−strong acceptor", one should incorporate in the polymer backbone a "strong acceptors" to lower the LUMO levels, decreasing the band gap of related polymers.

As already mentioned in the previous paragraphs, the most common D−A conjugated polymers consisting in 2,1,3-benzothiadiazole (unsubstituted or alkoxy functionalized) as the electron deficient units but other electron-withdrawing groups have been incorporated maintaining the thiophene ring as donor. These are for example thieno[3,4-b]pyrazine unit (**P36, P37, P41, P42, P43**)[77], diketopyrrolo[3,4-c]pyrrole unit[56] (**P38, P39**) and pyrazino[2,3-g]quinoxaline (**P40**) [78] (Chart 2.10). All the corresponding polymers have been synthesized using Stille or Suzuki cross-coupling reactions. The optical band gaps of the polymers are reported in Table 2.8.

One of the most well-studied electron acceptor block, except 2,1,3-benzothiadiazole, is thieno[3,4-b]pyrazine unit (TP), used in order to obtain LBG conjugated polymers through the donor-acceptor strategy. The interest about TP units is due to its ability to provide more planar backbone thanks to the less steric hindrance of the thiophene if compared to the benzene ring in benzothiadiazole polymers. **P36** and **P37** polymers present an identical band gap of about 1,30 eV independent of the presence of the alkyl chains on the thiophene ring as well the length of the alkyl chain on the phenyl rings of the TP unit.

The polymers **P36-37** show a structure similar to the macromolecules **P41-43** and, comparing the optical band gap of them, it is clear that the presence of the extra bond between two phenyl rings on the TP unit shifts the absorption spectra toward NIR region, providing a lower optical band gap of around 1.2 eV.

The lower band gap is due to the more planar structure of the acceptor. Unfortunately the hopolymers obtained from thieno[3,4-b]pyrazine and the thiophene showed poor photovoltaic properties.

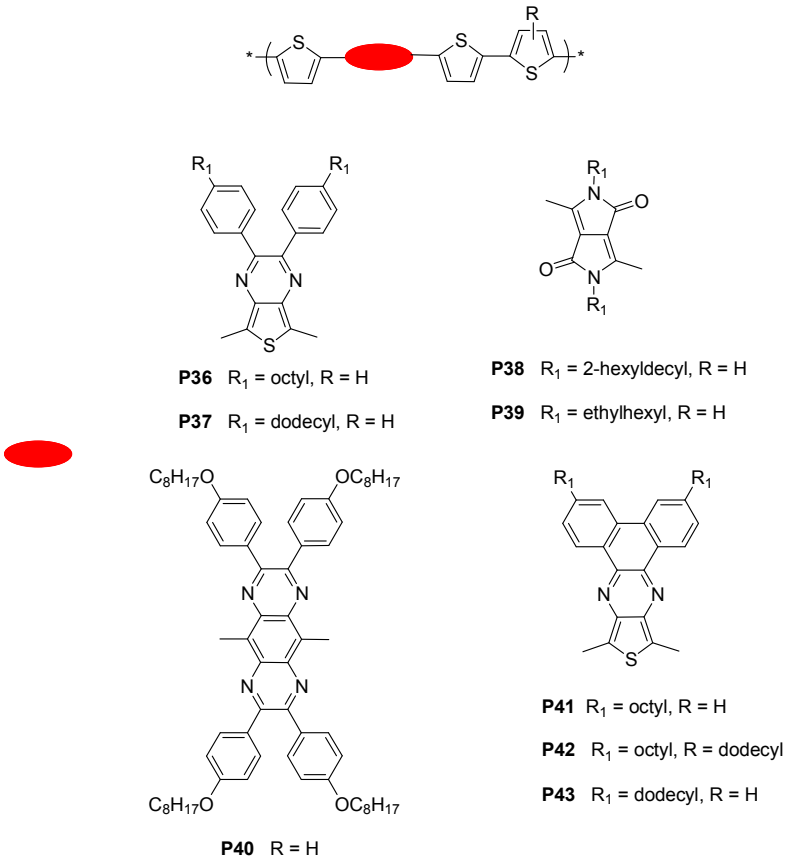

Chart 2.10: Chemical structures of different electron deficient units

Polymers	E_g^{opt} (eV)	LUMO (eV)	HOMO (eV)	PCE (%)
P36	1,30	-	-	0,22
P37	1,30	-	-	0,003
P38	1,3	3,61	5,17	4,70
P39	1,2	3,87	5,26	-
P40	1,10	3,90	5,64	2,10
P41	1,20	-	-	0,003
P42	1,20	-	-	0,014
P43	1,20	-	-	0,015

Tab. 2.8: Optical band gaps, electrochemical data and photovoltaic efficiency of P36-P43

Interesting results in terms of device efficiency was obtained from the same structure in which diketopyrrolo[3,4-c]pyrrole units (DPP) were introduced as electron acceptor group. DPP is a versatile building block due to its high electron withdrawing character. A large library of DPP based conjugated polymers and copolymers have been synthetized from many research groups using different electron donor block such as thiophene, carbazole, dibenzosilole and so on in order to tune the optoelectronic properties.[79]

As can be seen, the polymer **P38** with an unsubstituted terthiophene blocks between each pair of DPP units presents a PCE of 4.7% when blended with $PC_{71}BM$ in 1:2 (w/w) ratio. It has been shown how the molecular weight of the polymer plays a role in the final device performance: the higher the molecular weight (Mn = 54,000 g/mol), the higher the PCE. This behaviour is attributed to the fact that the lower Mn (10,000 g/mol) of **P38** presents a reduction in the photocurrent and as a consequence on the PCE (2.7% in blends with $PC_{71}BM$ in 1:2, w/w).[80]

Andersson and coworkers reported the synthesis of new D–A alternating oligothiophene polymers with pyrazino[2,3-g]quinoxaline as acceptor, substituted with octyloxy phenyl groups.

As reported in Table 2.8 the optical band gap of **P40** is 1.1 eV. Moreover, the HOMO and LUMO levels of the similar structure containing only one thiophene ring are located in suitable position matching to those of $PC_{61}BM$ but those of **P40** are close to $PC_{61}BM$, indicating that the electron transfer between **P40** and $PC_{61}BM$ is not so effective. BHJ solar cells based on **P40** with $PC_{71}BM$ in 1:3 (w/w) ratio showed PCE of 2.1% with a photoresponse extended to 1100 nm.

2.5 Conclusions

In this section it has been described how structural deviations on the backbone of conjugated polymers influence the optoelectronic properties and therefore the OPV performance.

Structural analysis of the conjugated polythiophene, based on donor-acceptor structures, reveals that the LUMO level of the polymers is mainly localized on the

acceptor unit. Thus, the proper selection of the acceptor unit can influence the LUMO level in these polymers. Also, the electron-withdrawing capability of the acceptor needs to be carefully arranged in order to avoid charge recombination and guarantees efficient electron transfer to the fullerene derivatives.

Another general conclusion is that the poly-fused aromatic rings ensure the planarity which makes them good donor materials since that usually show higher hole mobility, thereby efficient charge transport. In the polymer design, the side chain density and position should be taken into account: a good configuration, different for each polymer, minimizes the steric hindrance effect and, on the other hand, maximizes the solubility of the polymer.

The results reported before show that the structural tuning of the conjugated compound is one of the parameters that can be controlled to achieve good device performance, but other PCE improvements need the optimization of both (donor and acceptor) material properties. More detailed studies reported the role of the active layer morphology and how the device performance could be increased by suitable device architecture and processing.

[1] E. Bundgaard; F.C. Krebs, *Solar Energy Materials & Solar Cells* **2007**, 91, 954.

[2] E. Bundgaard, Low band Gap Polymers, *PhD dissertation*, June **2007**

[3] National Renewable Energy Laboratory (NREL), MS ExcelTM spreadsheet file downloaded from http://rredc.nrel.gov/solar/spectra/am1.5/

[4] G Dennler, *Materials Today* **2007**, 10, 56.

[5] V. Shrotriya; G. Li; Y. Yao; T. Moriarty; K. Emery; Y. Yang, *Adv. Mat*. **2006**, 16, 2016.

[6] J. M. Kroon; M. M. Wienk; W.J.H. Verhees; J.C. Hummelen, *Thin Solid Films* **2002**, 403, 223.

[7] M.C. Scharber; D. Mùhlbacher; M. Koppe; P. Denk; C. Waldauf; A.J. Heeger; C.J. Brabec, *Adv. Mater.* **2006**, 18, 789.

[8] L.J.A. Koster; V.D. Mihailetchi; P.W.M. Blom, *Appl. Phys. Lett*. **2006**, 88, 093511.

[9] A. Moliton; J.M. Nunzi, *Polym. Int*. **2006**, 55, 6, 583.

[10] R. Kroon; M. Lenes; J. C. Hummelen; P. W. M. Blom; A. B. De Boer, *Polymer Reviews*, **2008**, 48, 531.

[11] S.E. Shaheen; C. J. Brabec; N. S. Sariciftci; F. Padinger; T. Fromherz; J.C. Hummelen, *Appl. Phys. Lett*. **2001**, 78, 841.

[12] J.K. Lee; W.L. Ma; J.C. Brabec; J. Yuen; J.S. Moon; J. Y. Kim; K. Lee; G.C. Bazan; A.J. Heeger, *J. Am. Chem. Soc*. **2008**, 130, 3619.

[13] J. Peet, J; J.Y. Kim; N. E. Coates; W. L. Ma; D. Moses; A.J. Heeger; G. C. Bazan, *Nat. Mater*. **2007**, 6, 497.

[14] A. Cravino; P. Schilinsky; C.J. Brabec, *Adv. Func. Mat*. **2007**, 17, 3906.

[15] H. Zhou; L. Yang; W. You, *Macromolecules* **2012**, 45, 607.

[16] E.E. Havinga; W. Hoeve; H. Wynberg, *Synth. Met*. **1993**, 55, 1, 299.

[17] J.L Bre´das, *Synth. Met*. **1987**, 17, 115.

[18] B.A. Hess; L.J. Schaad; C.W. Holyoke, *Tetrahedron* **1972**, 28, 3657.

[19] M. Chen; E. Perzon; M.R. Andersson; S. Marcinkevicius; S.K.M. Jonsson; M. Fahlman; M. Berggren, *Appl. Phys. Lett.* **2004**, 84, 3570.

[20] K. Sivula; C.K. Luscombe; B.C. Tompson; J.M. Fréchet, *J. Am. Chem. Soc*. **2006**, 128, 13988.

[21] J. Roncali, *Chem. Rev.* **1997**, 97, 173.

[22] M. Chen; E. Perzon; M.R. Andersson; S. Marcinkevicius; S.K.M. Jo¨ nsson; M. Fahlman; M. Berggren, *Appl. Phys. Lett.* **2004**, 84, 3570.

[23] C. Kitamura; S. Tanaka; Y. Yamashita, *J. Chem. Soc. Chem. Commun*. **1994**, 1585.

[24] A. Ajayaghosh, *Chem. Soc. Rev*. **2003**, 32, 81.

[25] C. Kitamura; S. Tanaka; Y. Yamashita, *Chem. Mater.* **1996**, 8, 570.

[26] M. Jayakannan; P. A. Van Hal; R. A. J. Janssen, *J. Pol. Scien. A, Pol. Chem*. **2002**, 40, 251.

[27] U. Salzner, J.B. Lagowski; P.G. Pickup; R.A. Poirier, *Synth Met* **199**8, 96, 177.

[28] A. Facchetti, *Mater. Today* **2007**, *10*, 28.

[29] M. A. Green; K. Emery; Y. Hishikawa; W. Warta, *Prog. Photovolt Res. Appl*. **2011**, 19, 84.

[30] R.D. McCullough; R.D. Lowe, *J. Chem. Soc., Chem. Commun*. **1992**, 70.

[31] R.D. McCullough; R.D. Lowe; M. Jayaraman; D.L. Anderson, *J. Org. Chem*. **1993**, 58, 904.

[32] R.S. Loewe; S.M. Khersonsky; R.D. McCullough, *AdV. Mater.***1999**, 3, 250.

[33] E.E. Sheina; J. Liu; M.C. Iovu; D.W. Laird; R.D. McCullough, *Macromolecules* **2004**, 37, 3526.

[34] M.C. Iovu; E. Sheina; R.R. Gil; D.W. Laird, D; R.D. McCullough, Macromolecules **2005**, 38, 8649.

[35] A. Yokoyama; R. Miyakoshi; T. Yokozawa, *Macromolecules* **2004**, 37, 1169.

[36] R. Miyakoshi; A. Yokoyama; T. Yokozawa, *J. Am. Chem. Soc*. **2005**, 127, 17542.

[37] M.T. Dang; L. Hirsch; G. Wantz, *Advanced Materials* **2011**, 23, 31, 3597.

[38] A. Cravino ; P. Schilinsky; C. J. Brabec ; *Adv. Funct. Mater*. **2007** , 17 , 3906.

[39] R. Street; M. Chabinyc; F. Endicott , *Phys. Rev. B: Condens. Matter.* **2007** , 76, 045208.

[40] W. Ma; C.Yang; X. Gong; K. Lee; A.J. Heeger, *Adv Funct Mater.* **2005**, 15, 1617.

[41] A.J. Moule´; K. Meerholz, *AdV. Mater*. **2008**, 20, 240.

[42] A.L. Ayzner; D.D. Wanger; C.J. Tassone; S.H. Tolbert; B.J. Schwartz, *J. Phys. Chem. C* **2008**, 112, 18711.

[43] H. Kim; W. So; S. Moon , *Sol. Energy Mater. Sol. Cells* **2007** , 91 ,581.

[44] C. H. Woo; B. C. Thompson; B. J. Kim; M. F. Toney; J. M. J. Fréchet , *J. Am. Chem. Soc*. **2008** , 130 , 16324 .

[45] K. Sivula K; C.K. Luscombe; B.C. Thompson; J.M.J. Fréchet, *J. Am Chem Soc.* **2006**, 128, 13988.

[46] S. Miyanishi; K. Tajima; k. Hashimoto, *Macromolecules* **2009**, 42, 1610.

[47] G. Dennler; M.C. Scharber; C.J. Brabec, *Adv Mater.* **2009**, 21, 1323.

[48] L.M. Chen; Z. Hong; G. Li; Y. Yang, *Adv. Mater*. **2009**, 21, 1434.

[49] F. Padinger; C.J. Brabec; T. Fromherz; J.C. Hummelen; N.S. Sariciftci, *Opto-Electron Rev*. **2000**, 8, 280.

[50] C.N. Hoth; P. Schilinsky; S.A. Choulis; C.J. Brabec, *Nano Lett*. **2008**, 8, 2806.

[51] D. Vak; S.S Kim; J. Jo; S.H. Oh; S.I. Na; J. Kim; D.Y. Kim, *Appl. Phys. Lett*. **2007**,91, 081102/1.

[52] L.H. Nguyen; H. Hoppe; T. Erb; S. Gu¨nes; G. Gobsch; N.S. Sariciftci, *AdV. Funct. Mater*. **2007**, 17, 1071.

[53] D.W. Breiby; E.J. Samuelsen, *J. Pol. Sci. B: Pol. Phys*. **2003**, 41, 2375.

[54] K.E. Aasmundtveit; E.J. Samuelsen; M. Guldstein; C. Steinsland; O. Flornes; C. Fagermo; T.M. Seeberg; L.A.A. Pettersson; O. Ingana¨ s; R. Feidenhans'l; S. Ferrer, *Macromolecules* **2000**, 33, 3120.

[55] E.E.Sheina; S.M. Khersonsky; E.G.Jones; R.D.McCullough, *Chem. Mater.* **2005**, 17, 3317.

[56] M. Koppe; M. Scharber; C. Brabec; W. Duffy; M. Heeney; R.D. McCulloch, *Adv Funct Mater* **2007**,17,1371.

[57] J. Hou J; T.L. Chen; S. Zhang; L. Huo; S. Sista S; Y. Yang, *Macromolecules*, **2009**, 42, 9217.

[58] G. Wantz; F. Lefevre; M.T. Dang; D. Laliberté; P.L. Brunner; O.J. Dautel, *Sol Energy Mater Sol Cells* **2008**, 92,558.

[59] B.C. Thompson BC; B.J. Kim; D.F. Kavulak; K. Sivula; C. Mauldin; J.M.J. Fréchet, *Macromolecules* **2007**, 40, 7425.

[60] J.H. Tsai; W.Y. Lee; W.C. Chen; C.Y. Yu; G.W. Hwang; C. Ting, *Chem Mater* **2010**, 22, 3290.

[61] C.L. Chochos; S.A. Choulis, *Progress in Polymer Science* **2011**, 36, 1326.

[62] J. Hou; Z. Tan; Y. Yan; Y. He; C. Yang; Y. Li, *J. Am Chem Soc* **2006**, 128, 4911.

[63] E. Zhou; Z. Tan; L. Huo; Y. He; C.Yang; Y. Li, *J. Phys Chem B* **2006**, 110, 26062.

[64] Y.T. Chang YT,S.L. Hsu; M.H. Su; K.H.Wei, *Adv Mater* **2009**, 21, 2093.

[65] Y.T.Chang; S.L. Hsu; M.H Su; K.H. Wei, *Adv Funct Mater* **2007**,17, 3326.

[66] Y.T. Chang; S.L. Hsu; G.Y. Chen GY; M.H.Su; T.A. Singh; E.W.G. Diau; K.H. Wei, *Adv Funct Mater* **2008**, 18, 2356.

[67] H. Sirringhaus; P. J. Brown; R. H. Friend; M. M. Nielsen; K. Bechgaard; B. M.W. Langeveld-Voss; A. J. H. Spiering; R. A. J. Janssen; E. W. Meijer; P. Herwig; D. M. de Leeuw, *Nature* **1999**, 401, 685.

[68] A. Kokil; I. Shiyanovskaya; K. D. Singer; C. Weder; *J. Am. Chem. Soc*. **2002**, 124, 9978.

[69] E.J. Zhou; Z.A. Tan; C.H. Yang; Y.F. Li, *Macromol Rapid Commun* **2006**, 27, 793.

[70] E.J. Zhou; Z.A. Tan; Y. Yang; L.J. Huo; Y.P. Zou; C.H.Yang; Y.F. LI, Macromolecules **2007**, 40, 1831.

[71] E. Bundgaard; F.C. Krebs, *Macromolecules* **2006**, 39, 2823.

[72] W. Yue; Y. Zhao; H. Tian H; D. Song D; Z. Xie Z; D. Yan D; Y. Geng; F. Wang, *Macromolecules* **2009**,42,6510.

[73] F. Liang; J. Lu; J. Ding; R. Movileanu R; Y. Tao, *Macromolecules* **2009**, 42, 6107.

[74] M. Helgesen; S.A. Gevorgyan; F.C. Krebs; R.A.J. Janssen, *Chem Mater* **2009**, 21, 4669.

[75] M.M. Wienk; M.P. Struijk; R.A.J. Janssen, *Chem Phys Lett* **2006**, 422, 488.

[76] P.M. Beaujuge; J. Subbiah; K.R. Choudhury; S. Ellinger; T.D. McCarley; F. So; J.R. Reynolds, *Chem Mater* **2010**,
22, 2093.

[77] M.H. Petersen; O. Hagemann; K.T. Nielsen; M. Jorgensen; F.C. Krebs, *Sol Energy Mater Sol Cells* **2007**, 91, 996.

[78] E. Wang; L. Hou; Z. Wang; S. Hellstrom; W. Mammo; F. Zhang; O. Inganas; M.R. Andersson, *Org Lett*. **2010**, 12, 4470.

[79] Q. Sanyin; H. Tian, *Chem. Commun*., **2012**, **48**, 3039.

[80] J.C. Bijleveld; A.P. Zoombelt; S.G.J. Mathijssen; M.M. Wienk; M. Turbiez; D.M. de Leeuw DM; R.A.J. Janssen *J. Am Chem Soc* **2009**, 131, 16616.

3. A Novel Isomer of Pyrrolo-pyrrole-1,4-dione as a New Building Block for Polymer Solar Cells

3.1 Introduction

As reported Chapter 1 the need for low-cost renewable energy sources and the recent increase in power efficiency of OPV cells have motivated the design and synthesis of new donor materials for bulk heterojunction solar cells. Currently, BHJSCs achieve PCE surpassing 8.3%, but further improvements are required to make OPVs competitive with their inorganic counterparts.[1] In the Chapter 2 we describe in detail the guidelines for the design and synthesis of new polymeric materials for photovoltaic applications. This strategy is based on the incorporation of highly absorbing chromophore, in the visible and near infrared region, into π-conjugated polymer chains. Conjugated polymers based on alternate donor and acceptor moieties along the conjugated backbone have attracted great interest because, by a proper D and A units combination, their electronic properties can be finely tuned and their absorption ranges can be extended to the near infrared region.

Recently, 2,5-diketopyrrolo[3,4-*c*]pyrrole (DPP) based materials (Fig 3.1) have being attracting interest for their promising performance as a building block for polymer for photovoltaic applications.[2] The first synthesis of 3,6-diphenyl-substituted DPP (diphenyl-DPP) was reported by Farnum et al. in 1974 [3] but the yield was very low. In order to optimize the pathway, increasing the yield of the reaction, Iqbal, Cassar, and Rochat reported an elegant synthetic procedure for DPP derivatives in 1983.[4,5] It was discovered that DPP derivatives could be prepared in high yield in a single step by reacting benzonitrile (or other aromatic nitriles) with succinic acid diesters. Numerous DPP derivatives have since been synthesized and they rapidly became an important class of high-performance pigments with colours ranging from orange yellow via red to purple.[2] This chromophore shows a high

electron affinity, due to the electron-withdrawing effect of the lactam unit, and also the presence of the hydrogen, presented in diphenyl-DPP, favors the formation of a physically cross-linked structure in the solid state, which is the origin for the poor solubility. [6,7]

π-π interactions via molecular orbital overlapping and exciton coupling effects could be due to the short distance between the lactam planes (0.336 nm) and phenyl ring planes (0.354 nm),[8] while electronic interactions and strong intermolecular forces lead to a high thermal stability up to 500 °C. Afterward, because of exceptional stability as well as fluorescent properties, DPP has also been investigated for optical-electronic applications.[9,10,11]

To introduce the DPP core into conjugated polymers, the solubility of these compounds need to be increased and the chromophore requires to be functionalized with polymerizable groups. The solubility of the lactam units is increased by *N*-alkylation[12], arylation [13]or acylation[14] thus preventing hydrogen bond formation between the chromophores, while suitable polymerizable group (halogen atoms, hydroxyl, trifluoromethylsulfonate or aldehyde group) can be attached to the aryl units in the 3- and 6-positions of the central DPP chromophore,[15] or to the lactam substituent groups[16].

The general synthetic pathway to obtain the DPP unit is outlined in Scheme 3.1.

After these improvements, in a short time, DPP unit has emerged as a promising building block for the synthesis of copolymers for both thin-film transistors and solar cell devices, because it combine a low HOMO, a rigid planar core and high electron mobility.[2] Several research groups have synthesized D–A low-band gap copolymers using palladium-catalyzed polycondensation reactions such as Suzuki,[17] Stille[18] and Heck[19] coupling. More suitable polymerization reactions such as Ni-mediated Yamamoto coupling[20], Sonogashira coupling[21] or electrochemical polymerization have been reported[22].

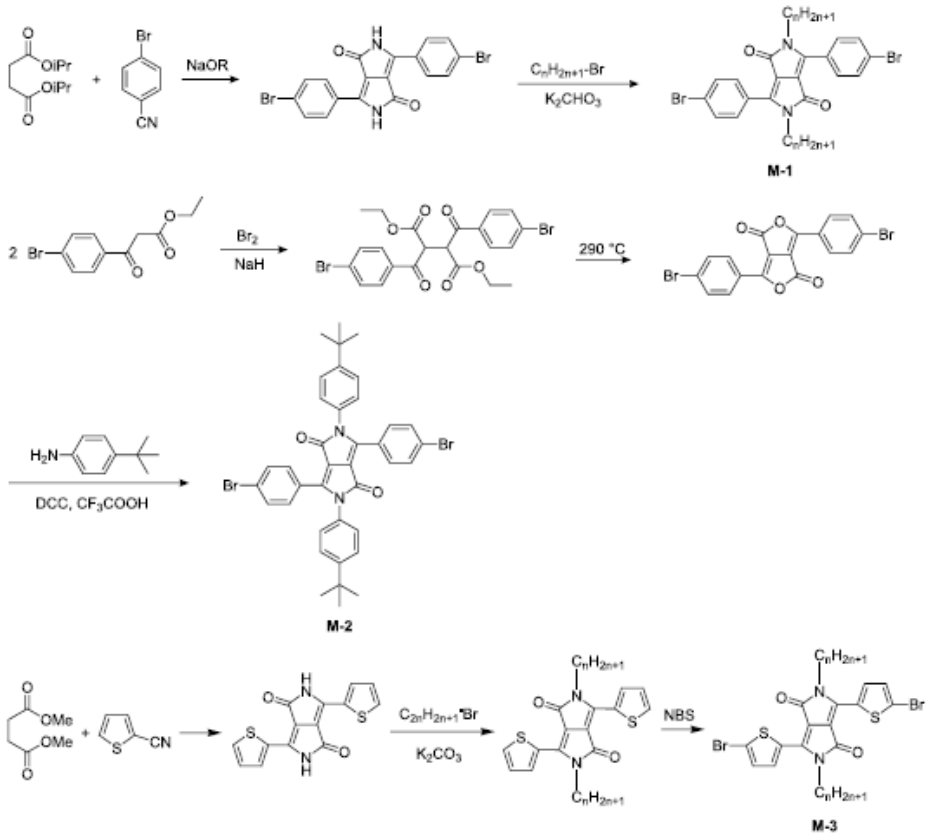

Scheme 3.1: Synthetic pathway of DPP monomer

The integration of DPP into high-performance polymer solar cells has been extensively reported, with many DPP-based polymers exhibiting PCEs higher than 4%.[23] Bijleveld et al. synthesized a polymer of terthiophene and DPP, which has a band gap of 1.30 eV and shows ambipolar transport in field-effect transistors (FET), with nearly balanced electron and hole mobilities in the 10^{-2} cm^2 V^{-1} s^{-1} range. Devices fabricated from blends of this polymer with $PC_{70}BM$ (Phenyl-C_{70}-butyric acid methyl ester) offer a PCE of 4.7%, along with a open-circuit voltage (V_{oc}) of 0.65 V, a short-circuit density current (J_{sc}) of 11.8 mA cm^{-2} and a fill factor (FF) of 60%.[24] Replacing the thiophene monomer with benzene led to a new polymer, which has a slightly larger band gap (1.53 eV) with a lower HOMO level (-5.35 eV). The optimized device resulted in a high PCE value of 5.5%, an enhanced V_{oc} of 0.80 V, a

J_{sc} of 10.3 mA cm^{-2} and an FF of 65%.[25] With coplanar thieno[3,2-*b*]thiophene units instead of thiophene as donor, the resulting polymer has an impressive FET hole mobility of 1.95 cm^2 /V s, which is the highest value for polymer-based FETs reported to date. BHJSCs comprising this polymer and $PC_{70}BM$ gave a PCE of 5.4%.[26] Janssen et al. synthesized a series alternating quaterthiophene and DPP units with a band gap of 1.4 eV, which is close to the optimum for polymer solar cells. After careful optimization of the processing conditions, the new donor polymer in combination with $PC_{60}BM$ and $PC_{70}BM$ derivatives afforded power conversion efficiencies of 3.2 and 4.0%, respectively.[27]

Despite the significant number of reports on DPP-based copolymers, there have been just few studies on the use of its isomer, diarylpyrrolo[3,2-*b*]pyrrole (Figure 3.1), as a building block for the synthesis of functional π-conjugated polymers (no references at the beginning of this projet). *N,N'*-diarylpyrrolo[3,2-*b*]pyrrole was first mentioned in the literature in the 1980s and an efficient multigram-scale synthesis was reported a few years later by Langer et al., suggesting its use as dye with tunable optical properties, high stability and low solubility.[28,29]

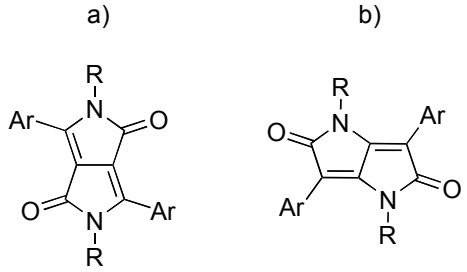

Figure 3.1: Structure of DPP dyes: (a) pyrrolo[3,4-*c*]pyrrole and (b) pyrrolo[3,2-*b*]pyrrole.

In a search for novel electron-deficient building blocks for the synthesis of conjugated donor-acceptor polymers, we have synthesized a new DPP derivative, 1,4-bis(4-butylphenyl)-3,6-di(2-thienyl)pyrrolo[3,2-*b*]pyrrole-2,5-dione. This unit was then copolymerized with thiophene and bithiophene stannanes, by palladium-catalyzed Stille coupling. The intrinsic optical and electronic properties of the resulting polymers and their performance in BHJSCs were evaluated. The choice of DPP isomer as acceptor unit is motivated by the fact that pyrrolo[3,2-*b*]pyrrole-2,5-

diones, as its positional isomer, consists of two fused lactam rings, which are planar and highly conjugated, resulting in strong π–π interactions. They can also be seen as resulting from the fusion of two maleimide units. The amide function increases the powerful electron-accepting ability of the flanking aromatic units and provides a low-lying HOMO energy level. The extended π system helps also to form highly ordered materials and facilitate charge transport.

3.2 Synthetic Route and Chemical Characterization of iso-DPP

Between the few examples reported in literature about pyrrolo[3,2-*b*]pyrrole-2,5-diones Mukai et al. in 1985 reported on the synthesis of 2,5-Dioxo-1,4-dihydropyrrolopyrrole by the one-pot oxidation of 3,6-di-*t*-butyl-2,5-dihydropyrrolo[3,2-b]pyrrole, using NBS.[30]

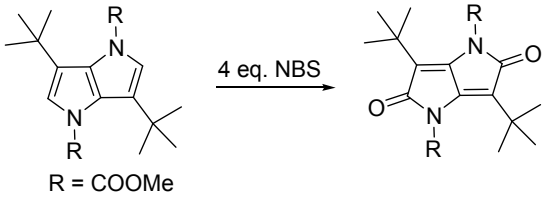

Scheme 3.2: one-pot oxidation of 2,5-dihydropyrrolo[3,2-b]pyrrole [31]

Moreover, selected pyrrolo[3,2-*b*]pyrrole-2,5-diones have been prepared in three steps starting with (*N*-phenylacetyl)acetic acid amino-ester,[29] or in one step from pulvinic acid using relatively harsh reaction conditions (autoclave reaction, 140-180 °C).[31]

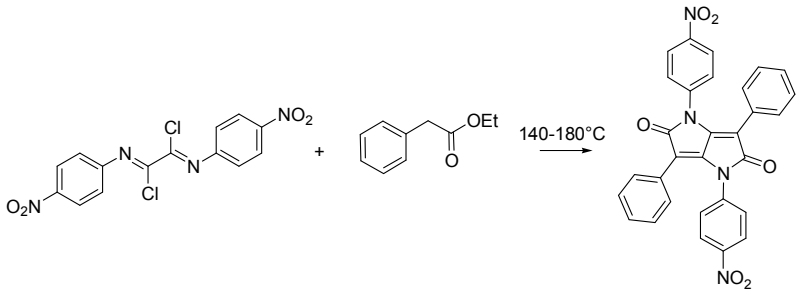

Scheme 3.3: one-pot oxidation of 2,5-dihydropyrrolo[3,2-b]pyrrole from pulvinic acid [32]

Langer et al. reported a synthetic strategy for preparing libraries of pyrrolo[3,2-*b*]pyrrole-2,5-diones, based on a new domino reaction of ester carbanions with oxalic acid-bis(imidoyl)chlorides.[32,30]

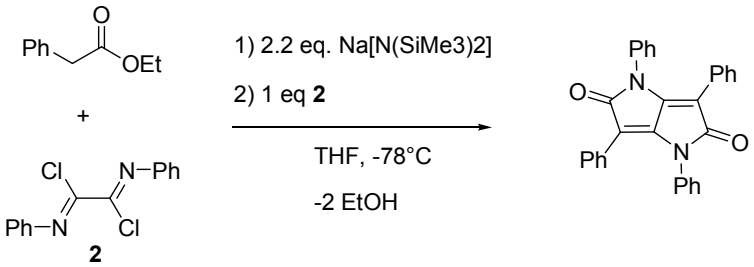

Scheme 3.4: Reaction of Ethyl Phenylacetate with Bis(imidoyl)chloride [33]

Inspired by this work, we have used this strategy for the synthesis of new thiophene-based [3,2-b]-DPP to be employed as a new electron-deficient building block for semiconducting polymers.

The synthesis of the DDP core started with symmetrical oxalic-bis(imidoyl)dichloride (**2**), which was prepared by a two-step reaction (Scheme 3.2). First oxalic-bis-amide (**1**) was prepared in excellent yield (90%) from commercially available oxalyl chloride and 4-butylaniline. The resulting *N,N′*-bis(4-butylphenyl)oxalamide (**1**) was reacted with phosphorus pentachloride giving oxalic-bis(imidoyl)dichloride (**2**) in moderate yield. The yield of this reaction depends strongly on the conditions: bis(imidoyl)dichloride is unstable in the presence of moisture, affording the starting bis-amide as the by-product of dichloride hydrolysis. The presence of an aryl group is necessary to increase its stability against hydrolysis; very poor yields were observed when alkylamine such as octylamine was used instead of 4-butylaniline, due to the prompt hydrolysis of the corresponding dialkyl-bis(imidoyl)dichloride. One molar equivalent of bis(imidoyl)chloride of oxalic acid was then reacted with two molar equivalents of ethyl 2-thiophene-acetate enolate (**3**), generated by LDA in THF at low temperature, affording the symmetrical 1,4-dioxo-3,6-dithiophen[3,2-b]pyrrole (**4**) in 60% yield. Dibromination of compound **4** with a slight excess of NBS in chloroform at room temperature provided monomer **5** in 65% yield. The resulting substituted derivatives

were fully characterized by ^{1}H NMR and high-resolution mass spectroscopy. (See Paragraph Exp. Section).

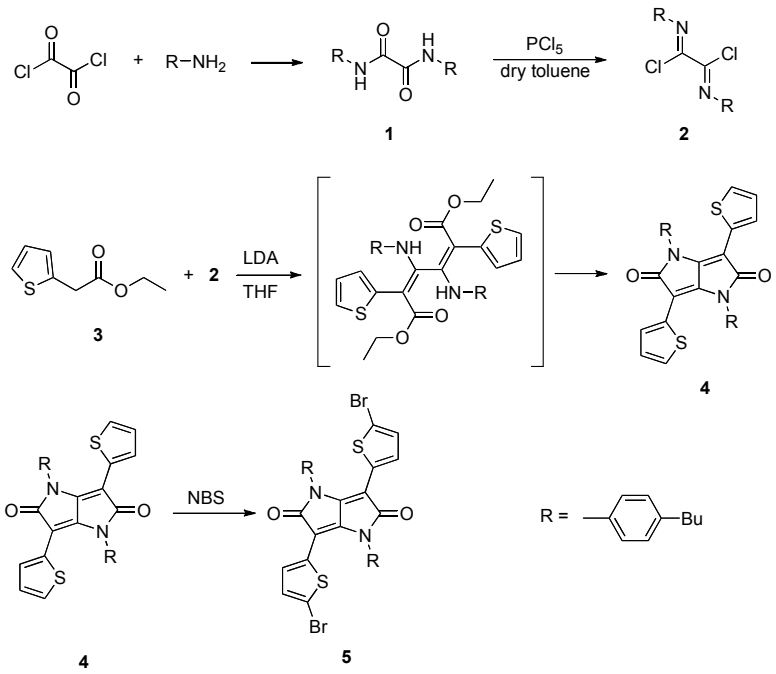

Scheme 3.2: Synthetic route to diarylpyrrolo[3,2-b]pyrrole monomer.

Two new polymers (**PDPPT** and **PDPPTT)** were synthesized by Stille coupling of monomer **5** with 2,5-bis(trimethylstannyl)thiophene and 5,5'-bis(trimethylstannyl)-2,2'-bithiophene, respectively, as shown in Scheme 3.3. The initial experiments followed the typical Stille coupling procedure, using $PdCl_2(PPh_3)_2$ as catalyst. The reaction mixture was heated overnight at 100 °C in toluene or at reflux in THF. GPC analysis showed M_w of 2.1 kg mol^{-1} and a polydispersity index (PDI) of 1.1. As it has been shown that the molecular weight of the material plays a significant role in determining the polymer optical and electrical properties,[33] it would be interesting to find a way of increasing it to approximately 20 kg mol^{-1}, which is usually the target for better performance. From the modest results in terms of molecular weight, we modified the reaction conditions, evaluating several factors, such as alternative catalysts and solvents. The use of microwave heating was also investigated. Unfortunately, only polymers with a moderate molecular weight (2.0-5.0 kg mol^{-1}),

with PDI ranging from 1.1 to 2.5 were obtained. Table 3.1 summarizes the polymerization results.

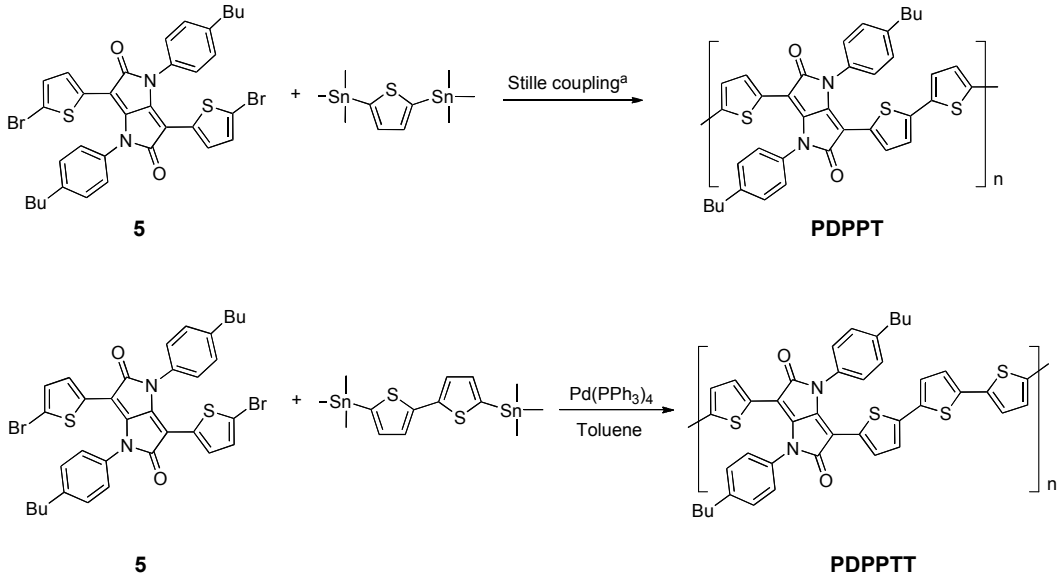

Scheme 3.3: Synthetic routes to **PDPPT** and **PDPPTT** polymers by Stille coupling. (1) $Pd(PPh_3)_4$, toluene or THF. (2) Pd_2dba_3, $P(o\text{-tolyl})_3$, dichlorobenzene, microwave heating, 150°C.

In the case of **PDPPT**, a first polymerization with $PdCl_2(PPh_3)_2$ as catalyst in toluene resulted in polymers of low molecular weight, 2.1 kg mol^{-1}, with a PDI of 1.1. Therefore, another catalytic system, $Pd(PPh_3)_4$ in toluene, was tried, and a higher molecular weight (3.8 kg mol^{-1}) was obtained, with a PDI of 2.1. To further increased molecular weights, **PDPPT** was synthesized by microwave-assisted Stille-polymerization using Pd_2dba_3 with $P(o\text{-tolyl})_3$ in dichlorobenzene. This resulted in a moderate improvement in number-averaged molecular weight M_n, (2.3 vs. 2.0 kg mol^{-1}) over that obtained from the polymerization in THF using $PdCl_2(PPh_3)_2$.

The results of these trials clearly show that the low molecular weight of the polymers is not due to a reduced reactivity, but to the low solubility of the growing polymer, causing its early precipitation during the polymerization. The lack of solubility is attributed to the low ratio of solubilizing alkyl chains relative to the aromatic units. Indeed, the repeating unit consists of two thiophene units, the DPP

core, and the butyl-benzene segment. The butyl chains were introduced to improve the solubility of resulting polymers, but, unfortunately, neither the length of this side-chain or the chain density, i.e. the number of side-chains per repeat unit, is enough to balance the chain packing and impart solubility to the resulting polymer.

Polymer samples were purified by precipitation from methanol, followed by Soxhlet extraction with methanol, diethyl ether and then hexane to remove low-molecular-weight products and catalyst. The soluble fraction of the polymers was Soxhlet extracted using chloroform, then precipitated into methanol, and filtered. The structures of the chloroform-soluble fractions were characterized by ^{1}H NMR in $CDCl_3$. The ^{1}H NMR spectrum of **PDPPT** shows broad peaks at 7.71, 7.53 and 7.21 ppm attributed to the thiophene moieties, at 7.46 and 7.05 ppm due to the phenyl group, and the triplet at 4.31 ppm is given by the benzylic methylene of the butyl chain. The NMR spectrum of **PDPPTT** shows corresponding peaks at 7.71, 7.53, 7.45 and 7.20 ppm, at 7.47 and 7.05 ppm and at 4.30 ppm.

Table 3.1: Experimental conditions and molecular weights of the polymers.

Polymer	Solvent	Catalyst	Temp. (°C)	Time (h)	M_n (g mol^{-1})	M_w (g mol^{-1})	PDI (M_w/M_n)
PDPPT	Toluene	$PdCl_2(PPh_3)_2$	100	12	1947	2066	1.01
PDPPT	Toluene	$Pd(PPh_3)_4$	100	10	1807	3791	2.01
PDPPT	THF	$Pd(PPh_3)_4$	66	10	1992	5022	2.05
PDPPT	THF	$Pd_2(Pdba)_3$ $P(o\text{-tolyl})_3$	180[b]	1	2262	4598	2.00
PDPPTT	Toluene	$Pd(PPh_3)_4$	100	10	1679	3197	1.09

a) DCB = o-dichlorobenzene. b) Microwave heating

3.2.1 Optical Properties

The optical properties of the polymers were investigated by UV-Vis absorption spectroscopy on dilute solutions in chloroform and spin-coated films on quartz plates.

Figure 3.2 shows the absorption spectra of both polymers, **PDPPT** and **PDPPTT**. Electronic absorption data including the absorption peak wavelength (λ_{max}), the absorption edge wavelength (λ_{edge}), and the optical band gap (E_g^{opt}) are collected in Table 3.2.

All the samples show a broad absorption band covering a range from 350-650 nm, and a distinct shoulder in the long-wavelength regions, which is related to the intramolecular charge transfer transition. Thin films show broad absorption spectra with two almost equally strong maxima at 500 and 620 nm. The red shift of the absorption peaks and the broadening of the absorptions from solution to film indicate strong π-stacking and aggregation in the solid state. The shape and position of the absorption bands are correlated with the average molecular weight of the polymers.

Figure 3.2: Left: UV-Vis absorption spectra of polymers in $CHCl_3$; right: spin-coated on a quartz plate from o-dichlorobenzene solution

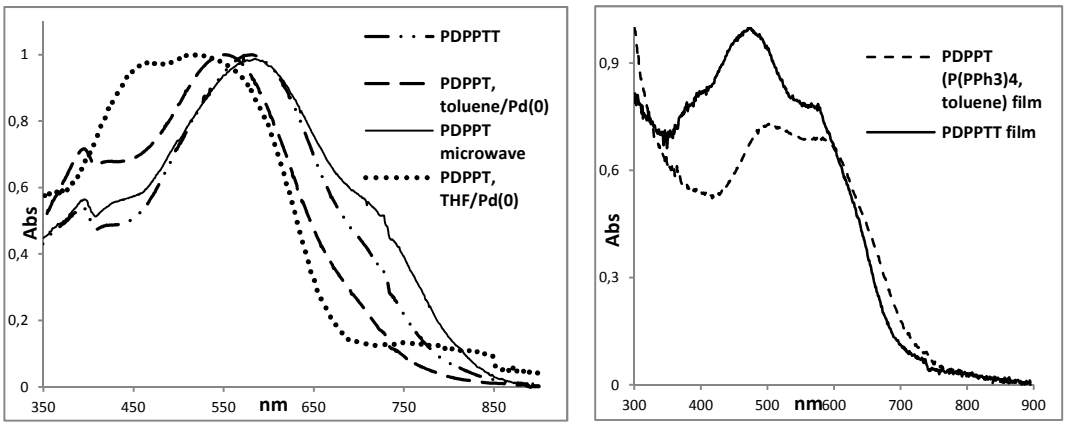

Table 3.2: Optical Properties of the Polymers **PDPPT** and **PDPPTT**

Polymer	Experimental conditions	Solution [(a)]	Film [(b)]		
		λ_{max} (nm)	λ_{max} (nm)	λ_{edge} (nm)	E_g^{opt} (eV) [(c)]
PDPPT	$Pd(PPh_3)_4$,toluene	552	500	759	1.63
PDPPT	$Pd(PPh_3)_4$,THF	529	-	-	-
PDPPT	Pd_2dba_3 P(o-tolyl)$_3$, DCB	585	-	-	-
PDPPTT	$Pd(PPh_3)_4$,toluene	584	480	725	1.71

(a) Measured in chloroform solution. (b) Casted film from DCB solution of polymers obtained by Stille coupling, using $Pd(PPh_3)_4$ in toluene. (c) Band gap calculated from the absorption edge wavelength of the optical absorption spectra.

The sample prepared using $Pd(PPh_3)_4$ and toluene as catalyst and solvent, respectively, has a relatively large band gap around 1.63 eV as thin film, with an absorption maximum in solution at 552 nm. As expected, the polymer prepared using microwave heating and DCB as solvent, shows a much longer maximum absorption wavelength with maximum at 585 nm, and the shoulder at 702 nm becomes more dominant. The optical band gap (determined from the absorption edge) is around 1.4 eV, which is 0.2 eV lower than for the polymer obtained using conventional heating.

The optical band gap values, determined from the onset of absorption of **PDPPT** and **PDPPTT** thin films are 1.63 and 1.71 eV, respectively.

3.2.2 Electrochemical Properties

Cyclic voltammetry (CV) has been employed to analyze the redox behavior and to estimate the HOMO-LUMO energy levels. Results for **PDPPT** and **PDPPTT** are

reported in Figure 3.3 and the related CV data (E_{ox}, E_{red}, HOMO and LUMO energy levels) are summarized in Table 3.3. Cyclic voltammetry was performed at room temperature and at a scan rate of 50 mV s^{-1}, under argon in chlorobenzene solution (0.5 mg mL^{-1}) with tetrabutylammonium hexafluorophosphate (n-Bu_4NPF_6) (0.1 M) as the supporting electrolyte, a glassy carbon working electrode, a platinum-wire auxiliary electrode, and Ag wire as pseudo-reference electrode. The CV curves showed reversible oxidation and reduction processes for both polymers. The **PDPPT** presents one oxidation process, with onset potential of 0.73 V and one reduction process with onset potential of -0.9 V. From the value of E_{ox}, the HOMO energy is calculated according to:

$$\text{HOMO} = -[E_{ox} - E_{1/2}(\text{ferrocene}) + 4.8]\ \text{V}$$

where E_{ox} is the onset oxidation potential measured vs. the pseudo-reference electrode. In the same way the lowest unoccupied molecular orbital (LUMO) levels were estimated from the values of E_{red} by:

$$\text{LUMO} = -[E_{red} - E_{1/2}(\text{ferrocene}) + 4.8]\ \text{V}$$

where E_{red} is the onset reduction potential measured vs. the pseudo-reference electrode. The electrochemical band gaps E_g^{ec}, calculated as $E_g^{ec} = e(E_{ox} - E_{red})$ are similar for the two copolymers (1.60 for and 1.62 eVfor PDPPT and PDPTT, respectively).

The HOMO values of **PDPPT** and **PDPPTT** were calculated to be -5.1 and -5.1 eV; their LUMO values were estimated to be -3.5 and -3.4 eV, accordingly. The addition of one thiophene ring to the polymer backbone, **PDPPTT**, does not alter significantly the positions of the HOMO and LUMO energy levels. To overcome the exciton binding energy of the polymer and to ensure efficient electron transfer from polymer to $PC_{60}BM$, the LUMO energy level of the polymer must be positioned above that of the $PC_{60}BM$ by at least 0.3 eV. It is worth comparing the energy level diagram of **PDPPT** and **PDPPTT** against $PC_{60}BM$, as shown in Figure 3.3. The LUMO levels of polymers are 0.8 eV higher than that of $PC_{60}BM$, which is well above the required energy for efficient exciton dissociation. The low HOMO levels of these polymers are essential to achieve large V_{oc} values in PV devices, since V_{oc}

is closely correlated with the energy difference between the HOMO of an electron-donor polymer and the LUMO of PCBM. It is worth mentioning that both a low HOMO level and a low band gap were obtained for the these polymers, which would therefore offer improved V_{oc} and enhanced J_{sc}, thereby leading to high efficiency BHJSCs.

Polymer	E_{ox} (V)	E_{red} (V)	HOMO (eV)	LUMO (eV)	E_g^{ec} (eV)	E_g^{opt} (eV)
PDPPT	0.73	-0.89	-5.12	-3.50	1.62	1.63
PDPPTT	0.70	-0.90	-5.09	-3.49	1.60	1.71

Table 3.3: Electrochemical Properties of PDPPT and PDPPTT.

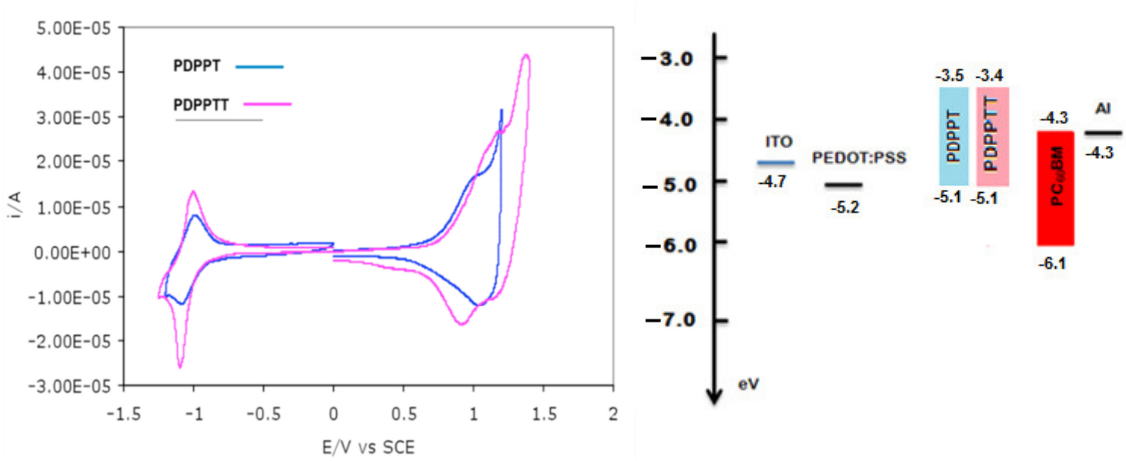

Figure 3.3: Left: cyclic voltammograms of PDPPT and PDPPTT films on glassy carbon in chlorobenzene solution containing 0.1 M Bu_4NPF_6 at scan rate of 50 mV s^{-1}. Right: Energy level diagram of the donor polymer (**PDPPT**), $PC_{60}BM$, buffer layer materials, and electrodes.

3.3 Photovoltaic solar cell characterization

To test the ability of iso-DPP based polymers to act as donor components in polymer solar cells, we fabricated bulk heterojunction solar cell devices. The device structure was ITO/PEDOT:PSS /polymer:$PC_{60}BM$/LiF/Al, where **PDPPT** and **PDPPTT** were used as electron donors and $PC_{60}BM$ was used as electron acceptor. The devices were characterized by means of a solar simulator under AM 1.5 G illumination at 100 mW cm^{-2}. The polymers investigated were those synthesized by Stille coupling using $Pd(PPh_3)_4$ in toluene. A PEDOT:PSS layer was used to facilitate hole extraction and LiF was used for electron injection. The active layers were spin-coated from DCB solutions of polymer and $PC_{60}BM$; the detailed conditions of device fabrication and characterization are described in the experimental section. To optimize the performance of the device, different polymer:$PC_{60}BM$ ratios, thicknesses and annealing temperatures were investigated. Device current density/voltage (J–V) curves are reported in the Figures 3.4-3.8 and show the characteristic trends. All parameters taken into account in order to improve the device performance are listed in Table 3.4.

To increase the PCE of the BHJ solar cells we studied first the effects of the composition of the photoactive layer. Two blends of polymer/$PC_{60}BM$ with different ratios (1:1 and 1:2, by weight) were investigated. The 1:1 ratio was found to be the better (Table 3.4). At this weight ratio, the device with **PDPPT**/$PC_{60}BM$ as active layer (140 nm) gave a V_{oc} of 0.86 V, a FF of 29%, and a J_{sc} value of 5.02 mA cm^{-2}, resulting in a PCE value of 1.24%. The same but with a thinner active layer (60 nm) showed a V_{oc} of 0.59 V, a J_{sc} of 1.98 mA cm^{-2}, and a FF of 27%, resulting in a PCE of 0.32%. With **PDPPTT** /$PC_{60}BM$ as active layer (100 nm) the device exhibited a V_{oc} of 0.57 V, a J_{sc} of 2.02 mA/cm^2, a FF of 28%, and a PCE of 0.32%.

Polymer	Annealing Temp. (°C)	Thickness (nm)	Jsc (mA/cm^2)	Voc (V)	FF	PCE (%)
PDPPT	120	120	-4.97	0.80	0.31	1.22
PDPPT	140	120	-5.02	0.86	0.29	1.24
PDPPT	160	120	-1.65	0.79	0.19	0.25
PDPPT	110	110	-4.39	0.81	0.27	0.95
PDPPT	110	120	-4.21	0.87	0.27	0.97
PDPPT	110	130	-4.22	0.88	0.26	0.96
PDPPT	140	60	-1.98	0.59	0.27	0.32
PDPPTT	140	70	-2.07	0.57	0.28	0.33
PDPPTT	140	100	-2.02	0.57	0.28	0.32
PDPPTT	120	70	-1.74	0.51	0.28	0.25
PDPPTT	160	70	-1.97	0.57	0.30	0.33

Table 3.4: Photovoltaic parameters of the BHJ devices fabricated with different annealing temperatures and active layer thicknesses.

Devices based on **PDPPT** had better photovoltaic performances than those based on **PDPPTT**. This may be attributed to a combination of factors such as absorption, molecular weight and hole mobility. A V_{oc} as high as 0.88 V was observed in devices based on **PDPPT**, which is consistent with its low HOMO level (-5.1 eV), resulting from the stronger electron-withdrawing ability of the DPP core. The modest device efficiency results from the disappointing value of FF, are largely due to poor phase segregation in the blend, as evidenced by morphological analysis.

a)

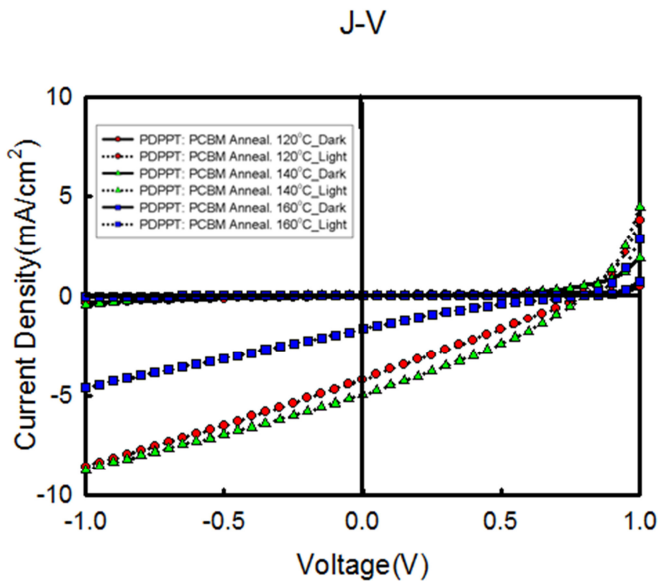

b)

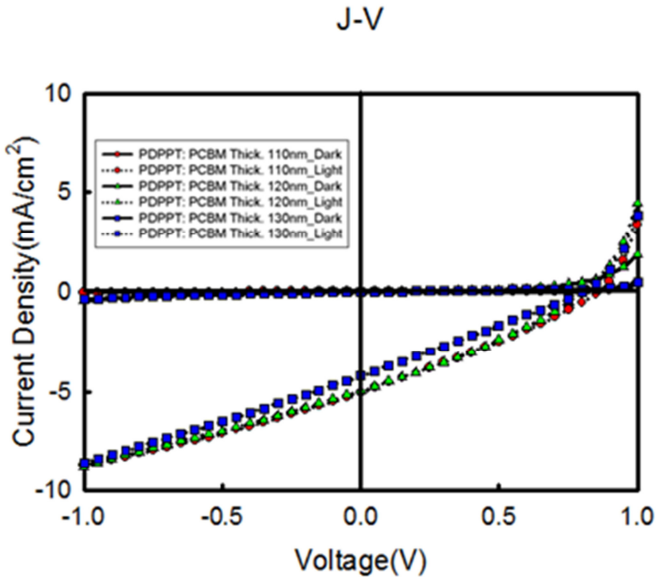

Figure 3.4: Current density-voltage characteristic of BHJSC made from **PDPPT**:$PC_{60}BM$ (1:1 weight ratio) at (a) different annealing temperature (b) different thickness, in the dark and under illumination.

a)

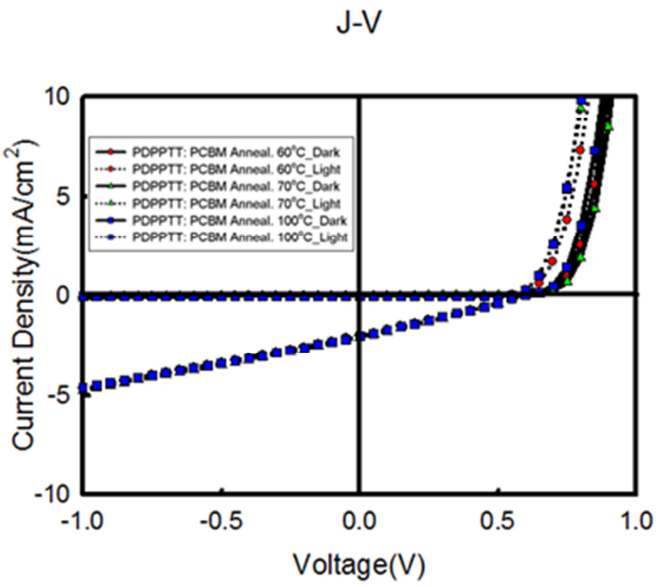

b)

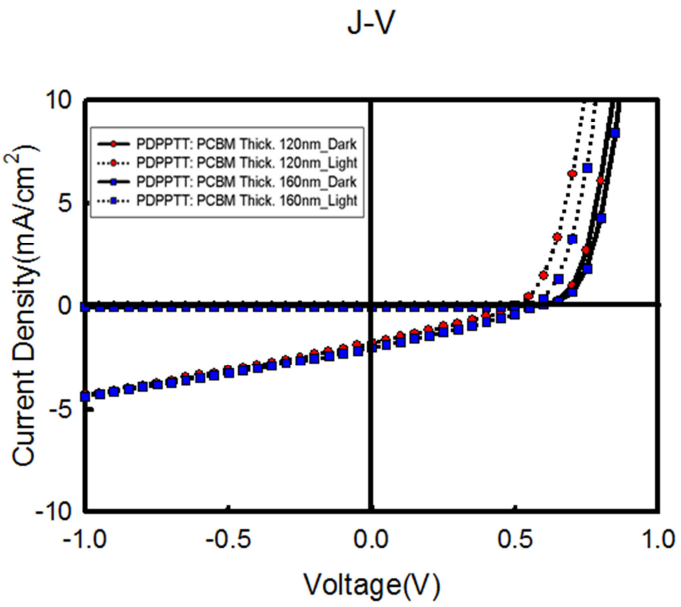

Figure 3.5: Current density-voltage characteristic of BHJSC made from **PDPPTT**:$PC_{60}BM$ (1:1 weight ratio) at (a) different annealing temperature (b) different thickness, in the dark and under illumination.

3.4 Atomic Force Microscopy characterization

Atomic Force Microscopy (AFM) analyses were carried out to investigate the morphology of the blended system. Figure 3.9 shows the surface of the PDPPT/$PC_{60}BM$ blend film on ITO/PEDOT substrate annealed at different temperatures. All films show well-defined interfaces where one can see clearly $PC_{60}BM$-rich domains embedded in the polymer matrix. The average domain size is estimated to be a few tens of nanometers, which is larger than the exciton diffusion length. For the film annealed at 100 °C, the surface is quite smooth and homogeneous, with a surface roughness of around 0.99 nm. As the annealing temperature is increased, the surface roughness increases (rms = 1.1 and 1.7 nm at 110 and 140°C, respectively) and the morphologies of the devices become less well defined with increasing aggregate size. Such coarse morphologies are known to result in poor performance.

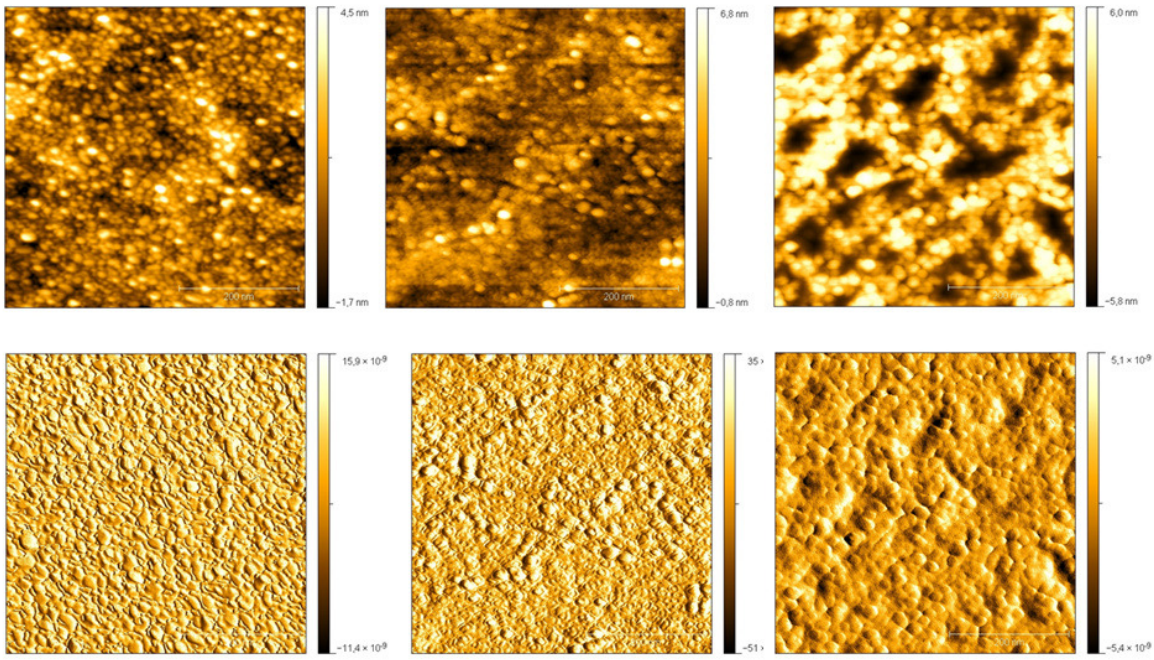

Figure 3.6: AFM height (top row) and phase (bottom row) images of **PDPPT**:$PC_{60}BM$ blends annealed at different temperatures (Left column: T = 100 °C, rms = 0.99 nm; central column: T = 120 °C, rms = 1.10 nm; right column: T = 140 °C, rms = 1.66 nm)

3.5 Conclusions

In summary, we have shown that 1,4-dibutyl-3,6-di(thiophene-2-yl)pyrrolo[3,2-*b*]pyrrole-2,5-dione can be used as a building unit in the design and synthesis of low-band gap conjugated polymers with interesting solar cell performance, as an alternative to its isomer, diketopyrrolo[3,4-*c*]pyrrole. The polymers examined, **PDPPT** and **PDPPTT**, have nearly identical optical and electronic properties. The incorporation of pyrrolo[3,2-*b*]pyrrole-2,5-dione into the conjugated backbone allows polymer with a deeper HOMO, while its electron- withdrawing nature causes a noticeable reduction of the HOMO-LUMO gap. Preliminary results on photovoltaic devices based on a **PDPPT**:$PC_{60}BM$ bulk heterojunction gave a PCE of 1.2%. These results show that **PDPPT** is a promising polymer material for use in solar cells. Further investigations on **PDPPT** and further syntheses of new low-band gap pyrrolo[3,2-b]pyrrole-2,5-dione-containing derivatives with improved solubility are currently in progress.

3.6 Experimental Section

3.6.1 Materials

All reagents and solvents were purchased from Aldrich and used without further purification. All reactions using dry solvents were carried out with oven-dried glassware and under inert atmosphere, unless otherwise stated.

3.6.2 Instruments

^{1}H NMR spectra were recorded on a Bruker (400 MHz) spectrometer; chemical shifts (δ) are given relative to TMS. HRMS analyses were performed on a JEOL GCMate II, using EI+ ionization. UV–visible absorption spectra were recorded on a JΛSCO V-570 spectrophotometer at room temperature. Molecular weights (M_n, M_w and M_p) and polydispersity indexes (M_w/M_n) were measured by the GPC Agilent

Technologies PL-GPC 220, using trichlorobenzene (TCB) as eluent at 80 °C, and polystyrene as a standard.

The cyclic voltammetry were performed in chlorobenzene solutions (0.5 mg polymer /1ml chlorobenzene) containing 0.1 M n-Bu_4NPF_6 as the supporting electrolyte at a scan rate of 50 mV s–1. A glassy carbon electrode and platinum wire were used as the working and counter electrodes, respectively. All potentials were recorded versus Ag as a pseudo-reference electrode. The ferrocenium/ferrocene redox couple in CB/ nBu_4NClO_4 occurs at a value of E_0 of +0.42V, with respect to Ag electrode.

Microwave experiments were performed in a CEM DISCOVER.

The morphologies of the polymer films were analyzed using a VEECO DICP-II atomic force microscope operated in the dynamic force mode at room temperature and an etiche Si probe operated under a resonant frequency of 131 kHz and a spring constant of 11 N m^{-1}.

3.6.3 Monomer and copolymers synthesis

Synthesis of *N,N'*-bis(4-butylphenyl)oxalamide (1)

A two-necked flask equipped with a magnetic stirring bar and a dropping funnel was charged with 4-butylaniline (3.00 g, 20 mmol) and pyridine (1.75 g, 22 mmol) in 25 mL of CH_2Cl_2. A solution of oxalyl chloride (1.20 g, 10 mmol) in 16 mL of CH_2Cl_2 was added dropwise through the addition funnel over a period of about 20 minutes at 0°C, and a resulting suspension stirred for 24 hours at room temperature. An aqueous saturated solution of $NaHCO_3$ (5 mL) was then added dropwise and the two-phase system stirred for 2 hours. The product is formed as a white solid, filtered off, washed with water and then with ethyl acetate in order to remove by-products. The solid was dried under vacuum. Yield = 90%. ^{1}H NMR (400 MHz, $CDCl_3$, 300 K): δ (ppm) = 9.29 (s, 1H, NH), 7.56 (d, 2H, -NHC$_6$*H*$_4$, ^{2}J = 10.1 Hz), 7.20 (d, 2H, -NHC$_6$*H*$_4$, ^{2}J = 10.8 Hz), 2.61 (t, 2H, ^{3}J = 10 Hz, -C*H*$_2$-Ph), 1.60 (m, 2H, -CH_2-CH_2-), 1.36 (m, 2H, -C*H*$_2$-CH_2-), 0.93 (t, 3H, ^{3}J = 10 Hz, –CH_2-CH_3).

Synthesis of oxalic-bis(imidoyl)dichloride (2)

A toluene solution (120 mL) of *N,N′*-bis(4-butylphenyl)oxalamide (**1**) (3.00 g, 8.5 mmol) and PCl_5 (3.53 g, 1.7 mmol) was refluxed for 8 hours under nitrogen. The solvent was removed under reduced pressure and the product extracted with petroleum ether; the starting material is not soluble in this solvent. The solvent was removed under reduced pressure affording the desired product as a yellow solid. Yield = 74%.

^{1}H NMR (400 MHz, $CDCl_3$, 300 K): δ (ppm) = 7.24 (d, 2H, -NHC$_6$*H*$_4$), 7.09 (d, 2H, - NHC$_6$*H*$_4$, 2J = 10.8 Hz), 2.64 (t, 2H, ^{3}J = 10 Hz, -CH_2-Ph), 1.61 (m, 2H, -CH_2-CH_2-), 1.38 (m, 2H, -CH_2-CH_2-), 0.94 (t, 3H, ^{3}J = 9.6 Hz, –CH_2-CH_3).

Synthesis of 1,4-bis(4-butylphenyl)-3,6-di(thiophen-2-yl)pyrrolo[3,2-b]pyrrole-2,5(1H,4H)-dione (4)

A dry THF solution (33 mL) of ethylthiophenacetate (**3**) (0.77 g, 4.5 mmol) was added dropwise to dry THF solution (6 mL) of LDA (3.78 mL, 2M in THF) under nitrogen atmosphere at 0 °C. The mixture was stirred for one hour at 0 °C and then cooled to -78 °C. A dry THF solution (20 mL) of oxalic-bis(imidoyl)dichloride (**2**) (0.8 g, 2.0 mmol) was then added dropwise. The mixture was allowed to warm to room temperature and stirred overnight. After 12 hours a brown suspension is formed and the solvent was removed under reduced pressure. The mixture was quenched with water, the organic phase extracted with CH_2Cl_2 (3x50 mL), dried over magnesium sulfate and the solvent evaporated. Petroleum ether (100 mL) was added to the crude product and a red solid precipitated into the brown-green solution. The solid was filtered off and washed with petroleum ether (3x20 mL). Yield = 60%.

^{1}H NMR (400 MHz, $CDCl_3$, 300 K): δ (ppm) = 7.29 (d, 1H, thiophene, ^{2}J = 1.3 Hz), 7.20 (m, 4H, -NHC$_6$*H*$_4$), 6.74 (t, 1H, thiophene, ^{3}J = 4.7 Hz), 6.40 (d, 1H, thiophene, ^{2}J = 4.7 Hz), 2.67 (t, 2H, ^{3}J = 10 Hz, -CH_2-Ph), 1.64 (m, 2H, -CH_2-CH_2-), 1.36 (m, 2H, -CH_2-CH_2-), 0.96 (t, 3H, ^{3}J = 9.6 Hz, –CH_2-C$\underline{H}_3$). HRMS-EI m/z = 564.1902 [M^+]. Calculated mass, m/z = 564.1905; error = -0.6.

Synthesis of 3,6-bis(5-bromothiophen-2-yl)-1,4-bis(4-butylphenyl)pyrrolo[3,2-b]pyrrole-2,5(1H,4H)-dione (5)

To a solution of 1,4-bis(4-butylphenyl)-3,6-di(thiophen-2-yl)pyrrolo[3,2-b]pyrrole-2,5(1H,4H)-dione (**4**) (0.20 g, 0.35 mmol) in $CHCl_3$ (50 mL), NBS (0.164 g, 0.9 mmol) was added portionwise at room temperature. After 2 hours the reaction was complete and the mixture was quenched with water, the organic phase extracted with CH_2Cl_2 (3x10 mL), dried over magnesium sulfate and the solvent evaporated. The crude product was dissolved in a large amount of ethyl ether (50 mL) in order to remove the by-product, succinimide. Yield = 98%.

^{1}H NMR (400 MHz, $CDCl_3$, 300 K): δ (ppm) = 7.19 (m, 4H, -NHC$_6$*H*$_4$), 6.68 (d, 1H, thiophene, ^{2}J = 5.0 Hz), 6.02 (d, 1H, thiophene, ^{2}J = 5.0 Hz), 2.68 (t, 2H, ^{3}J = 10 Hz, -CH_2-Ph), 1.62 (m, 2H, -CH_2-CH_2-), 1.37 (m, 2H, -CH_2-CH_2-), 0.96 (t, 3H, ^{3}J = 9.6 Hz, –CH_2-C<u>H</u>$_3$). HRMS-EI m/z = 722.0272 [M^+]. Calculated mass, m/z = 722.0272; error = 0.0.

Synthesis of PDPPT using $Pd(PPh_3)_4$ as catalyst in toluene or THF (6)

Dibrominated monomer (**5**) (120 mg, 0.165 mmol), 0.165 mmol of bis(tributylstannyl)thiophene were dissolved in 20 mL of solvent (toluene or THF). The solution was flushed with nitrogen for 10 min, and then $Pd(PPh_3)_4$ (9 mg, 5 mol%) was added. The solution was flushed again with nitrogen for 20 min. The mixture was heated at 100 °C (toluene) or refluxed (THF) overnight under nitrogen. The polymer was precipitated by pouring the toluene or THF solution into methanol (250 mL). The crude product was filtered and then Soxhlet extracted with methanol and hexane and diethyl ether to remove the oligomers and catalyst residues until the extraction solution was colorless. The chloroform-soluble fraction was then characterized.

GPC (TCB, 80 °C) for polymer synthesized in toluene: M_n = 1807 g mol^{-1}, M_w = 3791 g mol^{-1}, M_p = 3167 g mol^{-1}, PDI = 2.1.

GPC (TCB, 80 °C) for the polymer synthesized in THF: M_n = 1992 g mol^{-1}, M_w = 5022 g mol^{-1}, M_p = 4440 g mol^{-1}, PDI = 2.5. λ_{max} ($CHCl_3$) = 497 nm.

^{1}H NMR (400 MHz, $CDCl_3$, 300 K): δ (ppm) = 7.71 (m, 2H, thiophene), 7.53 (m, 2H, thiophene), 7.21 (m, 2H, thiophene), 7.46 (s, 4H, aromatic), 7.05 (s, 4H, aromatic), 4.31 (t, 4H, CH_2), 0.88 (t, 6H, CH_3), 1.25 (br, 4H CH_2), 1.54 (br, 4H CH_2).

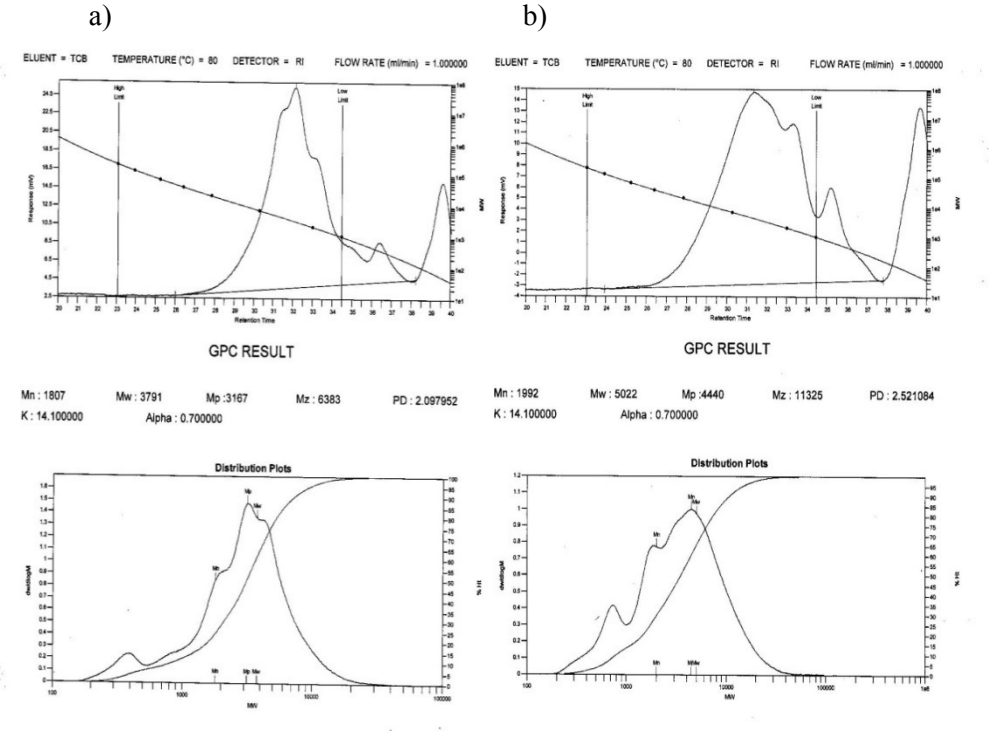

Figure 3.7: GPC report of PDPPT using $Pd(PPh_3)_4$ as catalyst in a) toluene, b) THF

Synthesis of PDPPT using Pd_2dba_3/P(o-tolyl)$_3$ as catalyst in chlorobenzene (microwave heating) (6)

A mixture of the bis(tributylstannyl)thiophene (131 mg, 0.2 mmol), dibrominated monomer (**5**) (120 mg, 0.165 mmol), Pd_2dba_3 (3.0 mg, 0.003 mmol) and P(o-tolyl)$_3$ (4.0 mg, 0.013 mmol) was placed in a 10 mL microwave vial and sealed. Dry chlorobenzene (4 mL) was injected into the vial and the mixture degassed with nitrogen for 20 min. The mixture was then heated at 120 °C for 3 min., 150 °C for 3 min. and finally at 180 °C for 1 hour under microwave heating. The reaction mixture was allowed to cool to r.t. The polymer was isolated as above.

GPC (TCB, 80 °C): M_n = 2262 g mol^{-1}, M_w = 4598 g mol^{-1}, M_p = 4344 g mol^{-1}, PDI = 2.0. λ_{max} ($CHCl_3$) = 585 nm.

^{1}H NMR (400 MHz, $CDCl_3$, 300 K): δ (ppm) = 7.71 (m, 2H, thiophene), 7.53 (m, 2H, thiophene), 7,21 (m, 2H, thiophene), 7.47 (s, 4H, aromatic), 7.05 (s, 4H, aromatic), 4.30 (t, 4H, CH_2) 0.88 (t, 6H, CH_3), 1.26 (br, 4H CH_2), 1.54 (br, 4H CH_2).

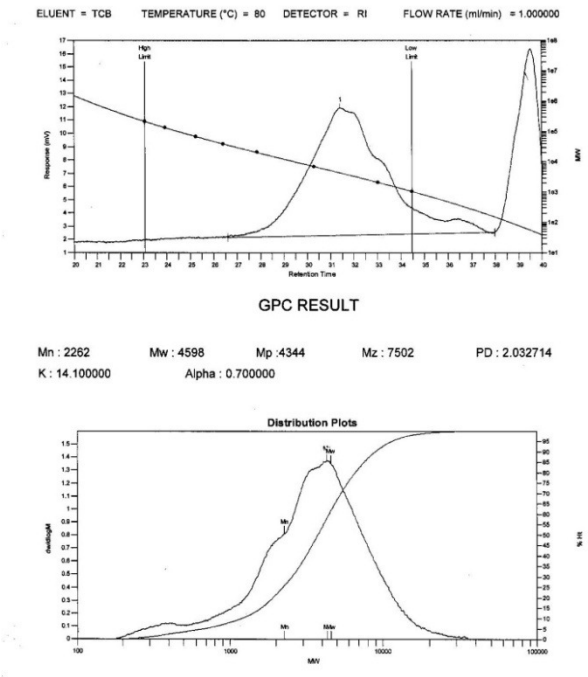

Figure 3.8: GPC report of PDPPT using Pd_2dba_3/P8o-Tolyl)$_3$ as catalyst in CB (microwave heating).

Synthesis of PDPPTT using $Pd(PPh_3)_4$ as catalyst in toluene (7)

Dibrominated monomer (**5**) (120 mg, 0.165 mmol), and 0.165 mmol of 5,5'-bis(tributylstannyl)-2,2'-bithiophene were dissolved into 20 mL of toluene. The solution was flushed with nitrogen for 10 min., and then $Pd(PPh_3)_4$ (9 mg, 5 mol%) was added into the flask. The solution was flushed again with nitrogen for 20 min. The solution was heated at 110 °C overnight under a nitrogen atmosphere. The polymer was isolated as above. GPC (TCB, 80 °C): M_n = 1679 g mol^{-1}, M_w = 3197 g mol^{-1}, M_p = 2568 g mol^{-1}, PDI = 1.9. λ_{max} ($CHCl_3$) = 509 nm.

^{1}H NMR (400 MHz, $CDCl_3$, 300 K): δ (ppm) = 7.71 (m, 2H, thiophene), 7.53 (m, 2H, thiophene), 7.45 (m, 2H, thiophene), 7,21 (m, 2H, thiophene), 7.47 (s, 4H, aromatic), 7.05 (s, 4H aromatic), 4.30 (t, 4H, CH_2), 0.88 (t, 6H, CH_3), 1.25 (br, 4H CH_2), 1.54 (br, 4H CH_2).

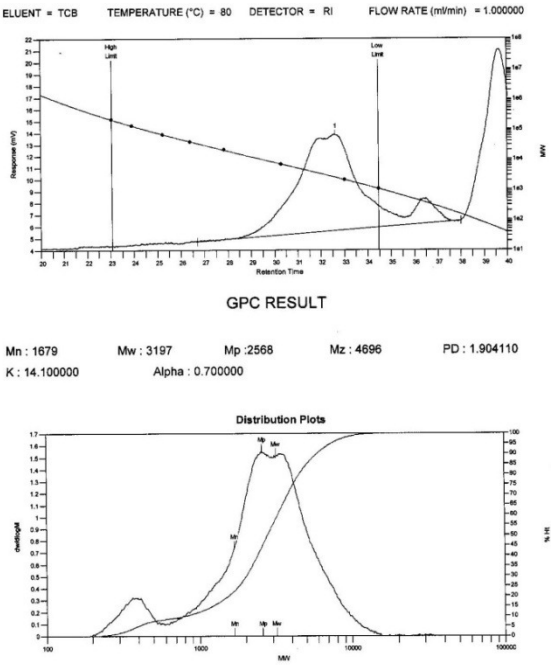

Figure 3.9: GPC report of PDPPTT using $Pd(PPh_3)_4$ as catalyst in toluene

3.6.4 Fabrication of Polymer Solar Cells

All bulk heterojunction photovoltaic cells were prepared using the same preparation procedures and device fabrication procedure as follows: glass-indium tin oxide (ITO) substrates (obtained from Xinyan Technologies, (< 20 Ω/cm^2) were first patterned by acid etching. Before processing, the patterned ITO glass was cleaned by sonication, first in a microelectronic detergent, then in deionized water for 45 min., and finally rinsed with acetone and isopropyl alcohol. After drying in a stream of nitrogen, substrates were cleaned in a UV-ozone chamber for 15 min. Poly(3,4-ethylenedioxythiophene):poly(styrenesulfonate) (PEDOT:PSS, Baytron 4083) was filtered through 0.4 μm filter before being spin coated onto ITO (thickness around 40 nm) at 3500 rpm for 30 s in nitrogen, and dried at 108 °C for 2 min. inside a glove box. Then, for the preparation of active layer, a mixture of the polymer and $PC_{60}BM$ DCB (2.2 wt.%) was spin-coated on top of the PEDOT:PSS layer at 1000 rpm for 45 s. The films were annealed at the desired temperature for 1 min. in a glove box. The solar cell devices were completed by thermal evaporation of LiF (1.2 nm) and Al (100 nm) at $<10^{-6}$ Torr. The deposition rates of LiF and Al were 0.1 and 2.5 Å/ s, respectively. The active area of the device is 0.28 cm^2. The current-voltage (I-V) measurements of the photovoltaic cells were performed on a computer-controlled Keithley 2635 source measurement unit (SMU) with a solar simulator (SolarCell Test 575 from KHS) under illumination of AM 1.5G at 100 mW cm^{-2}.

---

[1] M.A Green; K. Emery; Y. Hishikawa; W. Warta, *Prog. Photovoltaics* **2012**, *20*, 12.

[2] T. Bernd; R. A. Raman; Z. Kai; Z. Yu, *Beilstein J. Org. Chem.* **2010,** *6,* 830.

[3] D.G. Farnum; G. Metha; G.G.I Moore; F.P. Siegal, *Tetrahedron Lett.* **1974,** *29,* 2549.

[4] A. Iqbal; L. Cassar, U.S. Patent 4,415,685, Nov 15, **1983**.

[5] A.C. Rochat; L. Cassar, L; A. Iqbal, EP 94911, Nov 23, **1983**.

[6] J. Mizuguchi; G. Rihs, *Ber. Bunsen-Ges. Phys. Chem.* **1992,** 96, 597.

[7] J. Mizuguchi; A. Grubenmann; G. Wooden; G. Rihs, *Acta Crystallogr.* **1992,** B48, 696.

[8] J. Mizuguchi, *J. Phys. Chem. A* **2000,** 104, 1817.

[9] Y. Jiang; J.L. Wang; S.Y. Hua; S. Qu; H. Qian, *J. Polym. Sci., Part A: Polym. Chem.*, **2009**, 47, 4400.

[10] M. Fukuda; K. Kodama; H. Yamamoto; K. Mito; *Dyes Pigm*., **2004**, 63, 115.

[11] Z. Qiao; Y. Xu; S. Lin; J. Peng; D. Cao, Synth. Met., **2010**,160, 1544.

[12] T. Potrawa; H. Langhals, *Chem. Ber.* **1987,** *120,* 1075.

[13] H. Langhals; T. Grundel; T. Potrawa; K. Polborn, *Liebigs Ann.* **1996,** 679.

[14] J.S. Zombounis; Z. Hao; A. Iqbal, *Nature* **1997,** *388,* 131.

[15] W.K. Chan; Y. Chen; Z. Peng; L. Yu, *J. Am. Chem. Soc.* **1993,** 115,566.

[16] S.H. Eldin; A. Iqbal; Z. Hao, EP 0787730/EP0787731, Jan 22, **1997**.

[17] N. Miyaua; A. Suzuki, *Chem. Rev.* **1995,** 95, 2457.

[18] J.K. Stille, *Angew. Chem., Int. Ed. Engl.* **1986,** 24, 508.

[19] R.K. Heck, *Org. React.* **1982,** 27, 345.

[20] K. Sonogashira; Y. Tohnda; N. Hagihara, *Tetrahedron Lett.* **1975,** 50, 4467.

[21] T. Yamamoto; A. Morita; Y. Miyazaki; T. Maruyama; H. Wakayama; Z.H. Zhou; Y. Nakamura; T. Kanbara, *Macromolecules* **1992,** 25, 4, 1214.

[22] R. Danieli; R. Ostoja; M. Tiecco; C. Zamboni; C. Taliani, *J. Chem. Soc., Chem. Commun.* **1986,** 1473.

[23] S. Qu; H. Tian, *Chem. Commun*. **2012**, *48*, 3039.

[24] J.C. Bijleveld; A.P. Zoombelt; S. G. J. Mathijssen; M. M. Wienk; M. Turbiez; D.M. de Leeuw; R.A. Janssen, *J. Am. Chem. Soc.* **2009**, *131*, 16616.

[25] J.C. Bijleveld; V.S. Gevaerts; D. Di Nuzzo; M. Turbiez; S.G.J. Mathijssen; D.M. de Leeuw; M.M. Wienk; R.A. Janssen, *Adv. Mater,* **2010**, 22, E242–E246.

[26] H. Bronstein; Z. Chen; R.S. Ashraf; W. Zhang; J. Du; J.R. Durrant; P. Shakya Tuladhar; K. Song; S.E. Watkins; Y. Geerts; M.M. Wienk; R.A.J. Janssen; T. Anthopoulos; H. Sirringhaus; M. Heeney; I. McCulloch, *J. Am. Chem. Soc*. **2011**, 133, 3272.

[27] M.M. Wienk; M. Turbiez; J. Gilot; R.A.J. Janssen, *Adv. Mater*. **2008**, 20, 2556.

[28] H. Fürstenwerth, **1987**, DE 3525109 A1; Bayer AG *Chem. Abstr*. **1987**, 106, 1038150.

[29] J. Wuckelt; M. Döring; P. Langer; H. Görls; R. Beckert, *Tetrahedron Lett*. **1997**, 38, 5269.

[30] T. Mukai; A. Konno; T. Kumagai; K. Satake, *Chem. Lett.* **1985**, 14, 1809.

[31] A.C. Rochat; A. Iqbal; J. Pfenninger; L. Casser, Fur. Pat. Appl. **1984**, EP 016,309 (Chem. Abstr. 1984, 100, 87260)

[32] P. Langer; J. Wuckelt; M. Döring, *J. Org. Chem*. **2000**, 65, 729.

[33] G. Dennler; M.C. Scharber; C. Brabec, *J. Adv. Mater*. **2009**, 21, 1323.

4. Conjugated polymers based on Maleimide for photovoltaic applications

4.1 Introduction

Among the wide variety of electron deficient building blocks used in the prepartion of donor and acceptor polymers, aromatic diimide have been shown to be an excellent building block, because they combine a deep lying HOMO, a rigid planar core and high electron mobility.[1,2,3,4]

Leclerc *et al.* reported a new polymer using thieno[3,4-*c*]pyrrole-4,6-dione (TPD) as the new and interesting accepting building block.[5,6,7,8] Solar cells made of blends of TPD-based copolymers with soluble fullerene derivatives exhibited very promising performance, with a PCE up to 7.3%.[9] Jenekhe *et al*. reported on the BHJ solar cells based on the blend of the new low band gap donor-acceptor polymer, poly(N-(dodecyl)-3,6-bis(4-dodecyloxythiophen-2-yl)phthalimide) (PhBT12), and fullerene derivative ($PC_{61}BM$ or $PC_{71}BM$).[10] The performance of the solar cells varied significantly changing the composition between PhBT12 and fullerene, reaching a PCE of 2.0% with a current density of 6.43 mA/cm^2 and a fill factor of 0.55 for the 1:1 PhBT12/$PC_{71}BM$ blend devices.

a) b)

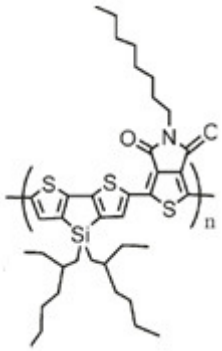

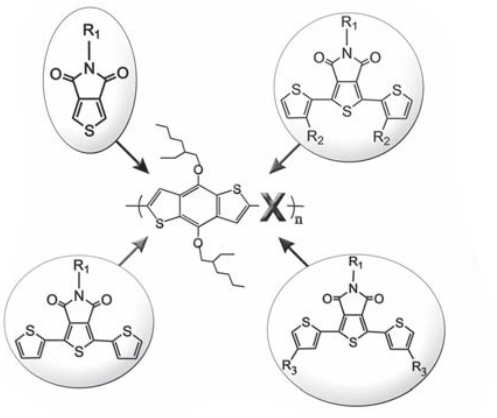

c)

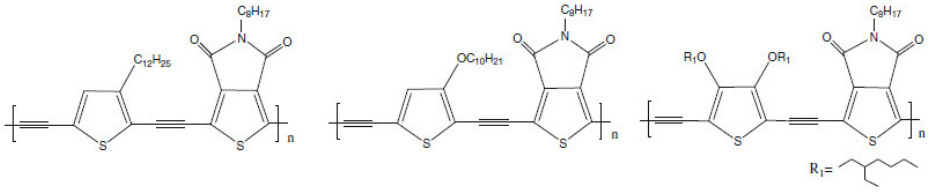

Chart 4.1: a) copolymer of dithienosiloleand thienopyrrole-4,6-dione (PDTSTPD)[9]; b) copolymers based on benzodithiophene (BDT) and thieno[3,4-c]pyrrole-4,6-dione (TPD); c) copolymers with alkylthiophene/alkoxythiophene and the thieno[3,4-c]pyrrole-4,6-dione[8].

Onimura and coworkers[11] reported on 2,3-diaryl-N-substituted maleimide such as model compounds of conjugate copolymers containing N-substituted maleimide and they studied the relationship between the fluorescence properties and structures of the conjugated copolymers.

In these regards, Chen et al. described the synthesis and characterization of a series of 3,4-diphenylmaleimide based conjugated polymers, which exhibit high fluorescence in both solution an in the solid state.[12,13] In fact, light-emitting diodes obtained from 3,4-diphenylmaleimide copolymer exhibited long wavelength electroluminescence from orange to the saturated red region, with satisfactory brightness and efficiency.

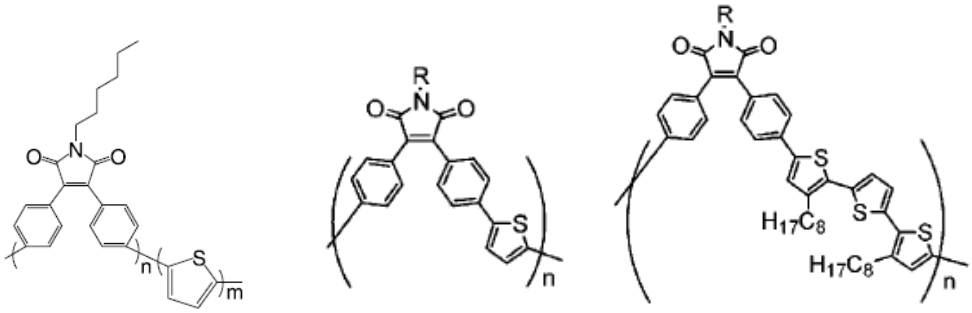

Chart 4.2: Polymers and copolymers containing 1,2-diphenylmaleimide[12,13]

Maleimide has the simplest structure within unsaturated imide family and meets the requirements of the common structural features of the aromatic diimides: extended aromatic ring flanked in both sides by carboxylic diimides, and their powerful electron accepting ability.

However, to our knowledge, there have been no reports about its simple structure. It is quite surprising that only few works have been made to study the maleimide core as building block to growth polymers for organic electronics.

During this PhD work, Lee et al. published a series of studies describing the synthesis and the photovoltaic properties of cross-linkable maleimide/thiophene copolymers [14] and others copolymers based on 3,4-diphenyl-maleimide.[15] The HOMO energy levels of the polymers presented by Chan et al.[15] were in the range of 5.63 - 5.73 eV, indicating the potential of these polymers to achieve high V_{oc}. The device was prepared using $PC_{61}BM$ or $PC_{71}BM$ as acceptor material. The best results were obtained with the device containing $PC_{71}BM$, with a V_{oc} of 0.74 V, J_{sc} of 7.4 mA cm^{-2}, a FF of 0.22 and a PCE of 1.20% under AM 1.5 G simulated solar light. While the best device obtained from $PC_{61}BM$ gave a V_{oc} of 0.80 V, J_{sc} of 4.9 mA cm^{-2}, a FF of 0.21 and a PCE of 0.82%. The poor results in terms of efficiency arise from the poor charge transport and light induced charge separation. However these preliminarily studies confirm the interest in maleimide as accepting unit.

a)

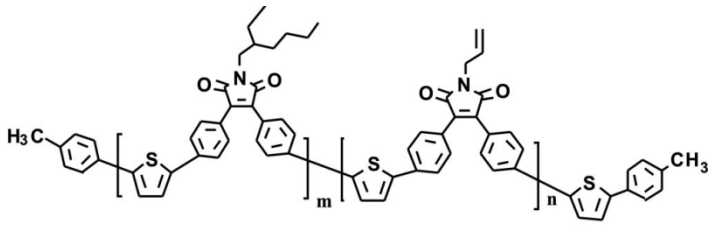

b)

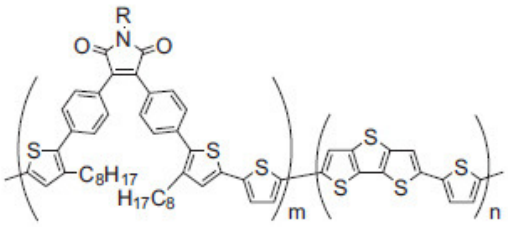

Chart 4.3: a) crosslinkable maleimide conjugated polymers[14]; b) random conjugated copolymers containing 3,4-diphenylmaleimide and thiophene derivatives[15]

This Chapter reports the synthesis of new D-A polymers containing bithienyl-maleimide and thiophene as electron acceptors and electron donor moiety, respectively. The first example on maleimide-based small molecule as third component in the P3HT/PCBM blend will be also presented.

Several studies report improvement in the PCE of BHJ devices based on P3HT:PCBM by incorporating additives via ternary mixing.[16,17,18] For example, in terms of optimizing the performance of P3HT/PCBM in the BHJ solar cells, Chu and co-workers have applied a small molecule to form a ternary cascade structure[19], resulting in about a 15% increase in PCE compared to a pristine P3HT:PCBM device. The offset of the energy levels of the donor and the acceptor normally gives rise to energy losses upon exciton dissociation and the mixing of three components can reduce the charge transfer barriers within the active layer, in this way the recombination of the excitons could be significantly reduced. For this purpose, many device architectures have been proposed.[20,21,22]Another solution is the addition of the organic component, with suitable energy level, to P3HT/PCBM mix in order to form a ternary cascade structure solar cells.

a)

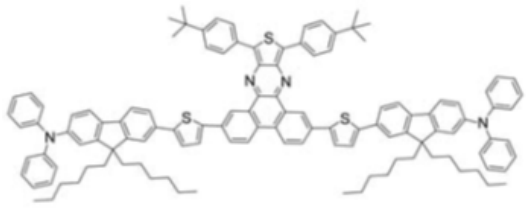

b)

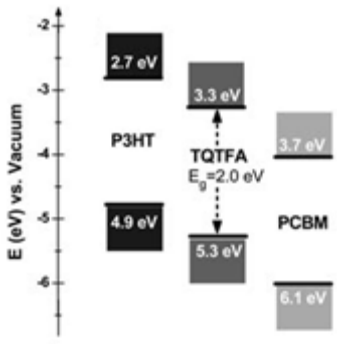

Fig 4.1: a) The chemical structure of 7,7'-{5,5'-[10,12-bis(4-tert-butylphenyl)-dibenzo[*f,h*]thieno[3,4-*b*]quinoxaline-2,7-diyl]bis(thiophene-5,2-diyl)}bis(9,9-dihexyl-N,N-diphenyl-9H-fluoren-2-amine) (TQTFA), b) Energy level diagram for P3HT, TQTFA, and PCBM.[19]

The maleimide small molecule, based on donor-acceptor architecture, exhibits levels that meet the requirement of the cascade energy levels between P3HT and PCBM. We demonstrated how the addition of this compound in P3HT:PCBM blend can show an improvement in efficiency compared to the traditional BHJ solar cells.

All conjugated D-A molecule and polymers were synthesized via Stille polycondensation and their optical, electrochemical, morphological and photovoltaic properties were investigated.

4.2 Synthetic Route and Chemical Characterization of Maleimide small molecules and polymers

Symmetrical or unsymmetrical maleimides substituted in 3 and 4 position were already presented in literature, for example diaryl-maleimides were commonly synthesized from acetonitrile derivatives but the yields of the reaction were not satisfactory in the case of thiophene as substituent group. [23,24] A modified Perking condensation was an alternative methods to prepare diaryl-maleimides or the corresponding diaryl-maleic anydrides or their precursors, involving sodium salts of arylglyoxylic acid and arylacetic acid with acetic anhydride[25], by oxidation of 2,5-dibromopyrrole in presence on HNO_3[26] or variations of these methods.[27,28,29] In order to improve the yield of the reaction it was chosen to apply the most direct

patway to obtain bis-(thien-2-yl)-maleimides, based on the direct bromination of maleic anhydride with Br_2, catalyzed by $AlCl_3$.[30]

Dibromo derivate can easily converted into the imide and the resulting compounds can be used in cross-coupling mechanism, based on Stille reaction, to get access to bis-aryl-maleimide in a better yield.[31,32,33,34,35 ,36 37]

As reported in the Scheme 2.1, 2,3-oligothiophene-N-substitued maleimide compounds (**3**, **5**, and **6**) were obtained by Stille coupling reaction starting from 2,3-dibromo-N-octylmaleimide, Pd^0 catalyzed (generated from $PdCl_2$).

In the first step maleic anhydride was treated with Br_2 in the presence of $AlCl_3$ in catalytic amount.[38] Imidization of dibromo product (**1**) with alkyl amine, in acetic acid, gave 3,4-dibromo-1-octyl-1H-pyrrole-2,5-dione (**2**) in a good yield. The intermediate **2** was reacted with 2-(tributylstannyl)thiophene, using $PdCl_2(PPh_3)_2$ as a catalyst and the resulting 2,3-dithiophene-N-octylmaleimide (**3**) was brominated with an excess of NBS, in chloroform at r.t., provided the 2,3-bis(2-bromothiophene)-N-octylmaleimide (**4**) in 90% yield. To extend the conjugation we carried out the coupling reaction of compound **4** with 2-tributylstannylthiophene and 2-tributylstannyl-3-hexyl-thiophene, affording compounds **5** and **6**, respectively.

All these new derivatives were purified by silica gel, obtaining the products in high purity. The resulting compounds were fully characterized by ^1H NMR and high-resolution mass spectroscopy.

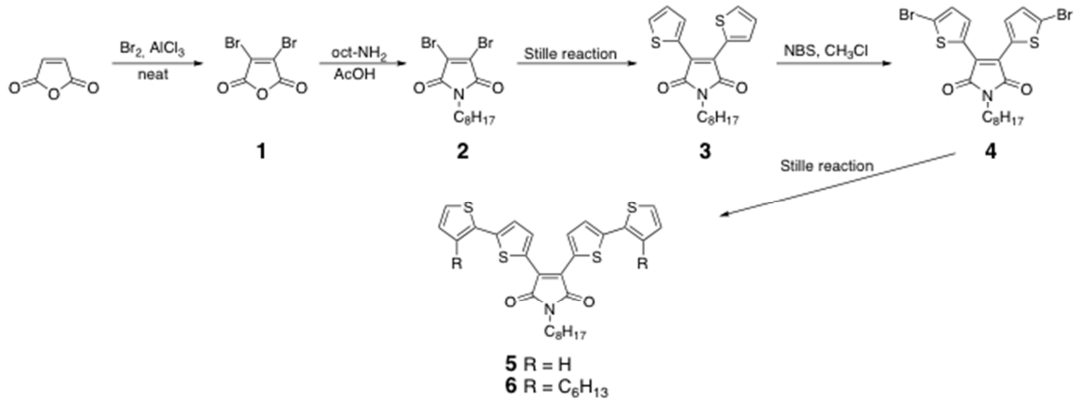

Scheme 2.1: Synthesis of the new 2,3-oligothiophene-N-substitued maleimide compounds.

In order to study the transformation of the maleimide derivatives into the new polymer **P1** and **P2**, two coupling reactions were tried with bis-stannylthiphene and bis-stannyl-bis-thiophene. Scheme 2.2 shows the synthetic pathway to obtain polymers **P1** and **P2** by Stille reaction. The monomers **4** and **2** were reacted with bis(stannyl) derivatives using DMF and Pd^{II} as solvent and catalyst, respectively. The reaction mixture was heated overnight at 90 °C in DMF.

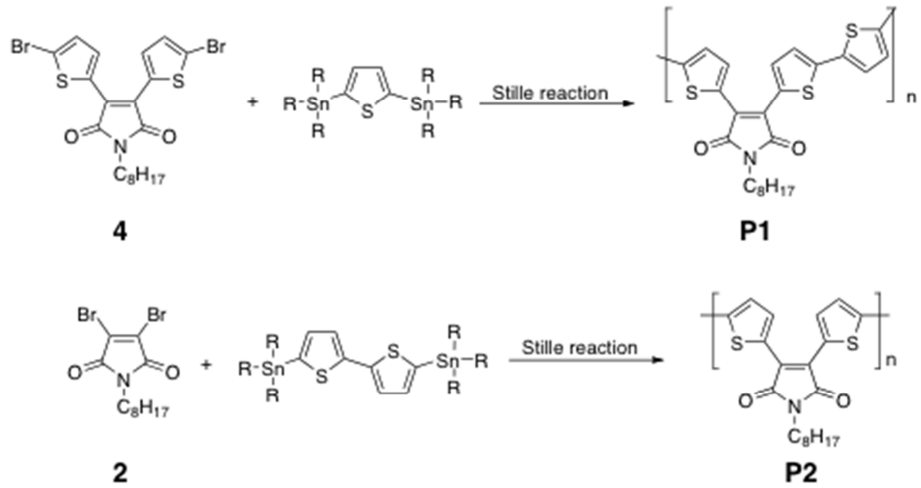

Scheme 2.2. Synthesis of copolymers based on maleimide

The products was precipitated in MeOH and purified by Soxhlet extractor using MeOH and diethylether, to remove residual catalyst and by product (low molecular weight molecules), respectively.

All polymers show good solubility in halogenated solvents, such as chloroform and DCB. GPC in THF at RT was used to determine the molecular weights: the number-average molecular weights (Mn) and the polydispersity index (PI) of the **P1** are 14397 g/mol and 1,26, respectively while for the P2 are 11650 g/mol and 1.45.

The GPC data confirm that the molecular weights of the polymers are very close to maleimide-based polymers already presented in literature obtained by Stille coupling.[15]

4.2.1 Optical Properties

The optical properties of **P1**, **P2** and their monomer **3, 5** were investigated both in chloroform solutions and thin films. The λ_{max} values for compounds **3** and **5** (422 and 520 nm) are very close to those reported in literature for (E)-1,2-bis(2-thienyl)vinylene and (E)-1,2-bis-[2,2'-bithienyl] vinylene, 422 and 435 nm respectively. This concordance suggests that introduction of the carboxylic imide onto the vinylene bridge has little influence on the electronic structure of the π-conjugated system.[39]

Figure 4.2-a shows the UV-visible spectra of **P1** and **P2** in chloroform solution while the **P2** as thin film (Fig. 4.2-b) shows broad absorption between 300 and 700 nm with a maximum red shifted by 100 nm in comparison with the polymer solution, indicating a strong intermolecular interaction in the polymer film. The optical band-gap of **P2**, calculated from the absorption edge in the UV–VIS spectrum of the thin film, is 1.85 eV.

The incorporation of the electron deficient maleimide unit in the polymer backbone, produces an intra-molecular charge transfer (ICT) between donor moiety (thiophene) and the acceptor one, resulting in electronic delocalization along the chain. In the case of **P2**, the absorption in solution is 180 nm red-shifted compared to the previously reported in literature for N-maleimide-1,4-phenylene based polymer.[12, 15] The much stronger ICT between the electon-donor thiophene unit and the electron-acceptor maleimide moiety affords a broadened and shifted absorption than previously reported in which phenyl group was employed as donor block.

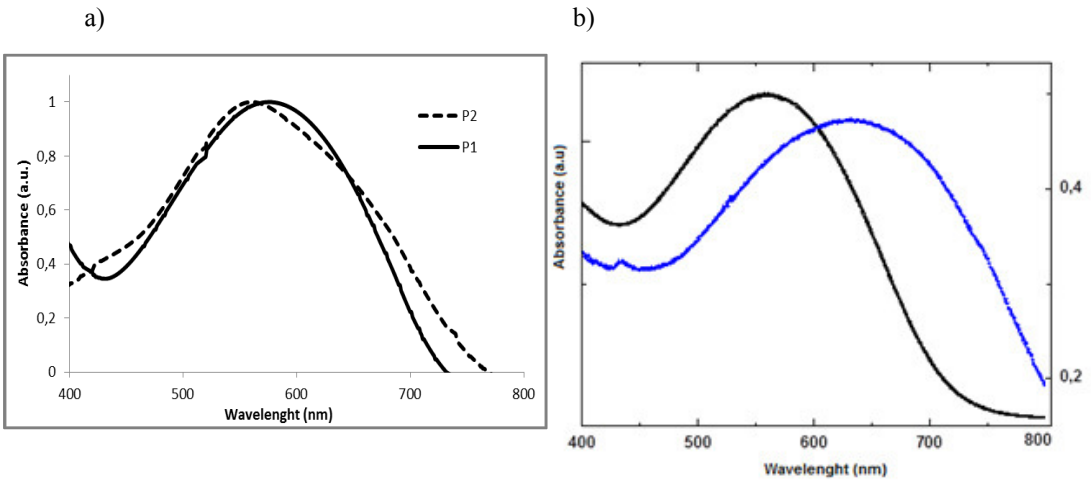

Figure 4.2: UV-visible absorption spectrum of a) **P1** and **P2** in CHCl3 solution; b) P2 as thin film (blue line) and chloroform solution (black line).

4.2.2 Electrochemical Properties

The electrochemical properties of the model compound **5** were examined by cyclic voltammetry (CV) to estimate the HOMO and LUMO energy levels. The corresponding potential profiles are reported in Figure 4.3-a (4 cycles). When the potential is scanned firstly just in the cathodic region, a reversible and stable redox process is present at potential ($E_{1/2}$) of -1.25 V vs. Fc. This process is attributed to the compound reduction in solution with the formation of the corresponding radical anion. On the contrary, when higher potential are explored in the anodic scan, an irreversible current peak is detected at 0.70 V vs. Fc which is due to the oxidation of the neutral compound to the radical cation. After the first cycle, the peak current grows cycle by cycle and a new redox process is observed at lower potential (between 0.40 and 0.65 V) which can be attribute to the p-doping/de-doping of a semiconducting polymer growing at the electrode surface. So it is evident that the fresh formed radical cations react chemically to give polymer chains attached to the electrode. To further confirm this hypothesis, we have also characterized the obtained film by cyclic voltammetry in monomer free solution. The results are

shown in Figure 4.3-b where the characteristic p- and n-doping behaviors of a conducting polymer can be observed. As expected, the p-doping/dedoping process lies at potential lower than the corresponding monomer oxidation, while the polymer n-doping takes place at almost the same potential of the monomer reduction. In any case, both the polymer redox processes are reversible and no changes in the current profiles are observed after the first cycle.

a) b)

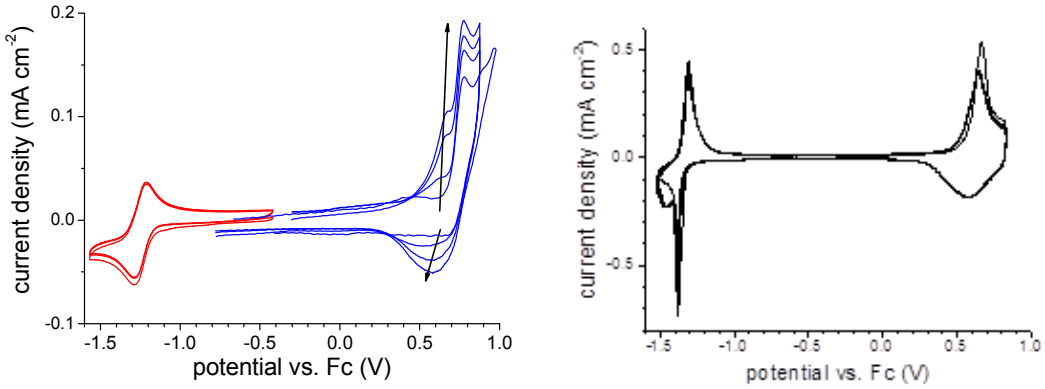

Figure 4.3: a) cyclic voltammetry curves of model compound **5** in solution and b) cyclic voltammetry curves of poly-**5** in monomer free solution.

The HOMO and LUMO energy levels of the compound **5** can be estimated from the current onset of the irreversible oxidation process at the first cycle and the $E_{1/2}$ value of the reversible reduction process, respectively. Potential values vs. Fc are converted to vacuum scale energies under the assumption that the Fc/Fc^{+} redox couple is 5.23 eV relative to a vacuum (using a potential value of 4.6±0.2 eV for NHE vs. vacuum.[40] The same procedure can also use to calculate the polymer energy levels.

The HOMO and LUMO levels determined for model compound **5** are -5.9 and -4.0 eV, respectively, therefore the energy levels are positioned between those of P3HT and PCBM, as reporte in Figure 4.4. These values indicate the utilization of the

small molecule as additive, in order to obtain a cascade energy levels and improved absorption photons.

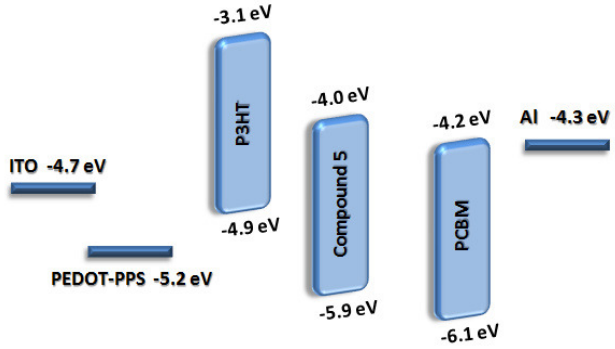

Figure 4.4: Energy level diagrams for P3HT, **5** and PCBM

The corresponding values for the polymer are -5.8 and -3.9 eV, respectively. The reduction potentials of the model compound is quite close to that of $PC_{61}BM$, with an offset of 0.2 eV (the $PC_{61}BM$ LUMO level was determined as -4.2 eV in our lab. under the same experimental conditions), while the corresponding values for polymers are -5.64 and -3.9 eV, respectively.

4.3 Photovoltaic solar cell and Atomic Force Microscopy characterization

Organic solar cell device based on blends of $PC_{61}BM$ as acceptor and oligomers and polymers, as electron donor materials, were fabricated with the common structure of ITO / PEDOT:PSS / polymer:$PC_{61}BM$ / LiF / Al.

Solar cell devices were characterized under AM1.5G illumination at 100 mW/cm^2 with a solar simulator. In order to optimize the performance of the device different ratio between DONOR and ACCEPTOR were investigated.

Small molecule containing the maleimide core was employed in **5**:$PC_{61}BM$ blend system but any photovoltaic behavior was observed, because of the lack of the offset of the LUMO levels between **5** and $PC_{61}BM$. The offset is 0.2 eV, which is slightly

lower than the minimum value required for efficient charge separation at the interface of the donor and acceptor; while in the case of the polymers the value of the LUMO levels are high enough to allow the excitons dissociation. Indeed when polymers were blended with $PC_{61}BM$ and used as active layer, a photovoltaic effect is observed. The device exhibited a short-circuit current of 0.11mA/cm^2, an open-circuit voltage of 0.62 V, a fill factor of 0.22, with a resulting PCE of 0.02%. The poor photovoltaic performances are in accordance with the examples reported previously in literature for maleimide based polymers.

The low J_{sc} could be attributed to the low LUMO offset between donor and acceptor, but also to the large-scale phase separation, which causes inefficient exciton dissociation.

The morphology of the films was investigated by IC-AFM. Figure 4.4 shows the topography and the phase IC-AFM images for the **P2**:$PC_{61}BM$ film, obtained with blend ratios from 1:1.

One can easy see from the IC-AFM phase contrast image that the blend exhibits poor segregation and circular aggregates are observed. The contrast in the IC-AFM phase images come from to the differences in the materials interaction with the AFM tip.[41] The bright contrast, corresponding to **P2** rich clusters, emerges at the sample surface; the average aggregate reaches a width of a few hundred nanometers, for 10 to 20 nm height.

The size of the domains is larger than the exciton diffusion length and their presence can be the origin of the poor results obtained with this materials. The presence of these aggregates can be explained to the limited solubility of **P2** in the solvent used to prepare the active blend solution. These suggest the presence of **P2** clusters of average sizes smaller than filter pore used for filtering the polymer solution before the spin coating of the film. Attempts have been made to optimize these devices, but performances were still poor.

Interesting results in terms of optimizing the device performance were obtained instead by sensitizing the P3HT:$PC_{61}BM$ bulk heterojunction with oligomers or polymers (**P2** and **5**) as a third component.

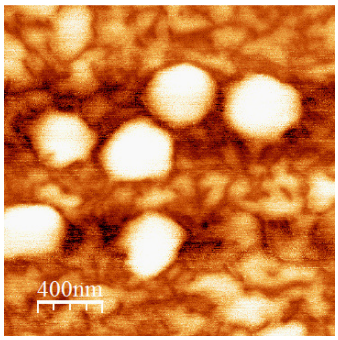

Figure 4.4: IC-AFM (a) topography and (b) phase images of ITO/PEDOT:PSS/**P2**:$PC_{61}BM$.

For the third semiconductor, as the additive, three criteria must be respected: (i) its energy levels must have the proper offset with respect to P3HT and PCBM, the blend counterpats, (ii) it should be able to operate as either an electron acceptor and trasporter as well electron donor and trasporter, (iii) it should have an high absorption coefficient in the range complementary to the other components of the BHJ blend.

Fig. 4.5 shows the J–V characteristics of the P3HT:**P2**:$PC_{61}BM$ ternary blend solar cells and the corresponding P3HT:$PC_{61}BM$ binary blend control device. The ternary blend solar cells exhibited a substantially improved performance compared to the binary blend control device. Hence, devices fabricated using P3HT:**P2**:$PC_{61}BM$ (0,8:0,2.:1) showed considerably enhanced performance (Figure 4.5, red line) with a PCE of 3.14% compared to the P3HT:$PC_{61}BM$ control device. The addition of **P2** improved the PCE from 1.73 to 3.14%, a 80% rise. The better performance from the P3HT: $PC_{61}BM$ to the P3HT:**P2**:$PC_{61}BM$ systems are due to the increase of J_{sc} (from 2.3 to 9.9 mA cm^{-2}) and the fill factor (FF, from 0.41 to 0.51).

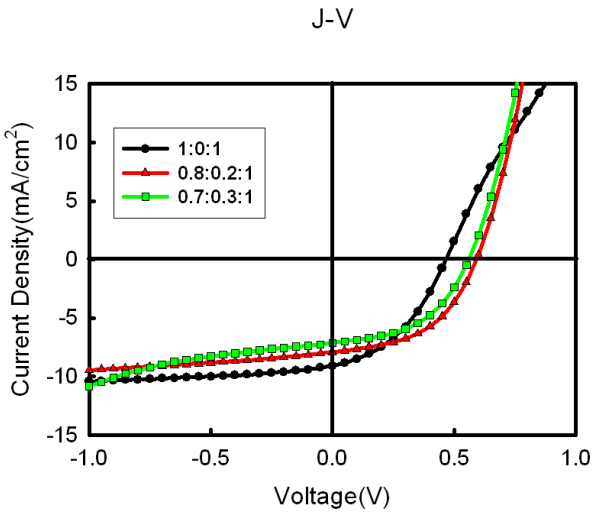

Figure 4.5: I-V characteristic of ITO/PEDOT:PSS/P3HT:**P2**:$PC_{61}BM$/LiF/Al with increasing amount of P2

In a second set of experiments, the third component employed in the ternary blend was compound **5**. Figure 4.6 displays J–V curves for devices incorporating different blend ratio of the three components compared to P3HT:PCBM (1:1 w/w) as a reference, under simulated AM 1.5 G irradiation (100mW/cm^2). The related parameters are summarized in Table 4.1.

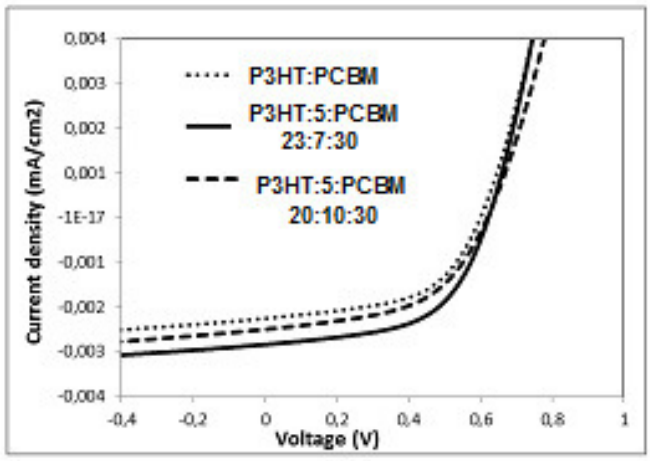

Fig 4.6: J-V characteristic of P3HT:**5**:PCBM films with different ratio of TTRMITT. The device has a configuration of the ternary blend BHJ solar cell.

The active layers were spin-coated from *o*-DCB solutions of PH3T, **5** and PCBM and the detailed conditions of the device fabrication and characterization are described in the Chapter 4.5.5. Two blends with different composition, P3HT:**5**:$PC_{61}BM$ 23:7:30 and 20:10:30 (% weight), were investigated, with a final thickness device of 120 nm.

The blend P3HT:PCBM was used as standard reference and shows a short current density (Jsc) of 2.60 mA/cm^2, an open circuit voltage (Voc) of 0.60 V, filling factor (FF) of 0.44 leading to PCE of 2.60%. The best performance is observed in the P3HT:**5**:$PC_{61}BM$ (23:7:30, w/w) blend, which shows an improved Voc of 0.62 V and Jsc of 10.11 mA/cm^2, whereas the FF of 0.48 is similar to those of that obtained for the device lacking additive. The corresponding PCE is 35% higher relative to that of the pristine P3HT:PCBM.

For concentrations of **5** greater than 10 wt% the device exhibited relatively lower current density. The lowered Jsc values can be explained by the decreased order within the P3HT domains. The crystallinity of P3HT could be destroyed if the amount of additive is too much, that means unfavorable morphology of the active layer and charge transport lowered.

Blend Composition	Jsc (mAcm^{-2})	Voc (V)	FF	PCE (%)
P3HT : $PC_{61}BM$ 30 : 30 (w/w)	8.03	0.60	0.44	2.60
P3HT : **5** : $PC_{61}BM$ 23 : 7 : 30 (w/w)	10.11	0.62	0.48	3.51
P3HT : **5**: $PC_{61}BM$ 20 : 10 : 30 (w/w)	8.90	0.61	0.48	2.86

Table 4.1: Photovoltaic performance of P3HT: $PC_{61}BM$ (1:1 w/w) device doped with different concentrations of **5**.

IC-AFM images (topography and phase) of the blends were recorded and compared in order to study the photovoltaic behavior and the blend morphology. Figures 4.6

a/c show topographic IC-AFM images that give an idea about the domain sizes and the roughness values announced. The topographic image, the phase IC-AFM (Fig. 4.6-b/d) is an effective tool to investigate phase separation and dispersion between donor and acceptor.

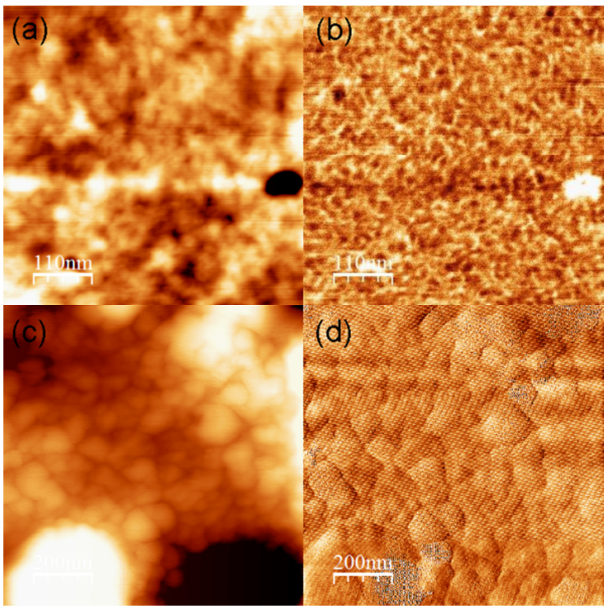

Figure 4.6: (a) IC-AFM topographic image and (b) phase image of the top surface of the P3HT:$PC_{61}BM$:**5**/ 23:30:7 (wt 3%) film. (c) IC-AFM topographic image and (d) phase image of the top surface of the P3HT:$PC_{61}BM$:**5**/ 23:30:10 (wt 17%) film.

In the case of P3HT:**5**:$PC_{61}BM$/23:7:30 ratio, a clear phase contrast is observed, the IC-AFM phase image of the film (Fig. 4.6-b) shows interpenetrating polymer networks. The average diameter of the nanocrystalline domains is less than 10 nm. The sizes of the domains, in this case match with the typical exciton diffusion length in a conjugated polymer (approximately 10 nm). Hence, the electron donor and acceptor materials forms nanoscale interpenetrating networks obtaining an efficient charge separation and transport throughout the whole active layer. As a result, the better solar cell performances were obtained from this 23:30:7/P3HT: $PC_{61}BM$:**5** film.

$PC_{61}BM$ molecules, at this concentration, are more uniformly dispersed than those prepared in the 30:30 and 20:10:30 composition. For the 20:30:10 P3HT: $PC_{61}BM$:**5** film, separated structure appeared effectively in the phase image (Fig. 4.6-d), with domain size of about 100 nm to 200 nm. The spots with bright contrast in the topographic images represent the P3HT-rich phase. In contrast, flat surface without any distinct structure was observed in the AFM images of the 30:30:0/P3HT: $PC_{61}BM$ sample (not shown). No obvious phase separation exists at the surface of the blend film.

4.4 Conclusion

A series of molecules and polymers based on maleimide, as electron poor moiety into the donor-acceptor structure, has been synthetized by simple and efficient route.
The optical properties of the polymer show a stronger internal charge transfer between the thiophene (donor) and the (maleimide) acceptor blocks, which leads larger and broadened absorptions than previously reported for maleimide based polymers. The poor photovoltaic properties are due to the limited solubility of the polymer, that produces domains in the active layer to much larger than the typical exciton diffusion length, as confirmed by AFM investigation.
The polymer could be employed as sensitizer in a mixture of three components with P3HT and PCBM.
The addition of P2, as third component improved the PCE from 1.73 to 3.14%, a 80% rise. The same improvement has been obtained if a small molecule containing the maleimide core was added to the standard blend. The good match of the electronic levels between the three components together the suitable morphology of the film produce an PCE of 35% greater than the reference cell without additive.

4.5 Experimental Section

4.5.1 Materials

All reagents and solvents were purchased from Aldrich and used without further purification. All reactions using dry solvents were carried out with oven-dried glassware and under inert atmosphere, unless otherwise stated.

4.5.2 Instruments

^{1}H NMR spectra were recorded on a Bruker (400 MHz) spectrometer; chemical shifts (δ) are given relative to TMS. HRMS analyses were performed on a JEOL GCMate II, using EI+ ionization. UV–visible absorption spectra were recorded on a JΛSCO V-570 spectrophotometer at room temperature. Molecular weights (M_n, M_w and M_p) and polydispersity indexes (M_w/M_n) were measured by the GPC Agilent Technologies PL-GPC 220, using tetrahydrofuran (THF) as eluent at RT, and polystyrene as a standard.

The morphologies of the polymer films were analyzed using a VEECO DICP-II atomic force microscope operated in the dynamic force mode at room temperature and an etiche Si probe operated under a resonant frequency of 131 kHz and a spring constant of 11 N m^{-1}.

Cyclic Voltammetries (CV) were performed at a scan rate of 50 mV/s with a PARSTA2273 EG&G potentiostat in a three-electrode electrochemical cell.

AFM measurements were performed using Nanotec Electronica microscope, operating in tapping mode or contact intermittent (IC-AFM). Scans were performed on areas close to the aluminum electrode. Both topographic and phase images are presented.

4.5.3 Monomer and copolymers synthesis

Synthesis of 2,3-dibromo-maleic anhydride (1)

The reaction was carried out under solvent free conditions. In a round-bottomed flask, equipped with a magnetic stirring bar and a nitrogen inlet, were added maleic anhydride (10.0 g, 102 mmol) and aluminum trichloride (1.0 g, 7.5 mmol). The mix was melted and then cooled at r.t., then 2 eq. of Br_2 (32.55 g, 203 mmol) were added in one portion and the reaction was stirred at 150°C overnight. After cooling to r.t., the solid was dissolved with ethyl acetate and the insoluble residue was filtered off. The solvent was removed under vacuum affording the desired product as white solid. Yield = 52%. M.p. and mass spectra were identical with those reported in literature.

Synthesis of 2,3-dibromo-N-octylmaleimide (2)

In a round-bottomed flask, equipped with a magnetic stirring bar and a nitrogen inlet, 1 equivalent of 2,3-dibromo-maleic anhydride (**1**, 5.0 g, 19.5 mmol) was dissolved in 25 mL of acetic acid. 1.5 eq.s of octylamine (3.78g, 29.25 mmol) were added to the solution, which was refluxed for 12 hours under nitrogen atmosphere. After cooling at r.t., the mixture was added to saturated solution of $NaHCO_3$ (100 mL) and then extracted with ethyl acetate (100 mL x 3). After drying over anhydrous magnesium sulfate, the filtrate concentrated in vacuo. The residue was purified by rapid filtration on a silica bed, using CH_2Cl_2, to afford the desired product as red solid. Yield = 43%

^{1}H NMR (500 MHz, $CDCl_3$, 300 K): δ (ppm) = 3.58 (t, 2H, N-*CH_2*, ^{1}J = 7.5 Hz, ^{2}J = 15 Hz), 1.58 (m, 2H, N-CH_2-*CH_2*-), 1.30-1.24 (m, 10H, -CH_2-), 0.86 (t, 3H, CH_3, ^{1}J = 7.0 Hz, ^{2}J = 15.0 Hz).

MS: m/z: 364 [M+].

Synthesis of 2,3-dithiophen-N-octylmaleimide (3)

To a solution of 2,3-dibromo-N-octylmaleimide (**2**, 2.0 g, 5.4 mmol) and 2-(tributylstannyl)thiophene (4.06 g, 10.8 mmol) in 40 mL of DMF, $Pd(PPh_3)_2Cl_2$ (76

mg, 0.108 mmol, 2%) was added. The mixture was refluxed for 12 hours at 100°C under nitrogen atmosphere. After cooling at r.t., the mixture was added to water and extracted with toluene (50 mL x 3). After drying over anhydrous magnesium sulfate, the filtrate concentrated in vacuo. The crude product was purified by flash column chromatography (SiO_2, petroleum ether: ethyl acetate 9:1) to afford the desired product as red oil. Yield = 91%

^{1}H NMR (500 MHz, $CDCl_3$, 300 K): δ (ppm) = 3.62 (t, 2H, N-*CH_2*, ^{1}J = 7.0 Hz, ^{2}J = 14.5 Hz), 1.65 (m, 2H, N-CH_2-*CH_2*-), 1.35 (m, 10H, -CH_2-), 0.87 (t, 3H, CH_3, ^{1}J = 6.5 Hz, ^{2}J = 14.0 Hz), 7.58 (dd 2H, CH thiophene, ^{1}J = 1 Hz, ^{2}J = 5 Hz), 7.13 (t, 2H, CH thiophene, ^{1}J = 4.5 Hz, ^{2}J = 9 Hz), 7.82 (dd, 2H, CH thiophene, ^{1}J = 1.5 Hz, ^{2}J = 4 Hz).

MS: m/z: 373 [M+].

Synthesis of 2,3-bis(2-bromothiophen)-N-octylmaleimide (4)

In a round-bottomed flask, equipped with a magnetic stirring bar and a nitrogen inlet, 1 equivalent of 2,3-dithiophen-N-octylmaleimide (**3**, 1.5 g, 4.02 mmol) was dissolved in 30 mL of chloroform. 2.2 eq. of NBS (1.5 g, 8.84 mmol) were added portionwise to this solution, which was kept under stirring at r.t. overnight. The mixture was added to water (100 mL) and then extracted with chloroform (50 mL x 3). After drying over anhydrous magnesium sulfate, the filtrate concentrated in vacuo affording the desired product as orange solid. Yield = 90%

^{1}H NMR (500 MHz, $CDCl_3$, 300 K): δ (ppm) = 3.59 (t, 2H, N-*CH_2*, ^{1}J = 7 Hz, ^{2}J = 14.5 Hz), 1.63 (m, 2H, N-CH_2-*CH_2*-), 1.30 (m, 10H, -CH_2-), 0.87 (t, 3H, CH_3, ^{1}J = 6.5 Hz, ^{2}J = 13 Hz), 7.10 (d, 2H, CH thiophene, J = 4 Hz), 7.62 (d, 2H, CH thiophene, J = 4 Hz).

MS: m/z: 531 [M+].

Synthesis of 2,3-bis(5,2'-bithiophen-2-yl)-N-octylmaleimide (5)

To a solution of 2,3-bis(2-bromothiophen)-N-octylmaleimide (**4**) in 5 mL of dry DMF (0.5 g, 0.94 mmol) and 2-(tributylstannyl)thiophene (0.7 g, 1.9 mmol),

$Pd(PPh_3)_2Cl_2$ (13 mg, 0.018 mmol, 2%) was added. The mixture was heated for 6 hours at 100°C under nitrogen. The reaction was monitored by TLC. After cooling to r.t., the mixture was added to water and extracted with ethyl acetate (50 mL x 3). After drying over anhydrous magnesium sulfate, the filtrate was concentrated in vacuo. The crude product was purified by flash column chromatography, (SiO_2, hexane: ethyl acetate 95 : 5) to afford the desired product as a purple solid. Yield = 60%

^{1}H NMR (500 MHz, $CDCl_3$, 300 K): δ (ppm) = 3.60 (t, 2H, N-CH_2, ^{1}J = 7.5 Hz, ^{2}J = 14.5 Hz), 1.68-1.63 (m, 2H, N-CH_2-*CH_2*-), 1.38-1.23 (m, 10H, -CH_2-), 0.88 (t, 3H, CH_3, ^{1}J = 7.0 Hz, ^{2}J = 14.0 Hz), 7.86 (d, 2H, CH thiophene, ^{1}J = 4.0 Hz), 7.3 (m, 4H, CH thiophene), 7.20 (d, 2H, CH thiophene, ^{1}J = 4.0 Hz), 7.05 (t, 2H, CH thiophene, ^{1}J = 4.5 Hz, ^{2}J = 8.5 Hz)

MS: m/z: 538 [M+].

Synthesis of 2,3-bis(3'-hexyl-5,2'-bithiophen-2-yl)-N-octylmaleimide (6)

To a solution of 2,3-bis(2-bromothiophen)-N-octylmaleimide (**4**) in 10 mL of dry DMF (1.00 g, 1.88 mmol) and 2-(tributylstannyl)-3-hexylthiophene (1.87 g, 5.64 mmol), $Pd(PPh_3)_2Cl_2$ (26 mg, 0.036 mmol, 2%) was added. The mixture was heated for 6 hours at 100°C under nitrogen. The reaction was monitored by TLC. After cooling to r.t., the mixture was added to water and extracted with toluene (50 mL x 3). After drying over anhydrous sodium sulfate, the filtrate was concentrated in vacuo. The crude product was purified by flash column chromatography, (SiO_2, hexane: ethyl acetate 9:1) to afford the desired product as purple oil. Yield = 81%

^{1}H NMR (500 MHz, $CDCl_3$, 300 K): δ (ppm) = 3.63 (t, 2H, N-CH_2, ^{1}J = 10 Hz, ^{2}J = 15 Hz), 2.80 (t, 4H, Thiophene-CH_2, ^{1}J = 5 Hz, ^{2}J = 15 Hz), 1.67-1.61 (m, 6H), 1.38-1.23 (m, 22H), 0.89-0.86 (m, 9H, CH_3), 6.95 (d, 2H, CH thiophene, ^{1}J = 5 Hz), 7.14 (d, 4H, CH thiophene, ^{1}J = 5 Hz), 7.23 (d, 2H, CH thiophene, ^{1}J = 5 Hz).

MS: m/z: 705 [M+].

Synthesis of poly (3-(2,2'-bithien-5-yl)-4-(thien-2-yl)-1-octyl-pyrrole-2,5-dione) (P1)

To a solution of **4** (200 mg, 0.38 mmol) and 2,5-bis(tributyl)stannyl-thiophene (270 mg, 0.41 mmol) dissolved in DMF (10 mL) $Pd(PPh_3)_2Cl_2$ (5 mg, 0.07 mmol, 2%) was added. The mixture was heated for 20 hours at 90°C under nitrogen atmosphere. The polymer was precipitated by pouring the DMF solution into methanol (200 mL). The crude product was filtered and then Soxhlet extracted with methanol and diethyl ether to remove the oligomers and catalyst residues until the extraction solution was colorless.

^{1}H NMR (500 MHz, $CDCl_3$, 300 K): δ (ppm) = 0.88 (br, 3H, CH_3), 1.27 (br, 6H, CH_2), 1.33 (br, 6H, CH_2), 3.62 (br, 2H, N-CH_2), 7.20 (br, 4H, CH thiophene), 7.88 (br, 2H, CH thiophene).

40 mg dark solid Yield = 21%

GPC (THF, 25 °C, RI Detector): M_n = 14397 g mol^{-1}, M_w = 18223 g mol^{-1}, M_p = 19432 g mol^{-1}, PDI = 1.26 λ_{max} (THF) = 590 nm.

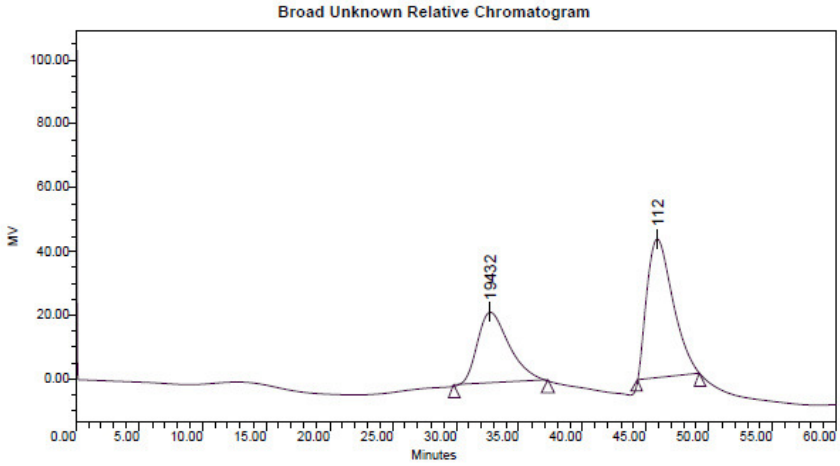

Broad Unknown Relative Peak Table

	Distribution Name	Mn (Daltons)	Mw (Daltons)	MP (Daltons)	Mz (Daltons)	Mz+1 (Daltons)	Polydispersity	Mz/Mw	Mz+1/Mw
1		14397	18223	19432	21893	25271	1.265693	1.201437	1.386777
2				112					

Synthesis of poly(3,4-di(2,2'-bithien-5-yl)-1-octyl-pyrrole-2,5-dione) (P2)

To a solution of **2** (250 mg, 0,68 mmol) and 2,5-bis(trimethyl)stannyl-bithiophene (0,56 mg, 0,75 mmol) dissolved in DMF (10 mL) $Pd(PPh_3)_2Cl_2$ (9,6 mg, 0,14 mmol, 2%) was added. The mixture was heated for 20 hours at 90°C under nitrogen atmosphere. The polymer was precipitated by pouring the DMF solution into methanol (200 mL). The crude product was filtered and then Soxhlet extracted with methanol and diethyl ether to remove the oligomers and catalyst residues until the extraction solution was colorless.

^1H NMR (500 MHz, $CDCl_3$, 300 K): δ (ppm) = 0.87 (br, 3H, CH_3), 1.25 (br, 6H, CH_2), 1.43 (br, 4H, CH_2), 1.57 (br, 4H, CH_2), 3.67 (br, 2H, N-CH_2), 6.98 (br, 2H, CH thiophene), 7.28 (br, 2H, CH thiophene).

150 mg dark solid. Yield = 60%

GPC (THF, 25 °C, RI Detector): M_n = 11650 g mol^{-1}, M_w = 16940 g mol^{-1}, M_p = 19621 g mol^{-1}, PDI = 1.45

λ_{max} ($CHCl_3$) = 561 nm

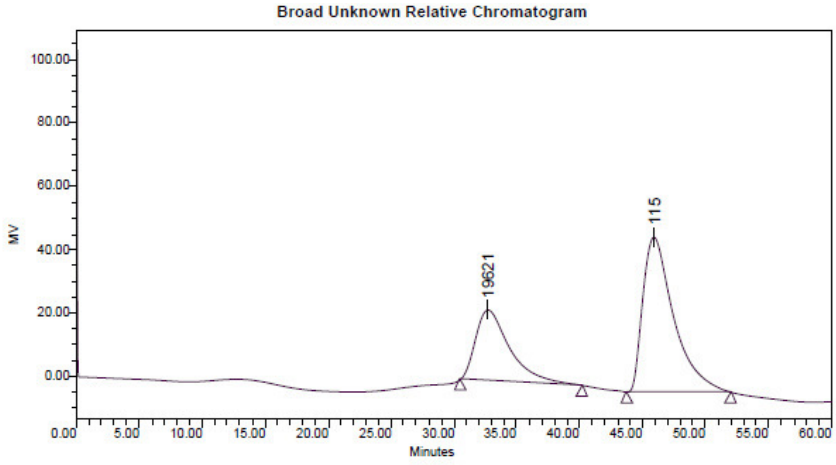

Broad Unknown Relative Peak Table

	Distribution Name	Mn (Daltons)	Mw (Daltons)	MP (Daltons)	Mz (Daltons)	Mz+1 (Daltons)	Polydispersity	Mz/Mw	Mz+1/Mw
1		11650	16940	19621	20895	23937	1.454110	1.233453	1.413009
2				115					

4.5.4 Electrochemical Characterization

Compound **5** was dissolved ($5x10^{-4}$ M) in a 0.1 M solution of tetrabutylammonium perchlorate ($TBAClO_4$) (Fluka, electrochemical grade, >99.0%) in anhydrous acetonitrile (Aldrich, 99.8%). Cyclic Voltammetries (CV) were performed at a scan rate of 50 mV/s with a PARSTA2273 EG&G potentiostat in a three-electrode electrochemical cell. All the measurements were carried out in a glove box filled with argon ($[O_2]$<1 ppm). The working, counter, and pseudoreference electrodes were a well polished Au pin, a Pt flag and a Ag/AgCl wire, respectively. The Ag/AgCl pseudoreference electrode was externally calibrated by adding ferrocene ($1x10^{-3}$ M) to the electrolyte. In the paper, all the potentials will be reported vs. the ferrocinium/ferrocene couple.

4.5.5 Fabrication of Polymer Solar Cells

All bulk heterojunction photovoltaic cells were prepared using the same preparation procedures and device fabrication procedure as follows: glass-indium tin oxide (ITO) substrates (obtained from Xinyan Technologies, (< 20 Ω/cm^2) were first patterned by acid etching. Before processing, the patterned ITO glass was cleaned by sonication, first in a microelectronic detergent, then in deionized water for 45 min., and finally rinsed with acetone and isopropyl alcohol. After drying in a stream of nitrogen, substrates were cleaned in a UV-ozone chamber for 15 min. Poly(3,4-ethylenedioxythiophene):poly(styrenesulfonate) (PEDOT:PSS, Baytron 4083) was filtered through 0.4 μm filter before being spin coated onto ITO (thickness around 40 nm) at 3500 rpm for 30 s in nitrogen, and dried at 108 °C for 2 min. inside a glove box. Then, for the preparation of active layer, a mixture of the polymer and $PC_{61}BM$ DCB (2.2 wt.%) was spin-coated on top of the PEDOT:PSS layer at 1000 rpm for 45 s. The films were annealed at the desired temperature for 1 min. in a glove box. The solar cell devices were completed by thermal evaporation of LiF (1.2 nm) and Al (100 nm) at $<10^{-6}$ Torr. The deposition rates of LiF and Al were 0.1 and 2.5 Å/s, respectively. The active area of the device is 0.28 cm^2. The current-voltage (I-V) measurements of the photovoltaic cells were performed on a computer-

controlled Keithley 2635 source measurement unit (SMU) with a solar simulator (SolarCell Test 575 from KHS) under illumination of AM 1.5G at 100 mW cm^{-2}.

[1] E. Zhou; J. Cong; Q. Wei, K. Tajima; C. Yang, K., *Angewandte Chemie International Edition*, **2011**, 50, 12, 2799.

[2] X. Zhan; A. Facchetti; S. Barlow; T. J. Marks; M. A. Ratner; M. R. Wasielewski, *Advanced Materials*, **2011**, 23, 2, 268.

[3] X. Zhao; X. Zhan, *Chemical Society Reviews*, **2011**, 40, 7, 3728.

[4] Y. Lin; Y. Li; X. Zhan, *Chemical Society Reviews*, **2012**, 41, 11, 4245.

[5] A. Najari; S. Beaupré; P. Berrouard; Y. Zou ; J. Pouliot; C. Lepage-Pérusse; M. Leclerc, *Adv. Funct. Mater*., **2011**, 21, 718.

[6] G. Zhang; Y. Fu; Z. Xie; Q. Zhang, *Polymer* **2011**, 52, 415.

[7] E. Zhou; J. Cong; K. Tajima; C.Yang; K. Hashimoto, *J. Phys. Chem*. C, **2012**, 116, 2608.

[8] W. Zhang; F. Tao; L. Xi; K. Meng; Z. Wang; Y. Li, *J Mater Sci,* **2012**, 47, 323.

[9] T.A. Chu; J. Lu; S. Beaupré; Y. Zhang; J.R. Pouliot; S. Wakim; J. Zhou; M. Leclerc; Z. Li; J. Ding, *Journal of the American Chemical Society*, **2011**, 133, 12, 4250.

[10] H. Xin; X. Guo; F. S. Kim; G. Ren; M. D. Watson; S. A. Jenekhe, *Journal of Materials Chemistry*, **2009**, 19, 30, 5303.

[11] K. Onimura; M. Matsushima; M. Nakamura; T. Tominaga; K. Yamabuki; T. Oishi, *Journal of Polymer Science Part A: Polymer Chemistry*, **2011**, 49, 3550.

[12] T.Z. Liu; Y. Chen, *Polymer,* **2005**, 46, 23, 10383.

[13] L. H. Chan; Y.D. Lee; T. Chen, *Macromolecules*, **2006**, 39, 9, 3262.

[14] R. H. Lee; J.L. Huang, *Polymers for Advanced Technologies*, **2011**, 22, 12, 2110.

[15] L.H. Chan; S.Y. Juang; M.C. Chen; Y.J. LinChan, *Polymer*, **2012**, 53, 12, 2334.

[16] S. Sista; Y. Yao; Y. Yang, *Applied Physics Letters* **2007**, 91, 223508.

[17] E. Lim; S. Lee; K. K. Lee, *Chem. Commun*., **2011**, 47, 914.

[18] J. Lee; M. Hee Yun; J. Kim; C. Yang, *Macromol. Rapid Commun*., **2012**, 33, 140.

[19] J. H. Huang; M. Velusamy; K. C. Ho; J. T. Lin; C. W. Chu, *J. Mater.Chem*., **2010**, 20, 2820.

[20] M. Reyes-Reyes; K. Kim; D.L. Carroll, *Appl. Phys. Lett.* **2005**, 87, 83506.

[21] Y. Kim; S. Cook; S.M. Tuladhar; S.A. Choulis; J. Nelson; J.R. Durrant; D.D.C. Bradley; M. Giles; I. Mcculloch; C.S. Ha; M. Ree, *Nat. Mater*. **2006,** 5, 197.

[22] J.Y. Kim; S.H. Kim; H.H. Lee; K. Lee; W. Ma; X. Gong; A.J. Heeger, *Adv. Mat*er. **2006**, 18, 572.

[23] H.C. Yeh; W.C. Wu; C.T. Chen, *Chemical Communications*, **2003**, 3, 404.

[24] L. H. Chan; Y. D. Lee; C.T. Chen; *Tetrahedron,* **2006**, 62, 41, 9541.

[25] H. Shih; R.J. Shih; D.A. Carson, *Journal of Heterocyclic Chemistry*, **2011**, 48, 6, 1243.

[26] D. S. Choi; S. Huang; M. Huang; T. S. Barnard; R. D. Adams; J. M. Seminario; J. M. Tour, *The Journal of Organic Chemistry*, **1998**, 63, 8, 2646.

[27] E.M. Beccalli; M.L. Gelmi; A. Marchesini, *European Journal of Organic Chemistry*, 6, **1999**, p. 1421.

[28] A.Terpin; K. Polborn; W. Steglich, *Tetrahedron,* **1995**, 51, 36, 9941.

[29] E. K. Fields; S. J. Behrend; S. Meyerson; M. L. Winzenburg; B. R. Ortega; H. K. Hall Jr., *The Journal of Organic Chemistry*, **1990**, 55, 17, 5165.

[30] M. Dubernet; V. Caubert; J. Guillard; M. C. Viaud-Massuard; *Tetrahedron*, **2005**, 61, 19, 4585.

[31] H. Wang; Q. Shi; Y. Lin; H. Fan; P. Cheng; X. Zhan; Y. Li; D. Zhu, *Macromolecules*, **2011**, 44, 4213.

[32] P.S. Deore; N.P. Argade, *The Journal of Organic Chemistry*, **2011**, 77, 1, 739.

[33] K. Onimura; M. Matsushima; M. Nakamura; T. Tominaga; K. Yamabuki; T. Oishi, *Journal of Polymer Science Part A: Polymer Chemistry*, **2011**, 49, 16, 3550.

[34] K. Onimura; M. Matsushima; K. Yamabuki; T. Oishi, *Polymer Journal*, **2010**, 42, 4, 297.

[35] S.V. Shorunov; M.M. Krayushkin; F.M. Stoyanovich; M. Irie, *Russian Journal of Organic Chemistry*, **2006**, 42, 10, 1497.

[36] C. Marminon; A. Pierre; B. Pfeiffer; V. Perez; S. Leonce; P. Renard; M. Prudhomme, *Bioorganic & Medicinal Chemistry*, **2003**, 11, 5, 687.

[37] D. Waghray; W. Nulens; W. Dehaen, *Organic Letters*, **2011**, 13, 20, 5519.

[38] M. Dubernet; V. Caubert; J. Guillard; M.C. Viaud-Massuard, *Tetrahedron*, **2005**, 61, 19, 4593.

[39] P. Frere; J.M Raimundo; P. Blanchard; J. Delaunay; P. Richomme; J.L. Sauvajol; J. Orduna; J. Garin; J. Roncali, *The Journal of Organic Chemistry*, **2003**, 68, 19, 7265.

[40] J. O. M. Bockris; S. U. M. *Khan, Surface Electrochemistry* – A Molecular Level Approach, Kluwer *Academic/Plenum Publishers*, New York, **1993**

[41] Y.C. Huang; Y.C. Liao; S.S. Li; M.C. Wu; C.W. Chen; W. F. Su, *Solar Energy Materials & Solar Cells*, **2009**, 93, 888.

5. Amphiphilic Conjugated block copolymers for Bulk Heterojuction Cells

5.1 Introduction

In the previous Chapter it was explained how the OPV research has progressed remarkably both in terms of new materials and device performances. And we have shown also that the relevant figures of merit of organic solar cells (J_{sc}, V_{oc}, FF, and PCE) are strongly dependent on charge generation and transport, which are ultimately dominated by the phase behavior of the donor and acceptor materials blend. An unfavorable nano-morphology of donor–acceptor blend limits the PCE; precise control of the morphology at the nanoscale is the key challenge for the development of efficient organic solar cell devices. The main morphological factors that must be controlled for the development of efficient organic solar cell devices are:

(i) The two components should phase-segregate into domains with the highest interfacial area for optimized exciton dissociation.

(ii) The domains size should be at the nanoscale, with a mean domain size comparable to the exciton diffusion length (about 10 nm[1,2,3]); if the domain sizes are larger than the diffusion length of the photoinduced excitons, excitons will not reach an interface within their lifetime.

(iii) Conversely, if the phase separation is too fine, with larger interfacial area, geminate and/or bimolecular recombination are enhanced.

(iv) The two components must be fully interdispersed, to avoid the formation of isolated donor or acceptor domains where the charges can be trapped.

(v) A complete immiscibility of the two components is strongly desirable. The formation of mixed phased can decrease the measured V_{oc} and in general the electronic properties of mixed phases are less predictable and more complex.[4]

In this context, beyond tailoring the chemical structure of the materials, different production parameters (during or after the film formation) have been used to achieve an optimal morphology. The most significant parameters that influence the nanoscale morphology of polymer–fullerene blends are:

a) the spin casting solvent and the solution concentration;

b) the ratio between polymer and fullerene;

d) temperature and length of thermal annealing processes.

Obviously, the success of these strategies mostly depends on the nature of donor polymers; for example, while the thermal annealing process was effective in P3HT/PCBM system, it failed completely used other donor polymer, leading to a dramatic decrease in device performance.[5] The chemical structure of polymers determines the solubility in common organic solvents and the solid state miscibility with $PC_{61}BM$.

It is now known that smaller domain size and lower surface roughness are crucial to the device performance. These intrinsic properties of the active layer can be achieved by using different solvent which influences crystallization and diffusion of one or both compounds in the blend. Solvent nature and thermal annealing and more recently the use of additives (such as Diiodooctane, DIO) are standard tools to improve phase separation and crystallinity of the polymer phase.[6,7]

Alternatively, nanostructured BHJ can be realized by using molecules or polymers with the ability to self-assemble and form stable nanostructure in the range comparable to the exciton diffusion length. In this regards, block copolymers (BCPs), made of two covalently linked polymer chains, have been proposed with the purpose to improve the morphology.[8]

When the mixing entropy is small (the mixing entropy changes inversely with the molecular weight) the polymers with different structures can be immiscible and tend to separate in macro-phase separation to minimize the interfacial energy.

In the case of BCPs it’s not possible to have macro-phase separation because the immiscibility of the blocks and, at the same time, the presence of a covalent bond between them, lead to the spontaneous formation of ordered nanodomains, providing

a larger interface for charge separation and improving the formation of a bicontinuous pathway for charge transport. If BCPs form separated phases of the order of 5-50 nm, the length scale is comparable to the exciton diffusion length.

The balance between the spontaneous phase separation and the chemical bond between blocks gives to the BCPs the properties of self-assemble and the possibility to form meso-to nanostructures.[9] The self-assembly due to phase separation, typical of BCPs, can be exploited to produce a nanostructured morphology, highly ordered and close to ideal morphology for efficient BHJ solar cells.

BCPs can produce complex nanostructures in which the solvent plays a role in the resultant morphology.[10] This latest also depends on the relative volume fraction of the blocks respect the total volume, the length of the segment and the reciprocal miscibility.

The opportunities offered by BCPs for OPV are not limited to the control of domain size but, they are also of interest in controlling the orientation of the domains and the degree of the crystallinity.

In order to offer a not hindered pathway towards the electrodes, the ideal orientation of donor-acceptor layer is perpendicular to them. In particular, lamellar or cylindrical domains parallel to the substrates are the ideal morphology to allow high value of photocurrent.[11,12]

On the basis of their structure, the BCPs for OPV applications can be classified as follows (Figure 5.1):

1) coil-coil BCPs: not conjugated main chain bearing both donor and acceptor as side groups to the main chain

2) rod-coil BCPs: flexible coil-like chains are covalently bonded to one or more blocks with rod-like chains due to π-conjugation.

3) rod-rod BCPs: combining of two or more different rigid-rod blocks due to π-conjugation.

In general, semiconducting polymers are classified as “rod” blocks, for the higher rigidity of conjugated system and due to their interaction between π-conjugated systems, while blocks formed by aliphatic main chains are classified as “coil” for

their higher flexibility. This simplified classification doesn't cover the entire scenery of the BCPs. More complex system has been presented in literature concerning triblock copolymers,[13] cross-linked copolymers,[14] or BCPs with blocks made with mixtures of different comonomers.

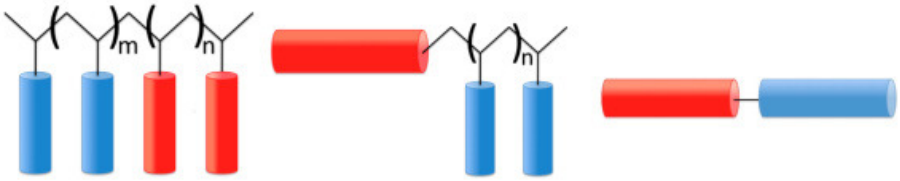

Figure 5.1: Main types of BCPs used for PV application: from the left, coil-coil, rod-coil and rod-rod DBCs.

Rod-coil and coil-coil BCPs offer similar function and in fact, for instance, have been applied to OPV of solar cell devices along two directions: first, conjugated copolymers have been proposed as active layer in BHJ, affording very promising results; [15,16] second, they have been investigated as compatibilizers for blends of P3HT/PCBM. In these systems the confinement at domain interfaces of the connections between the different blocks, reduces the interfacial tension, suppresses coalescence, limiting domain sizes, and helps to improve the nanoscale morphology and stability.[17]

While the synthesis of coil-coil copolymers for OPV can easily rely on the well-established knowledge acquired on the synthesis of classical BCPs, the development of rod-coil BCPs required the development of new strategies to combine blocks with different properties and which requires different syntheses.

The synthesis of all-conjugated block copolymers remains arduous, and there have been only a few recent reports on their synthesis, via Suzuki-type cross-coupling[18] or Grignard metathesis polymerization (GRIM).[19] There have been several reports on the synthesis of rod–rod block copolymers that contain a P3HT block and observations of the microphase separation. However, the synthesis of all-conjugated block copolymers reported so far involved first the polymerization of 3 hexylthiophene, followed by P3HT chain extension with polythiophene substituted with alkyl chains of different length or nature.[16,17,20,21]

GRIM polymerization, which was discovered by McCullogh and co-workers for the one-pot synthesis of P3HT [22], has been recently extended to a large variety of random or all-conjugated block copoloymers. [23,20,16,] Lin and co-workers[17] reported on the photovoltaic properties of the poly(3-butylthiophene)-b-poly(3-hexylthiophene), reaching PCE of the order of 4.0%, the best device performance reported so far using BCPs as active layer material. The PCE was also improved, controlling the nanoscale morphology, using BCPs as additive in the P3HT/$PC_{61}BM$.[21] Other research groups studied BCPs with amphiphilic structure: the crystallinity of the copolymers, due to the presence of poly(3-alkylthiophene), and a better interconnectivity between ordered domains are considered as the origin for the improved mobility.[24,25]

In the following we will report the synthesis of amphiphilic block copolymers, by GRIM polymerization, with fixed hydrophobic block. The BCPs was used as active layer in blend with $PC_{61}BM$, employed as classical acceptor material. The photovoltaic properties and morphologies of the blends were investigated as a function of block composition.

5.2 Synthetic Route and Chemical Characterization of Block and Random Copolymers

At the beginning we focused our attention on the synthesis of block and random copolymers containing P3HT and a new carboxy-functionalized thiophene, in order to compare the results in terms of structure and photovoltaic properties. For the synthesis of both materials it was necessary prepare the intermediate 2,5-dibromo-3-(6-ethyl-ethoxy-pentanoate)-thiophene. This molecule was prepared by Williamson reaction of 3-thiophene ethanol and 5-bromovaleric acid, the carboxylic acid was then protected as ester, followed by its electrophilic dibromination with NBS, in 30% overall yield. Isopropylmagnesium bromide (iPrMgBr) was employed to control the ability of 2,5-dibromo-3-ethylethoxy-pentanoatethiophene to undergo GRIM polymerization. Under optimized conditions, the Br–Mg exchange was complete after 1 h in THF at -50 °C affording the Grignard reagent. The high region-

selectivity was checked by ^{1}H NMR and GC mass analysis and the results are in accordance with theory that the GRIM method is well tolerated by ester, thanks to the possibility to exchange magnesium and bromine at low temperature[26] on the thiophene derivates bearing sensitive functional group. It was verified that this method is a new route to obtain regioregular polythiophene with carboxylic acid as side chain.[27] Obtaining the intermediate 2,5-dibromo-3-(6-ethyl-ethoxy-pentanoate)-thiophene (monomer **2**) random copolymer was synthetized by mixing of **2** with 2,5-dibromo-3-hexylthiophene while the synthesis of block copolymer was obtained starting from the same reagents but by sequential method (Scheme 5.1).

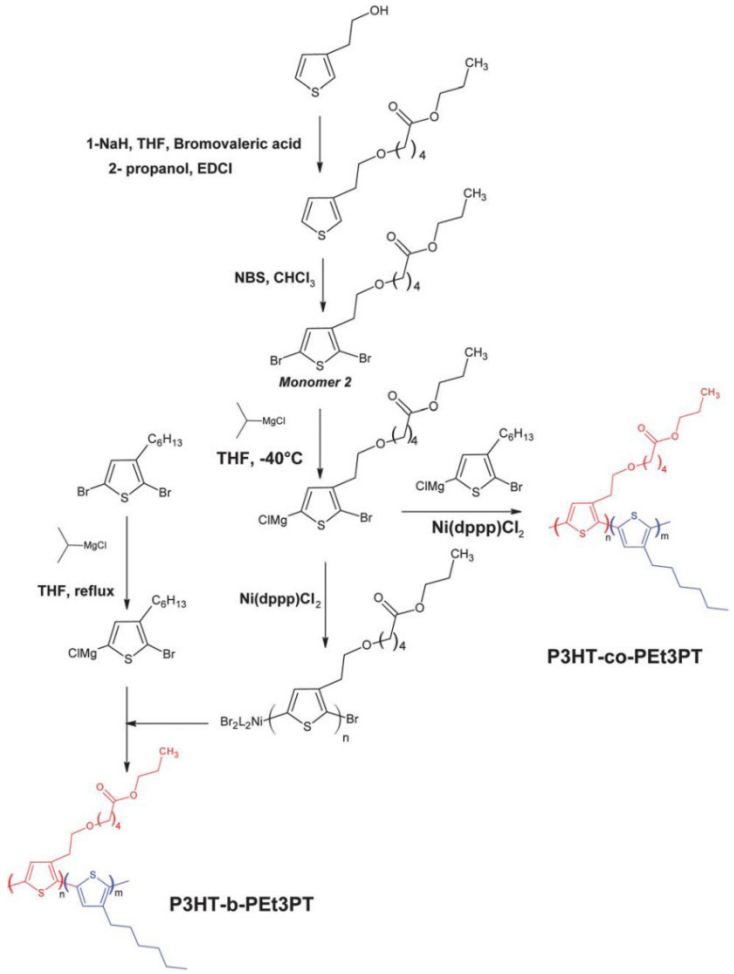

Scheme 5.1: Synthetic route to P3HT-co-P3EtPT and P3HT-b-P3EtPT

In the first case, poly([3-hexylthiophene-2,5-diyl]-co-[3-(6- ethyl-ethoxy-pentanoate) thiophene-2,5-diyl]), (**P3HT-*co*-P3EtPT**), was prepared by mixing the Grignard derivative of monomer **2** with 2-bromo-5-chloro-magnesium-3-hexylthiophene, at a molar ratio of 1:2. The polymerization was initiated by the addition of a catalytic amount (0.5% molar) of Ni(dppp)Cl_2. The resulting copolymer was purified by sequential Soxhlet extraction using methanol, ether, and chloroform, respectively. The GPC analysis of the chloroform fraction showed a monomodal peak at Mn = 16 600 g mol^{-1} with a narrow molecular weight distribution (PDI = 1.12). The ^{1}H NMR spectrum of P3HT-co-P3EtPT (Fig. 5.2) confirms the structure and the composition of the copolymer. The peak at 2.34 ppm, which corresponds to the methylene group adjacent to the ester carbonyl, confirms that the ester group survived exposure to the Grignard reagent. The peaks at 2.80, 3.09, 3.50, 3.71 and 4.01 arise from P3HT and **2** segments, respectively.

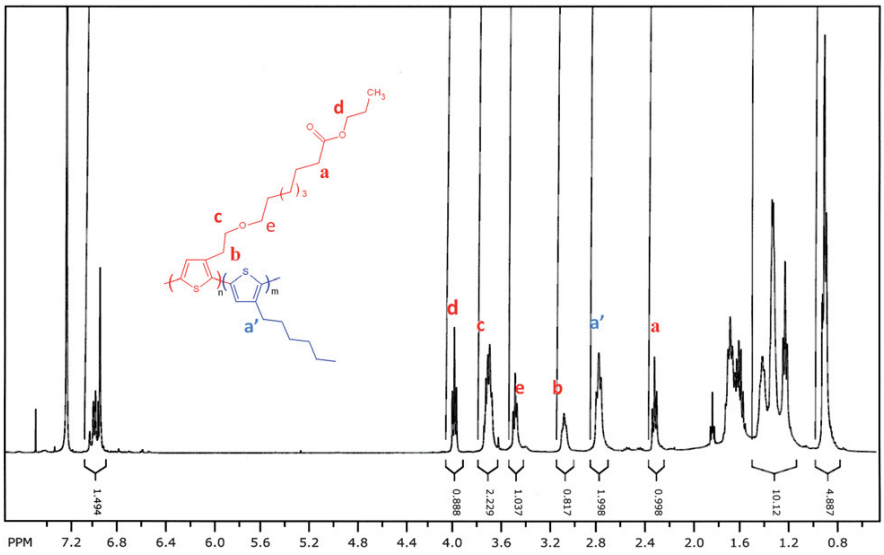

Figure 5.2: ^{1}H NMR spectrum of P3HT-co-P3EtPT.

P3HT-co-P3EtPT consists of 64 mol% of 3-hexyl-thiophene and 36 mol% of thiophene unit substituted with ester groups. The actual composition, calculated from the integral ratio between the triplet at 2.80 ppm assigned to methylene protons of the hexyl group and the triplet at 3.09 of oxyethylene protons next to the

thiophene ring in monomer **2,** is very close to the feed ratio (66–33%) of the monomers.

A block copolymer, P3HT-*b*-P3EtPT, was synthesized by GRIM polymerization as reported by McCullough and co-workers.[22] The first block was obtained using Ni(dppp)Cl_2 on the monomer **2** to give a polymer with a living chain-end, which was chain-extended into the diblock structure by addition of 2-bromo-5-bromomagnesium-3-hexylthiophene. The resulting block copolymer was purified by sequential Soxhlet extraction. The GPC analysis showed a monomodal peak with PDI = 1.16 and Mn= 17 000 g mol^{-1}.

Fig. 5.3 shows the ^{1}H NMR spectrum of P3HT-*b*-P3EtPT, the signals at 2.80 and 3.08 ppm are assigned to the protons of the α-methylene units in the α position of the thiophene ring of the P3HT segment and the oxyethylene protons of the P3EtPT segment, respectively.

The integration of these peaks gave the molar ratio of the two units and resulted 37:63/ P3EtPT:P3HT.

The measured composition is very close to the feed molar ratio (33:66).

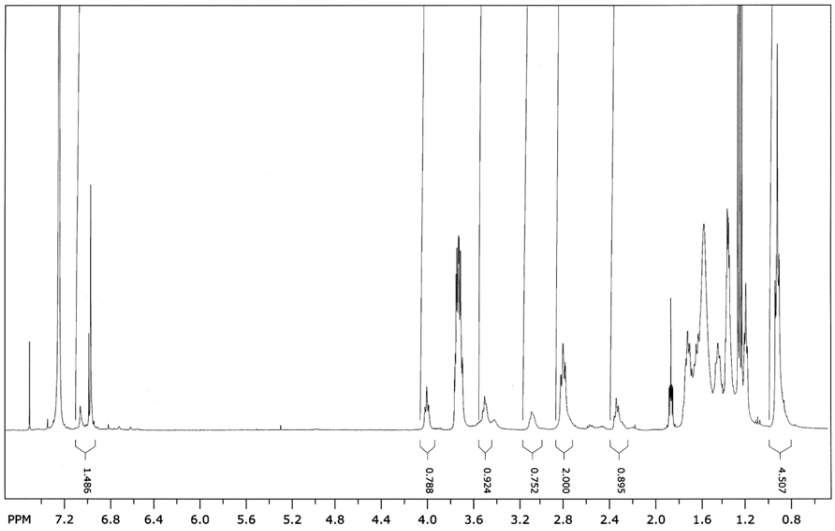

Figure 5.3: ^{1}H NMR spectrum of P3HT-*b*-P3EtPT.

It's worthwhile noting that in the aromatic region, the random copolymer shows four singlets at 6.98, 7.02, 7.04 and 7.07 ppm (Fig. 5.4). The peak at 6.98 is assigned to the HT–HT triad of P_3HT. That at 7.07 ppm has the same shift as the aromatic proton in the HT–HT triad of homopolymer obtained from monomer 2. The peaks at 7.02 and 7.04 arise from the other two triads resulting from coupling of 3-hexylthiophene and monomer 2. This confirms the statistical distribution of the monomers in the chain. In contrast, the block copolymer shows two singlets in the aromatic region at 6.98 and 7.07 ppm corresponding to each block.

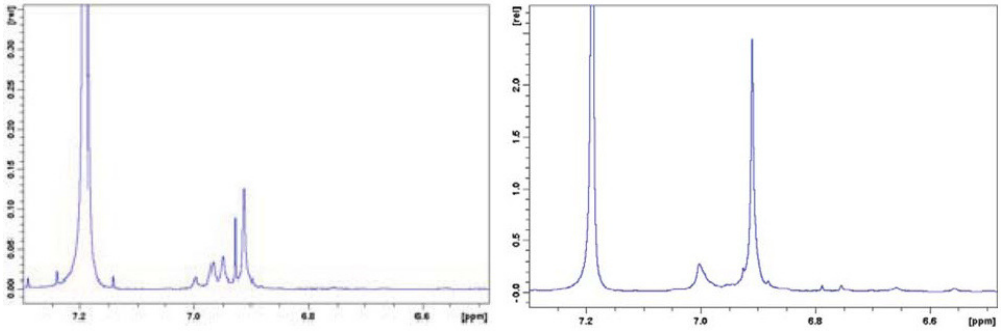

Figure 5.4: ^{1}H NMR spectra of the aromatic region of P3HT-*b*-P3EtPT (left) and P3HT-co-P3EtPT (right)

It has been tested the saponification of the ester group in both copolymers using NaOH in THF; the reaction gave a dark red solid, which was insoluble in both organic solvents and water. The lack of solubility is not entirely unexpected, because the solubility of rigid polyelectrolytes has been shown to be driven by the hydrophilic–lipophilic balance and electrostatic interactions.[28]

To overcome solubility problems associated with lipophilicity, it was chose to decrease the hydrophilic block in order to increase the solubility in organic solvents.

For this purpose, a diblock copolymer with shorter polar block was prepared through a combination of GRIM polymerization and post-functionalization.

The method reported in the Scheme 5.2 involved the synthesis of 3,2-(5 bromopentyl)oxyethyl-thiophene, followed by dibromination with NBS. To prepare

the block copolymer, the 2,5-dibromo-3-hexylthiophene was reacted with i-PrMgBr and the catalyst, Ni(dppp)Cl_2, was added to promote the polymerization.

In a separate vessel, the bromo-alkyl-substituted thiophene monomers were reacted and added to the polymerization reaction after the 3-hexylthiophene monomer was consumed. The resulting copolymer (P3HT-*b*-P3BrPT) was purified as describe before, by precipitation in MeOH followed by Soxhlet extraction.

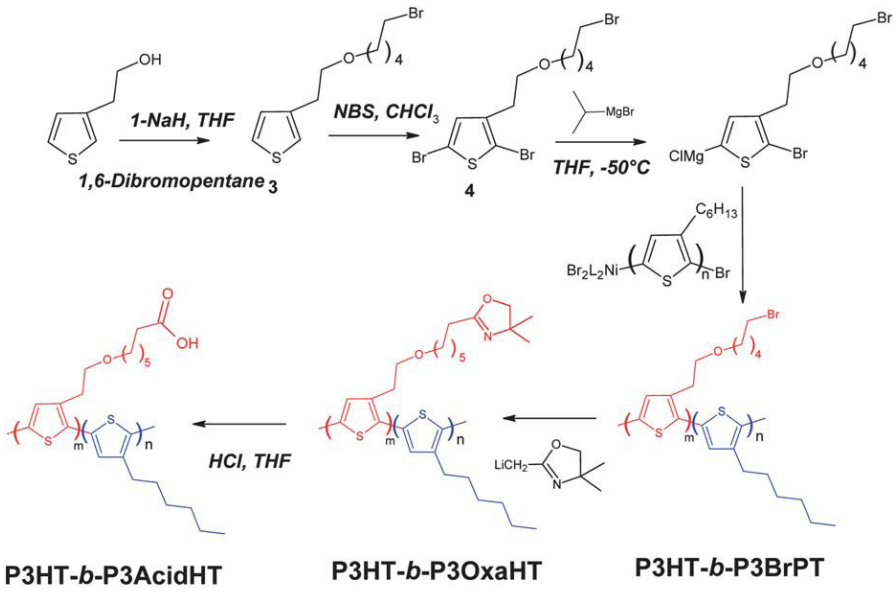

Scheme 5.2: Synthetic route to P3HT-*b*-P3AcidHT

The molecular weight and polydispersity index, determined by Size Exclusion Chromatography (SEC), were found to be 15000 g mol^{-1} and 1.37, respectively. The integration of the signals of the ^{1}H-NMR spectrum compared the methylene proton at α-position of thiophene and the signal of the methylene protons at 3.39 ppm for $BrCH_2$ gives the relative block lengths and ratio of the copolymer. The ratio was estimated to be 95 : 5.

The post-functionalization of the polymer was carried out as following: the bromide groups in P3HT-*b*-P3BrPT were transformed into oxazoline-protected carboxylic functions by treating the chloroform-soluble fraction with excess of lithiated 2,4,4-trimethyloxazoline at low temperature. The conversion was confirmed by 1H-NMR

with the appearance of a new signal at δ =2.22 ppm and disappearance of the triplet at δ = 3.38 ppm, assigned to the terminal methylene group a of bromine. The intermediate P3HT-*b*-P3OxaHT was then treated with HCl in order to hydrolyze the protecting group afforded the soluble amphiphilic diblock copolymer, P3HT-*b*-P3AcidHT.

5.2.1 Optical Properties

In order to compare the degree of π-conjugation of the new copolymers with P3HT, the photophysical characteristic and absorption spectra were examined in solution and in the solid state.

The presence of the hydrophilic pendant do not appear to significantly affect the photophysical properties of the copolymers, since absorption spectra in the solid state showed similar result for both polymers employed in the blend with PCBM. Figures 5.5 reported the absorption spectra of random and block copolymers compared with P3HT. The thin films, spin coated from a $CHCl_3$ solution, had λ_{max} at 516 nm, with an optical band gap of 1.9 eV.

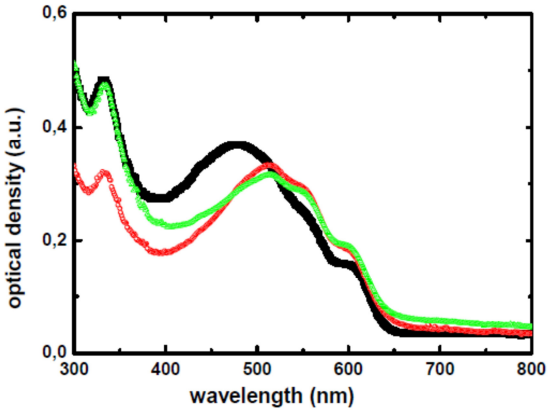

Figure 5.5: The absorption spectra of blend films of **P3HT**:PC61BM (red), **P3HT-b-P3AcidHT**:PC_{61}BM (green) and **P3HT-co-P3EtPT**:PC61BM (black).

5.2.2 Electrochemical Properties

The electrochemical behaviors of the copolymers were examined by cyclic voltammetry (CV). The HOMO levels are calculated from the onset of the oxidation peak and referenced to the HOMO of ferrocene (-4.8 eV, below the vacuum level), using the following equation.[29]

$$E^{HOMO} = [-e\ (E_{onset\ (vs\ SEC)} - E_{onset\ (Fc/Fc+\ vs\ SEC)}] - 4.8\ eV. \qquad \text{(eq 5.1)}$$

Figure 5.6 shows an example of cyclic voltammogram of the synthesized copolymers. CV was performed at room temperature and at a scan rate of 50 mV s^{-1}, under argon in chlorobenzene solution (0.5 mg/mL) with tetrabutylammonium hexafluorophosphate (n-Bu_4NPF_6) (0.1 M) as the supporting electrolyte, a glassy carbon working electrode, a platinum-wire auxiliary electrode, and a SCE as standard electrode.

The CV curves show reversible oxidation and reduction processes for both polymers. According to the equation 5.1, the HOMO level of the copolymer was −5.11 eV. The electrochemical measurements showed reversible oxidation processes for all the copolymers, which have LUMO and HOMO levels and band gap similar to those of P3HT.[30]

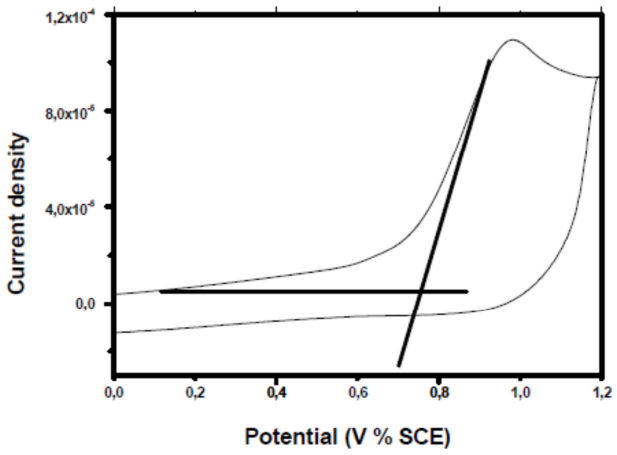

Figure 5.6: Example of cyclic voltammogram of the synthesized copolymers.

5.3 Photovoltaic solar cell characterization

The photovoltaic properties of the copolymers were investigated with a conventional device configuration ITO/PEDOT:PSS/copolymer:PC61BM/LiF/Al, where poly(3,4 ethylenedioxythiophene): poly(styrenesulfonate) (PEDOT:PSS) and lithium fluoride were used to ease hole and electron extraction, respectively.

The active area of the devices was 0.26 cm^2, three devices of each composition were fabricated and their short-circuit current density (Jsc), open-circuit potential (Voc), fill factor (FF) and power conversion efficiency (PCE) were calculated from J–V curves. The active layers were spin-coated from ortho-dichlorobenzene (o-DCB) solutions of polymer and $PC_{61}BM$.

A control device ITO/PEDOT:PSS/P3HT:$PC_{61}BM$/LiF/Al was also fabricated and tested, in order to minimize variation in the results that might arise due to different processing conditions. The rrP3HT was purchased from Aldrich, electronic grade quality. Both sets of BHJ devices (control and copolymers:$PC_{61}BM$) were fabricated and characterized during the same batch processing.

Details on device fabrication and characterization are provided at the end of this chapter in the Experimental section.

Fig. 5.7 shows the J–V characteristics of the polymer solar cells under 1000 W m^{-2} AM1.5 solar illumination and the Table 5.1 summarizes the device performance data. All the copolymers show excellent photovoltaic properties with an overall power conversion efficiency over 4%. Both random and block copolymers exhibited an open circuit voltage (0.6–0.7 V) comparable to those of P3HT (0.6 V), which is consistent with their relative HOMO levels, found by electrochemical characterization.

Compared the results in Table 5.1, P3HT-*b*-P3AcidHT showed the best performance with a PCE of 4.2%, open-circuit voltage of 0.60 V, short-circuit current density of 13.0 mA cm^{-2}, and fill factor of 0.60, while its analogous random copolymer only exhibited a PCE of 1.3% with a Voc of 0.66 V, Jsc of 4.3 mA cm^{-2}, and FF of 0.44. The control device exhibited a Voc of 0.62 V, a Jsc of 12.66 mA cm^{-2}, a FF of 0.45,

and a PCE of 3.24%. As a result, the efficiency of the best performing device showed a 30% improvement compared to the control device.

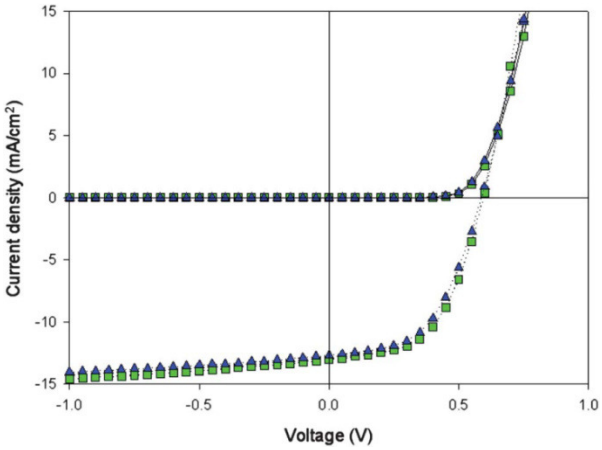

Figure 5.7: The current density–voltage characteristic of the BHJ solar cell made of P3HT-b-3AcidHT:PC61BM in a weight ratio of 1 : 1 in the dark and under illumination, annealed at 120°C (squares) and 140 °C (triangles).

Copolymers:PC61BM (w/w)	T (°C)	Thick. (nm)	Jsc (mA/cm^2)	Voc (V)	FF	PCE (%)	Rs(Ω)	Rsh(Ω)
P3HT-b-P3AcidHT 1 : 1	120	200	13,01	0,60	0,54	4,2	12	400
P3HT-b-P3AcidHT 1 : 1	140	200	12,72	0,59	0,52	3,9	13	450
P3HT-b-P3AcidHT 1 : 1	120	230	12,24	0,60	0,53	3,8	12	308
P3HT-b-P3AcidHT 1 : 1	120	240	12,24	0,60	0,51	3,6	13	340
P3HT-b-P3AcidHT 1 : 1	120	260	11,82	0,60	0,53	3,7	14	532
P3HT-b-P3AcidHT 1 : 2	120	140	3,94	0,70	0,34	0,9	56	340
P3HT-co-P3EtPT 1 : 2	120	200	2,04	0,71	0,4	0,6	73	715
P3HT-co-P3EtPT 2 : 1	120	240	4,31	0,66	0,44	1,2	42	500
P3HT-co-P3EtPT 1 : 1	120	90	2,03	0,44	0,42	0,4	26	660
P3HT-co-P3EtPT 1 : 1	120	180	0,79	0,49	0,26	0,1	27	624
P3HT-co-P3EtPT 1 : 1	120	220	1,59	0,70	0,4	0,4	74	790
P3HT-co-P3EtPT 1 : 1	120	240	1,5	0,68	0,41	0,4	17	780
P3HT-co-P3EtPT 1 : 1	120	350	11,13	0,74	0,38	0,3	97	1060
P3HT-co-P3EtPT	120	95	NA	NA	0,28	0,4	NA	NA
P3HT 1 : 1	110	100	12,66	0,62	0,45	3,2	NA	NA

Table 5.1: Photovoltaic performance of block and random copolymers

To study the effects of the composition of the photoactive material on the photovoltaic parameters, two blends of P3HT-*b*-P3AcidHT:$PC_{61}BM$ with different compositions (1 : 1 and 1 : 2 weight/weight) were investigated. The thickness of the active layer film was approximately 100 nm for all the blends. The 1:1 ratio was found to give the best performance. Also the thickness of the active layer was systematically varied between 100 and 260 nm by adjusting the spin rate during the coating process, while keeping the same P3HT-*b*-P3AcidHT:$PC_{61}BM$ ratio (1 : 1).
Despite some spreading in the data, a clear trend is observed: the performance gradually decreases while increasing the film thickness, mainly as a result of lowered current densities.

5.4 Atomic Force Microscopy characterization

Atomic Force Microscopy (AFM) analyses were carried out to investigate the self-assembly and film morphology of the blended system. As shown in Fig. 5.8, the surface of the P3HT-*b*-P3AcidHT:PC61BM blend film on the ITO/PEDOT substrate, annealed at 120 °C, is quite smooth, with a root-mean-square roughness of 0.7 nm. One can clearly observe well-defined interfaces where the phase separation within the P3HT-*b*-P3AcidHT:PC61BM appears as bright and dark regions, which are attributed to copolymer-rich and $PC_{61}BM$-rich domains, respectively. The average domain size is estimated to be 11 nm, close to the exciton diffusion length. The fine phase separation confirms the intimate mixing of P3HT-*b*-P3AcidHT and $PC_{61}BM$ at the nanoscale.

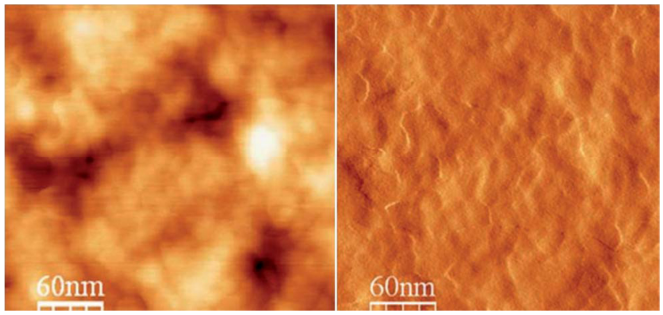

Figure 5.8: Height (left side) and phase (right side) AFM images of the P3HT-b-P3AcidHT:$PC_{61}BM$ blend film on the ITO/PEDOT

Nevertheless, the surface of the random copolymer, P3HT-*co*-P3EtPT:$PC_{61}BM$ blend, is much rougher, with an rms roughness of 7.4 nm (Fig. 5.9). The large domains (larger than 100 nm) on the surface of the film indicate a non-optimal morphology, which is not favorable for charge separation and thus limits the efficiency of the resulting devices. The reduced domain size and finer nanoscale morphology of P3HT-*b*-P3AcidHT:$PC_{61}BM$ suggest a stronger interchain interaction between the P3HT-*b*-P3AcidHT and $PC_{61}BM$ chains, which is primarily due to the presence of polyacid blocks in the copolymer, which are capable of forming hydrogen bonds between the carboxy-alkyl chains and the ester groups of $PC_{61}BM$. Evidence for hydrogen bonds in BHJ of regioregular poly(3-(carboxyalkyl)thiophene):$PC_{61}BM$ has been recently discussed and investigated through infrared spectroscopy and X-ray diffraction.[31] In this case, the polymer domain size was estimated to be 10 nm.

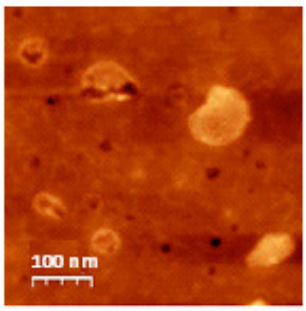

Figure 5.9: Phase image of **P3HT-*co*-P3EtPT**: PC61BM (1:1) blend annealed at 120°C

5.5 Conclusions

By employing GRIM method it has developed a straightforward and simple strategy to introduce carboxy-terminated chains into highly regioregular copolymers of 3-hexylthiophene in order to synthetize a series of random and diblock copolymers on 3-hexylthiophene and a new thiophene derivative (propyl-5-(2-(thiophen-3-yl)ethoxy) pentanoate), bearing an acidic function protected as propyl ester.

An alternative synthetic strategy, based on the postfunctionalization of a copolymer (P3HT-*b*-P3BrPT), obtained from a bromo-terminated alkyl-thiophene, was also explored and the corresponding acids were easily prepared by saponification in THF.

All the copolymers were tested for photovoltaic device, blended with $PC_{61}BM$ in the architecture composed on ITO/PEDOT:PSS/copolymer:$PC_{61}BM$/LiF/Al.

Among the amphiphilic copolymers, P3HT-*b*-P3AcidHT showed the best performance with a PCE of 4.2%, open-circuit voltage of 0.60 V, short-circuit current density of 13.0 mA cm^{-2} and fill factor of 0.60. This higher performance can be rationalized in terms of an improved interaction between the acid functions of P3HT-b-P3AcidHT and $PC_{61}BM$, thanks to the formation of non-covalent interaction, hydrogen bonds, between the carboxy-alkyl chains and the ester group of $PC_{61}BM$.[32]

5.6 Experimental Section

5.6.1 Materials

2,5-Dibromo-3-hexythiophene was prepared as described in the literature. 3-Thiophene ethanol, 5-bromovaleric acid, [1,3-bis (diphenyl-phosphino)propane]dichloro-nickel(II), (Ni(dppp)Cl_2), and isopropyl magnesium bromide were purchased from Aldrich and used without further purification. All reactions were carried out with oven-dried glassware, in dry solvents and under argon atmosphere, unless otherwise stated.

5.6.2 Instruments

^{1}H NMR spectra were recorded on a Bruker (400 MHz) spectrometer; chemical shifts (δ) are given relative to residual solvent peaks. UV-visible absorption spectra were collected with a Cary-Varian spectrophotometer. Molecular weights (Mws) and polydispersity indices (PDIs) were measured by GPC on a Model Dionex UltiMate 3000, equipped with a pump, an absorbance detector (UV, λ = 254 nm), a pre-column filter and polystyrene gel columns based on a conventional calibration curve using polystyrene standards. THF was used as a carrier solvent at a flow rate of 1.0 mL min^{-1} at room temperature.

5.6.3 Monomer and copolymers synthesis

Synthesis of 5-(2-(thiophen-3-yl)ethoxy)pentanoic acid (1).

To a solution of 5-bromovaleric acid (8.5 g, 47 mmol) in 100 mL of freshly distilled THF cooled to -78 °C under argon in a 500 mL three-necked flame-dried round-bottom flask was slowly added sodium hydride (60% in mineral oil, 1.9 g, 47 mmol) with vigorous stirring. The reaction mixture was stirred at -78 °C until completion of H_2 emission. In a separate flask, to a solution of 3-thiophene-ethanol (5 g, 39 mmol) in 150 mL of freshly distilled THF under argon was slowly added sodium hydride (60% in mineral oil, 2.8 g, 70 mmol) with vigorous stirring. The reaction mixture was stirred at room temperature until completion of H_2 emission.

The solution of sodium 5-bromovalerate was then slowly added to the solution of sodium

3-thiopheneethanolate and the mixture was stirred for 1 h at room temperature and for 15 h at 80 °C under argon. The reaction was quenched with a 1 M solution of NaOH and after washing with diethyl ether the aqueous phase was acidified with a 2M solution of hydrochloric acid (37%) to pH ≈ 2 to 3. The organic phase was extracted with diethyl ether (3 x 50 mL), dried over magnesium sulfate and the solvent was evaporated. The residue was purified by distillation (80 °C, 0.1 mbar) to afford the desired compound as a pale yellow oil (2.9 g, η = 33%).

^{1}H NMR (400 MHz, $CDCl_3$, 300 K): δ (ppm) = 1.68 (m, 4H, $CH_2CH_2CH_2$), 2.38 (t, 2H, CH_2COOH), 2.91 (t, 2H, ^{3}J = 7.1 Hz, thiopheneCH_2), 3.43 (t, 2H, $OCH_2CH_2CH_2$), 3.64 (t, 2H, ^{3}J = 7.1 Hz, OCH_2CH_2), 6.97 (dd, 1H, ^{3}J = 4.8 Hz, ^{4}J = 1.2 Hz, CCHCHS), 7.01 (m, 1H, ^{4}J = 1.2, 3 Hz, CCHS), 7.24 (dd, 1H, 3J = 4.8 Hz, ^{4}J = 3 Hz, CCHCHS).

^{13}C{1H} NMR (400 MHz, $CDCl_3$, 300 K): δ (ppm) = 21.3 ($CH_2CH_2CH_2$), 29.0 ($CH_2CH_2CH_2$), 31.2 (thiopheneCH_2), 36.1 (CH_2COOH), 72.2 ($OCH_2CH_2CH_2$), 76.6 (O CH_2CH_2), 121.4 (CHthiophene), 125.9 (CHthiophene), 128.3 (CHthiophene), 142.3 (Cthiophene), 178.2(COOH).

IR (ATR, cm^{-1}): 3100 broad (ν O–H), 3062 (ν C–Hthiophene), 2978 (ν_{as} C–H), 2927 (ν_{s} C–H), 1699 (ν C]O), 1542 (ν_{as} C]C), 1452 (ν_{s} C=C), 1231 (ν C–O), 769 (γ C–Hthiophene).

Synthesis of propyl 5-(2-(thiophen-3-yl)ethoxy)pentanoate (2).

To a solution of **1** (2.3 g, 10 mmol) and 1-propanol (0.9 mL, 12 mmol) in 20 mL of DMF in a 100 mL round-bottom flask were added at 0 °C N,N'-dicyclohexylcarbodiimide (2.3 g, 11 mmol) and 4-(dimethylamino)pyridine (123 mg, 1 mmol). The reaction mixture was stirred at room temperature for 48 h. The precipitated by product, N,N'-dicyclohexylurea, was filtered and rinsed with DMF. The solution was then poured into water and the organic phase extracted with diethyl ether (3 x 30 mL). Washing with water, drying over magnesium sulfate and evaporation of the solvent afforded the desired compound as a pale yellow oil (2.6 g, η = 96%).

^{1}H NMR (400 MHz, $CDCl_3$, 300 K): δ (ppm) = 0.93 (t, 3H, CH_3), 1.65 (m, 6H, $CH_2CH_2CH_2$ + $OCH_2CH_2CH_3$), 2.32 (t, 2H, CH_2COO), 2.89 (t, 2H, ^{3}J = 7.0 Hz, thiopheneCH_2), 3.45 (t, 2H,

$OCH_2CH_2CH_2$), 3.62 (t, 2H, ^{3}J = 7.0 Hz, OCH_2CH_2thiophene), 4.02 (t, 2H, $OCH_2CH_2CH_3$), 6.97 (dd, 1H, ^{3}J = 4.8 Hz, ^{4}J = 1.2 Hz, CCHCHS), 7.00 (m, 1H, ^{4}J = 1.2, 3 Hz, CCHS), 7.23 (dd, ^{1}H, 3J = 4.8 Hz, ^{4}J = 3 Hz, CCHCHS).

$^{13}C\{1H\}$ NMR (400 MHz, $CDCl_3$, 300 K): δ (ppm) = 10.6 (CH_3), 21.9 ($CH_2CH_2CH_2$), 22.1 ($OCH_2CH_2CH_3$), 29.3 ($CH_2CH_2CH_2$), 30.9 (thiopheneCH_2), 34.2 (CH_2COO), 66.0 ($OCH_2CH_2CH_3$), 70.6 ($OCH_2CH_2CH_2$), 71.1 (OCH_2CH_2thiophene), 121.2 (CHthiophene), 125.3 (CHthiophene), 128.6 (CHthiophene), 139.5 (Cthiophene), 173.8 (COO).

IR (ATR, cm^{-1}): 3055 (ν C–Hthiophene), 2933 (ν_{as} C–H), 2857 (ν_s C–H), 1732 (ν C=O), 1523 (ν_{as} C=C), 1447 (ν_s C=C), 1112 and 1165 (ν C–O), 774 (γ C–Hthiophene).

Synthesis of propyl 5-(2-(2,5-dibromothiophen-3-yl)ethoxy)pentanoate (3).

To a solution of **2** (2.6 g, 10 mmol) in 50 mL of chloroform in a 100 mL round-bottom flask was added N-bromosuccinimide (3.8 g, 21 mmol)portion by portion. The mixture was stirred at room temperature for 15 h in the dark. The resulting solution was washed with a saturated solution of sodium bisulfite, dried over magnesium sulfate and the solvent was evaporated.

The residue was then dissolved in hexane and the precipitated succinimide filtered and rinsed with hexane. The solvent was finally evaporated to afford the desired compound as a pale yellow oil (3.8 g, η = 92%).

^{1}H NMR (400 MHz, $CDCl_3$, 300 K): δ (ppm) = 0.94 (t, 3H, CH_3), 1.64 (m, 6H, $CH_2CH_2CH_2$ + $OCH_2CH_2CH_3$), 2.33 (t, 2H, CH_2COO), 2.78 (t, 2H, ^{3}J = 6.8 Hz, thiopheneCH_2), 3.44 (t, 2H, $OCH_2CH_2CH_2$), 3.55 (t, 2H, ^{3}J = 6.8 Hz, OCH_2CH_2thiophene), 4.03 (t, 2H, $OCH_2CH_2CH_3$), 6.86 (s, 1H, CCHCBrS).

$^{13}C\{1H\}$ NMR (400 MHz, $CDCl_3$, 300 K): δ (ppm) = 10.6 (CH_3), 21.9 ($CH_2CH_2CH_2$), 22.2 ($OCH_2CH_2CH_3$), 29.2 (thiopheneCH_2), 30.2 ($CH_2CH_2CH_2$), 34.2 (CH_2COO), 66.1 ($OCH_2CH_2CH_3$), 69.6 ($OCH_2CH_2CH_2$), 70.6 (OCH_2CH_2thiophene), 109.1 (CBr), 111.1 (CBr), 131.6 (CHthiophene), 142.0 (Cthiophene), 172.5 (COO).

IR (ATR, cm^{-1}): 3060 (ν C–Hthiophene), 2935 (ν_{as} C–H), 2862 (ν_s C–H), 1731 (ν C=O), 1540 (ν_{as} C=C), 1449 (ν_s C=C), 1112 and 1165 (ν C–O), 733 (γ C–Hthiophene).

Synthesis of P3HT-*co*-P3EtPT.

Compound **3** (870 mg, 2 mmol) and 2,5-dibromo-3-hexylthiophene (1.33 g, 4 mmol) were dissolved in 30 mL of anhydrous THF in a 100 mL three-necked flame-dried round-bottom flask under argon. After cooling at -50 °C, i-PrMgBr (3M in 2-methylTHF, 2.2 mL, 6.6 mmol) was added via a syringe. The reaction medium was maintained at -50 °C under stirring for 2 h. After warming at room temperature, Ni(dppp)Cl_2 (16.5 mg, 0.5 mol%/monomers) was added in one portion. The mixture was stirred at room temperature for 15 h and the reaction was then quenched by pouring into 300 mL of methanol. The precipitated polymer was filtered into a Soxhlet thimble and sequentially extracted with methanol, diethyl ether and chloroform. The chloroform fraction was evaporated to dryness to afford the desired copolymer as a violet solid (480 mg, η = 40%).

^{1}H NMR (400 MHz, $CDCl_3$, 300 K): δ (ppm) = 0.91 (t, CH_3), 1.24–1.71 (m, $CH_2CH_2CH_2$ + $CH_2CH_2CH_3$), 2.34 (t, CH_2COO), 2.80 (t, thiopheneCH_2 (P_3HT)), 3.09 (t, ^3J = 7.0 Hz, thiopheneCH_2 (P3EtPT)), 3.50 (t, $CH_2CH_2CH_2$), 3.71 (t, ^3J = 7.0 Hz, OCH_2CH_2thiophene), 4.01 (t, $OCH_2CH_2CH_3$), 6.98 (s, CHthiophene (HT–HT triad P3HT)), 7.02 (s, CHthiophene (HT–HT other triad)), 7.04 (s, CHthiophene (HT–HT other triad)), 7.07 (s, CHthiophene (HT-HT triad P3EtPT)). The ratio of P3EtPT:P3HT estimated from ^{1}H NMR is 36 : 64.

IR (ATR, cm^{-1}): 3054 (ν C–Hthiophene), 2927 (ν_{as} C–H), 2856 (ν_s C–H), 1736 (ν C=O), 1514 (ν_{as} C=C), 1458 (ν_s C=C), 1112 and 1166 (ν C–O), 825 (γ C–Hthiophene).

GPC (PS calibration, THF, 1 mL min^{-1}, room temperature): Mw = 18 600 g mol^{-1}, Mn = 16600 g mol^{-1}, PDI = 1.12.

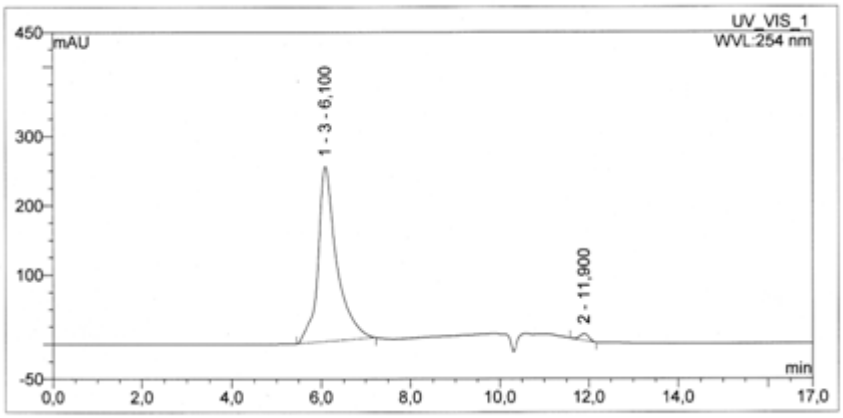

Figure 5.8: SEC chromatograms of **P3HT-*co*-P3EtPT** recorded at 40 °C, using RI and UV-visible detector, and THF as eluent.

Synthesis of P3HT-*b*-P3EtPT.

Compound 3 (870 mg, 2 mmol) was dissolved in 20 mL of anhydrous THF in a 100 mL three-necked flame-dried round-bottom flask under argon. After cooling at -50 °C, i-PrMgBr (3M in

2-methyl THF, 733 µL, 2.2 mmol) was added via a syringe. The reaction medium was maintained at -50 °C under stirring for 2 h. After warming at room temperature, $Ni(dppp)Cl_2$ (16.5 mg, 0.5 mol%/monomers) was added in one portion. The mixture was stirred at room temperature for 30 min.

In a separate flask, 2,5-dibromo-3-hexylthiophene (1.33 g, 4 mmol) was dissolved in 20 mL of anhydrous THF under argon. i-PrMgBr (3 M in 2-methyl-THF, 1.47 mL, 4.4 mmol) was then

added via a syringe and the mixture was heated at reflux under stirring for 2 h. After cooling to room temperature, the magnesium derivative of 2,5-dibromo-3-hexylthiophene was added to the P3EtPT homopolymer and the resulting mixture was stirred at room temperature for 15 h. The reaction was then quenched by pouring into 300 mL of methanol. The precipitated polymer was filtered into a Soxhlet thimble and sequentially extracted with methanol, diethyl ether and chloroform. The chloroform fraction was evaporated to dryness to afford the desired copolymer

as a violet solid (350 mg, η = 29%).

^{1}H NMR (400 MHz, $CDCl_3$, 300 K): δ (ppm) = 0.91 (t, CH_3), 1.19–1.71 (m, $CH_2CH_2CH_2$ + $CH_2CH_2CH_3$), 2.33 (t, CH_2COO), 2.80 (t, thiopheneCH_2 (P3HT)), 3.08 (t, ^{3}J = 7.0 Hz, thiopheneCH2 (P3EtPT)), 3.49 (t, $OCH_2CH_2CH_2$), 3.73 (t, ^{3}J = 7.0 Hz, OCH_2CH_2thiophene), 4.00 (t, $OCH_2CH_2CH_3$), 6.98 (s, CHthiophene (HT–HT triad P3HT)), 7.07 (s, CHthiophene (HT–HT triad P3EtPT)). The ratio of P3EtPT:P3HT estimated from ^{1}H NMR is 37 : 63.

IR (ATR, cm^{-1}): 3056 (ν C–Hthiophene), 2927 (ν_{as} C–H), 2856 (ν_s C–H), 1734 (ν C=O), 1514 (ν_{as} C=C), 1457 (ν_s C=C), 1110 and 1166 (ν C–O), 829 (γ C–Hthiophene).

GPC (PS calibration, THF, 1 mL min^{-1}, room temperature): Mw = 19 800 g mol^{-1}, Mn = 17000 g mol^{-1}, PDI = 1.16.

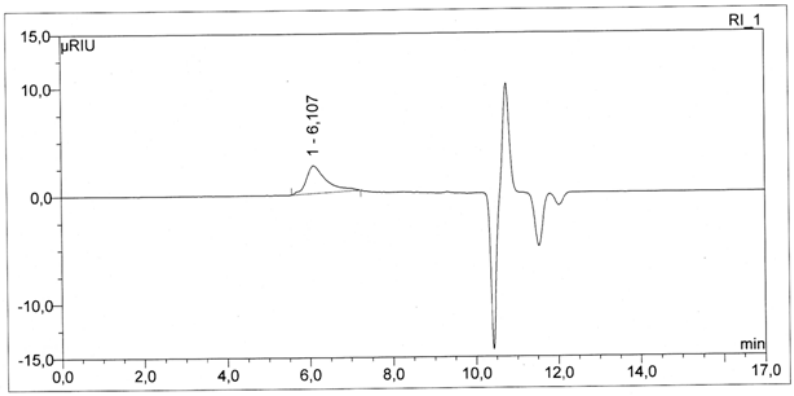

Figure 5.9: SEC chromatograms of **P3HT-*b*-P3EtPT** recorded at 40 °C, using RI and UV-visible detector, and THF as eluent.

Synthesis of 3-(2-(5-bromopentyloxy)ethyl)thiophene (4).

To a solution of 3-thiopheneethanol (3 g, 23 mmol) in 50 mL of freshly distilled THF under argon in a 250 mL three-necked flame-dried round-bottom flask was slowly added sodium hydride (60% in mineral oil, 1.2 g, 30 mmol) with vigorous stirring.

The reaction mixture was stirred at room temperature until completion of H_2 emission. 1,5 dibromopentane (26.9 g, 0.117 mol) was then added and the mixture was stirred for 1 h at room

temperature and for 15 h at 80 °C under argon. The reaction was quenched with water, the organic phase was extracted with diethyl ether (3 x 20 mL), dried over magnesium sulfate and the solvent was evaporated. The residue was purified by distillation (70 °C, 0.1 mbar) to afford the desired compound as a pale yellow oil (3.2 g, η = 49%).

^{1}H NMR (400 MHz, $CDCl_3$, 300 K): δ (ppm) = 1.54 (m, 4H, $CH_2CH_2CH_2$), 1.87 (p, 2H, 3J = 6.8 Hz, CH_2CH_2Br), 2.91 (t, 2H, ^{3}J = 7.0 Hz, thiopheneCH_2), 3.40 (t, 2H, ^{3}J = 6.8 Hz, CH_2Br), 3.45 (t, 2H, $OCH_2CH_2CH_2$), 3.63 (t, 2H, ^{3}J = 7.0 Hz, OCH_2CH_2), 6.98 (dd, 1H, ^{3}J = 4.8 Hz, ^{4}J = 1.2 Hz, CCHCHS), 7.02 (m, 1H, ^{4}J = 1.2, 3 Hz, CCHS), 7.25 (dd, 1H, ^{3}J = 4.8 Hz, 4J = 3 Hz, CCHCHS).

^{13}C{1H} NMR (400 MHz, $CDCl_3$, 300 K): δ (ppm) = 24.3 ($CH_2CH_2CH_2$), 29.0 ($CH_2CH_2CH_2$), 31.1 (thiopheneCH_2), 32.5 (CH_2CH_2Br), 33.8 (CH_2Br), 72.2($OCH_2CH_2CH_2$), 76.8 (OCH_2CH_2), 121.7 (CHthiophene), 125.9 (CHthiophene), 128.1 (CHthiophene), 142.5 (Cthiophene).

IR (ATR, cm^{-1}): 3060 (ν C–Hthiophene), 2973 (ν_{as} C–H), 2929 (ν_s C–H), 1542 (ν_{as} C=C), 1455 (ν_s C=C), 1189 (ν C–O), 765 (γ C–Hthiophene).

Synthesis of 2,5-dibromo-3-(2-(5-bromopentyloxy)ethyl)thiophene (5).

To a solution of 4 (3.2 g, 11.5 mmol) in 40 mL of chloroform in a 100 mL round-bottom flask was sequentially added N-bromosuccinimide (4.5 g, 25.4 mmol). The mixture was stirred at room temperature for 15 h in the dark. The resulting solution was washed with a saturated solution of sodium bisulfite, dried over magnesium sulfate and the solvent was evaporated. The residue was then dissolved in hexane and the precipitated succinimide filtered and rinsed with hexane. The solvent was finally evaporated to afford the desired compound as a pale yellow oil (4.7 g, η = 94%).

^{1}H NMR (400 MHz, $CDCl_3$, 300 K): δ (ppm) = 1.54 (m, 4H, $CH_2CH_2CH_2$), 1.87 (p, 2H, ^{3}J = 6.8 Hz, CH_2CH_2Br), 2.79 (t, 2H, ^{3}J = 6.7 Hz, thiopheneCH_2), 3.41 (t, 2H, ^{3}J = 6.8 Hz, CH_2Br), 3.43 (t, 2H, O $CH_2CH_2CH_2$), 3.55 (t, 2H, ^{3}J = 6.7 Hz, OCH_2CH_2), 6.86 (s, 1H, CCHCBrS).

^{13}C{1H} NMR (400 MHz, $CDCl_3$, 300 K): δ (ppm) = 25.1 ($CH_2CH_2CH_2$), 29.0 ($CH_2CH_2CH_2$), 30.2 (thiopheneCH_2), 32.7 (CH_2CH_2Br), 33.9 (CH_2Br), 69.6 ($OCH_2CH_2CH_2$), 70.8 (OCH_2CH_2), 109.1 (CBr), 110.5 (CBr), 131.7 (CHthiophene), 139.8 (Cthiophene).

IR (ATR, cm^{-1}): 3068 (ν C–Hthiophene), 2968 (ν_{as} C–H), 2927 (ν_{s} C–H), 1542 (ν_{as} C=C), 1457 (ν_{s} C=C), 1191 (ν C–O), 739 (γ C–Hthiophene).

Synthesis of P3HT-*b*-P3BrPT.

2,5-Dibromo-3-hexylthiophene (1 g, 3 mmol) was dissolved in 25 mL of anhydrous THF in a 100 mL three-necked flame-dried round-bottom flask under argon. i-PrMgCl·LiCl (Turbo Grignard, 1.3 M in THF, 2.6 mL, 3.3 mmol) was added via a syringe and the mixture was heated at reflux under stirring for 2 h. After cooling to room temperature, Ni(dppp)Cl_2 (8.7 mg, 0.5% mol/monomers) was added in one portion. The mixture was stirred at room temperature for 30 min. In a separate flask, **5** (67 mg, 0.15 mmol) was dissolved in 5 mL of anhydrous THF under argon. i-PrMgCl·LiCl (Turbo Grignard, 1.3 M in THF, 130 mL, 0.17 mmol) was then added via a syringe and the mixture was heated at reflux under stirring for 2 h. After cooling to room temperature, the magnesium derivative of **5** was added to the P3HT homopolymer and the resulting mixture was stirred at room temperature for 15 h. The reaction was then quenched by pouring into 300 mL of methanol. The precipitated polymer was filtered into a Soxhlet thimble and sequentially extracted with methanol, diethyl ether and chloroform. The chloroform fraction was evaporated to dryness to afford the desired copolymer as a violet solid (235 mg, η = 42%).

^{1}H NMR (400 MHz, $CDCl_3$, 300 K): δ (ppm) = 0.91 (t, CH_3), 1.20–1.71 (m, $CH_2CH_2CH_2$ + $CH_2CH_2CH_3$), 2.80 (t, thiophene CH_2 (P3HT)), 3.1 (t, ^{3}J = 7.1 Hz,

thiopheneCH_2 (P3BrPT)), 3.38 (t, CH_2Br), 3.50 (t, $OCH_2CH_2CH_2$), 3.72 (t, ^3J = 7.1 Hz, OCH_2CH_2thiophene), 6.98 (s, CH thiophene (HT–HT triad P3HT)), 7.08 (s, CH thiophene (HT–HT triad P3BrPT)).

The ratio of P3BrPT:P3HT estimated from ^1H NMR is 5 : 95.

IR (ATR, cm^{-1}): 3055 (ν C–Hthiophene), 2927 (ν_{as} C–H), 2857 (ν_s C–H), 1511 (ν_{as} C=C), 1456 (ν_s C=C), 1155 (ν C–O), 822 (γ C–Hthiophene).

GPC (PS calibration, THF, 1 mL min^{-1}, room temperature): Mw = 20 550 g mol^{-1}, Mn = 15000 g mol^{-1}, PDI = 1.37.

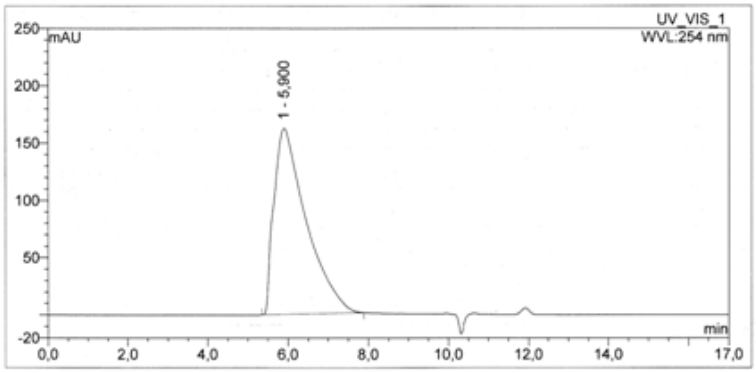

Figure 5.10: SEC chromatograms of **P3HT-*b*-P3BrPT** recorded at 40 °C, using RI and UV-visible detector, and THF as eluent.

Synthesis of P3HT-*b*-P3oxaHT.

To a solution of 2,4,4-trimethyl-2-oxazoline (1.1 mL, 8.7 mmol) in 20 mL of freshly distilled THF cooled to -78 °C under argon in a 100 mL threenecked flame-dried round-bottom flask was added dropwise via a syringe n-butyllithium (2.5 M in hexanes, 3.1 mL, 7.9 mmol) with vigorous stirring. The reaction mixture was stirred at -78 °C for 2 h under argon. A solution of P3HT-*b*-P3BrPT (150 mg, 0.87 mmol) in 20 mL of freshly distilled THF was then added at-78 °C to the 2,4,4-trimethyl-2-oxazoline lithium salt. The reaction mixture was stirred under argon for 15 h and allowed to warm to room temperature. The resulting solution was then poured into 300 mL of hexane. The precipitated polymer was filtered into a Soxhlet thimble and sequentially extracted with hexane and chloroform. The chloroform fraction was

evaporated to dryness to afford the desired copolymer as a violet solid (140 mg, η = 93%).

^{1}H NMR (400 MHz, $CDCl_3$, 300 K): δ (ppm) = 0.91 (t, CH_2CH_3), 1.24 (s, CCH_3), 1.27–1.70 (m, $CH_2CH_2CH_2$ + $CH_2CH_2CH_3$), 2.22 (t, CH_2CNO), 2.80 (t, thiopheneCH_2 (P3HT)), 3.09 (t, ^3J = 7.0 Hz, thiopheneCH_2 (P3oxaHT)), 3.48 (t, $OCH_2CH_2CH_2$), 3.71 (t, ^3J = 7.0 Hz, OCH_2CH_2thiophene), 3.87 (s, OCH_2CN), 6.98 (s, CHthiophene (HT–HT triad P3HT)), 7.06
(s, CHthiophene (HT–HT triad P3oxaHT)).
The ratio of P3oxaHT:P3HT estimated from 1H NMR is 5 : 95.
IR (ATR, cm^{-1}): 3055 (ν C–Hthiophene), 2924 (ν_{as} C–H), 2855 (ν_s C–H), 1666 (ν C=N), 1509 (ν_{as} C=C), 1459 (ν_s C=C), 1110 (ν C–O), 820 (γ C–Hthiophene).

Synthesis of P3HT-*b*-P3AcidHT.

To a solution of P3HT-*b*-P3oxaHT (140 mg, 0.81 mmol) in 50 mL of THF in a 100 mL round-bottom flask was added hydrochloric acid (37%, 3 mL). The reaction mixture was heated with stirring at 70 °C for 15 h. The resulting solution was then poured into 300 mL of methanol.

The precipitated polymer was filtered, rinsed with methanol and redissolved in 50 mL of THF in a 100 mL round-bottom flask. A solution of sodium hydroxide (10 M, 5 mL) was then added and the reaction mixture was heated with stirring at 70 °C for 15 h. After cooling to room temperature, the copolymer was reprotonated with a 2 M solution of hydrochloric acid (37%). The resulting solution was then poured into 300 mL of methanol. The precipitated polymer was filtered into a Soxhlet thimble and sequentially extracted with methanol and chloroform. The chloroform fraction was evaporated to dryness to afford the desired copolymer as a violet solid (120 mg, η = 87%).

^{1}H NMR (400 MHz, $CDCl_3$, 300 K): δ (ppm) = 0.91 (t, CH_2CH_3), 1.24–1.71 (m, $CH_2CH_2CH_2$ + $CH_2CH_2CH_3$), 2.29 (t, CH_2COOH), 2.80 (t, thiopheneCH_2 (P3HT)), 3.09 (t, ^3J=7.0 Hz, thiophene CH_2 (P3AcidHT)), 3.49 (t, $OCH_2CH_2CH_2$), 3.71 (t, ^3J = 7.0 Hz, OCH_2CH_2 thiophene), 6.98 (s, CH thiophene (HT–HT triad P3HT)), 7.08 (s,

CH thiophene (HT-HT triad P3AcidHT)). The ratio of P3AcidHT:P3HT estimated from ^{1}H NMR is 5 : 95.

IR (ATR, cm^{-1}): 3056 (ν C–H thiophene), 2926 (ν_{as} C–H), 2857 (ν_s C–H), 1707 (ν C=O), 1509 (ν_{as} C=C), 1456 (ν_s C=C), 1235 (ν C–O), 821 (γ C–H thiophene).

5.6.4 Fabrication and Characterization of Copolymer Solar Cells

All the bulk-heterojunction photovoltaic cells were prepared using the same preparation procedures and device fabrication procedure referring to as follows: the glass-indium tin oxide

(ITO) substrates (obtained from Xinyan Technologies (inf. 20 Ω sq^{-1})) were first patterned by acid etching. Before processing, the patterned ITO glass was cleaned by sonication, first in a microelectronic detergent, then in de-ionized water for 45 minutes, and finally rinsed by acetone and isopropyl alcohol. After drying by blowing nitrogen gas, substrates were irradiated in the UV–ozone chamber for 15 minutes. Poly(3,4-ethylenedioxy- thiophene):poly(styrenesulfonate) (PEDOT:PSS, Baytron 4083) was filtered through a 0.4 mm filter before being deposited on ITO with a thickness of around 40 nm by spin coating at 3500 rpm for 30 s in the nitrogen atmosphere, and dried at 108 °C for 2 min inside a glovebox. Then, for an active layer, the copolymer:$PC_{61}BM$ in an o-DCB blend of 2.2 weight% was spin-coated on the PEDOT:PSS layer at a speed rate of 1000 rpm for 45 s on the top of the PEDOT:PSS layer. The films were annealed at determined temperatures for 1 min in a glovebox. The solar cell devices were completed by thermal evaporation of LiF (1.2 nm) and Al (100 nm) under $<10^{-6}$ Torr pressure. The deposition rates of LiF and Al were 0.1 and 2.5 Å s^{-1}, respectively.

The active area of the device is 0.28 cm^2. The current–voltage (I–V) measurement of the polymer photovoltaic cells was conducted by a computer-controlled Keithley 2635 source measurement unit (SMU) with a solar simulator (SolarCell Test 575 from KHS) under the illumination of AM1.5G, 100 mW cm^{-2}. Atomic Force Microscopy (AFM) images were carried out with a dimension 3000 microscope from Digital Instruments.

[1] T. Stubinger; W. Brutting, *Journal of Applied Physics*, **2001**, 90, 7, 3632.

[2] D.E. Markov; J.C. Hummelen; P.W. Blom; A.B. Sieval, *Physical Review B*, **2005**, 72, 4, 045216.

[3] A. Haugeneder; M. Neges; C. Kallinger; W. Spirkl; U. Lemmer; J. Feldmann; U. Scherf; E. Harth; A. Gugel; K. Mullen, *Physical Review B*, **1999**, 59, 23, 15346.

[4] C. Groves; O.G. Reid; D.S. Ginger, *Accounts of Chemical Research* **2010**, 43, 5, 612.

[5] J.C. Guo; Y.Y. Liang; J. Szarko; B. Lee; H.J. Son; B.S. Rolczynski; L.P. Yu; L.X. Chen, *Phys. Chem. B* **2010**, 114, 742.

[6] F. Padinger; R.S. Rittberger; N.S. *Advanced Functional Materials*, **2003**, 13, 1, 85.

[7] G. Li; V. Shrotriya; J. Huang;Y. Yao; T. Moriarty; K. Emery; Y. Yang. Nat. Mater., **2005**, 4, 11, 864.

[8] A. Yassar; L. Miozzo; R. Gironda; G. Horowitz *Progress in Polymer Science* doi:10.1016/j.progpolymsci.**2012**.10.001

[9] T. Smart; H. Lomas; M. Massignani; M. V. Flores-Merino; L. Perez; G. Battaglia, *Nano Today*, **2008**, 3, 38.

[10] M.C. Orilall; U. Wiesner, *Chemical Society Reviews*, **2011**, 40, 2, 520.

[11] Y.J. Lee; S.H. Kim; H. Yang; M. Jang; S.S Hwang; H.S. Lee; K.Y. Baek, *The Journal of Physical Chemistry C*, **2011**, 115, 10, 4228.

[12] X. Yu; K. Xiao; J. Chen; N. V. Lavrik; K. Hong; B.G. Sumpter; D.B. Geohegan *ACS Nano*, **2011**, 5, 5, 3559.

[13] H.C. Moon; A. Anthonysamy; Y. Lee; J.K. Kim, *Macromolecules*, **2010**, 43,4, 1747.

[14] K.H. Nakabayashi; H. Oya; H. Mori, *Macromolecules*, **2012**, 45,7, 3197.

[15] G. Ren; P.T. Wu; S. A. Jenekhe, *Chem. Mater*., **2010**, 22, 2020.

[16] M. He; W. Han; J. Ge; Y. Yang; F. Qiu; Z. Lin; *Energy Environ. Sci.*, **2011**, 4, 2894.

[17] S. Rajaram; P.B. Armstrong; K.J. Bumjoon; J.M. Frechet, *J. Chemistry of Materials*, **2009**, 21, 9, 1775.

[18] T. Yokozawa; H. Kohno; Y. Ohta; A. Yokoyama, *Macromolecules*, **2010**, 43, 7095.

[19] I. Osaka; R. D. McCullough, *Acc. Chem. Res*., **2008**, 41, 1202.

[20] K. Ohshimizu; M. Ueda, *Macromolecules*, **2008**, 41, 5289.

[21] Y.C. Lai; K. Ohshimizu; A. Takahashi; J.C. Hsu; T. Higashihara; M. Ueda; W.C. Chen, *J. Polym. Sci., Part A: Polym. Chem.*, **2011**, 49, 2577.

[22] M. C. Iovu; E. E. Sheina; R. R. Gil; R. D. McCullough, Macromolecules, **2005**, 38, 8649.

[23] Y. Zhang; K. Tajima; K. Hirota; K. Hashimoto, *J. Am. Chem. Soc.*, **2008**, 130, 7812.

[24] R. H. Lohwasser; M. Thelakkat *Macromolecules,* **2012**, 45, 3070.

[25] C.R. Craley; M. Iovu; R.D. McCullough, *Polymer Preprints,* **2006**, 47, 2, 532.

[26] P. Knochel; W. Dohle; N. Gommermann; F. F. Kneisel; F. Kopp; T. Korn; I. Sapountzis; V. A. Vu, *Angew. Chem., Int. Ed*., **2003**, 42, 4302.

[27] P. Vallat; J. P. Lamps; F. Schosseler; M. Rawiso; J. M. Catala, *Macromolecules*, **2007**, 40, 2600.

[28] B. Kim; L. Chen; J. Gong; Y. Osada, *Macromolecules*, **1999**, 32, 3964.

[29] Y. Liu; M. S. Liu; A. K. Y. Jen, *Acta Polym.*, **1999**, 50, 105.

[30] M. Al-Ibrahim; H. K. Roth; U. Zhokhavets; G. Gobsch; S. Sensfuss, *Sol. Energy Mater. Sol. Cells*, **2005**, 85, 13.

[31] B. J. Worfolk; D. A. Rider; A. L. Elias; M. Thomas; K. D. Harris; J. M. Buriak, *Adv. Funct. Mater*., **2011**, 21, 1816.

[32] N. Sary; F. Richard; C. Brochon; N. Leclerc; P. Lévêque; J.N. Audinot; S. Berson; T. Heiser; G. Hadziioannou; R. Mezzenga, *Adv Mater*, 22, **2010**, 763.

6. Conclusions

Literature analysis about conjugated polymers, as donors in BHJ solar cells, reveals that the majority of them has been synthesized through the alternation of donor and acceptor moieties, in order to obtain low band gap polymers, increasing the efficiency of the OPV device due to a better overlap with the solar spectrum. The LUMO energy level of the D–A conjugated polymers is mainly localized on the acceptor unit, so a proper selection of the electron withdrawing block can influence the LUMO level of these polymers. Also, to avoid charge recombination of the free carriers after exciton separation, the electron-withdrawing ability of the acceptor needs to be carefully regulated.

Conjugated oligo-aromatic and heteroaromatic compounds with enforced planarity show great promise as DONOR material since that π-conjugation length and intra-chain charge transfer should be taken into account in the design of new polymers.

New low band gap polymers based on thiophene, as the donor unit, and iso-DPP or maleimide, as the acceptor moieties, were designed with these considerations in mind. All conjugated D-A molecules and polymers were synthesized via Stille polycondensation and their chemical behavior was investigated.

Bulk heterojunction solar cells based on new small bang gap materials, blended with PCBM, have been investigated and the effects on the morphology and phase separation were also investigated using AFM technique. Different parameters have been evaluated during the study of the device: the influence of different donor-acceptor ratio or thermal annealing was assigned to changes of the nanomorphology of blends.

The incorporation of pyrrolo[3,2-b]pyrrole-2,5-dione (iso-DPP) into the thiophene backbone allows to obtain polymers with a noticeable low band-gap and deep HOMO level. Preliminary results on photovoltaic devices based on a **PDPPT**:$PC_{60}BM$ have shown a PCE of 1.2%, therefore the new acceptor building

block is a promising molecule to use in solar cells. The problem of these polymers is the low molecular weight, due to poor solubilty of the oligomeric compounds during polymerization. Side alkyl chain, related to the phenyl group of the DPP core, should play a crucial role in improving the molecular weight, solubility, and processability of conjugated polymers.

Different results have been obtained employing the maleimide core to constitute the conjugated chain. AFM investigation showed domains between the polymer and the $PC_{61}BM$ too much larger than the typical exciton diffusion length, avoiding the formation of the typical interpenetrating network between DONOR and ACCEPTOR material.

The maleimide based polymer or molecules could be instead employed as a third component in the P3HT/PCBM blend. The photovoltaic results showed a PCE improved of 80% in the case of **P2** and 35% greater than pristine device if the small molecule **5**, consisting in two thiophene units for both side of the maleimide core, was added to the conventional mix.

From a chemical standpoint, the requirements for highly efficient solar cells are therefore not limited to the design of conjugated backbone with its electronic properties; crystallinity of polymer phase, miscibility with $PC_{61}BM$, morphology control and stability of the blend at the nanoscale are also critical factors.

In parallel the low band gap polymers studies, a series of new block copolymers, able to self-assemble in nano-domains, have been taken into account in order to better control the role of morphology.

Amphiphilic block copolymers, obtained by GRIM method, were synthesized and mixed with $PC_{61}BM$ in order to investigate the morphologies and the photovoltaic properties as a function of block composition.

Among the amphiphilic copolymers, **P3HT-b-P3AcidHT** showed the best performance with a PCE of 4.2%. These satisfactory performances can be rationalized in terms of non-covalent interaction between the carboxy-alkyl chains of the BCP and the ester functionality of the PCBM, which leads to the spontaneous

formation of ordered nanodomains, improving the formation of a larger interface and a bicontinuous network for the charge separation and transport, respectively.

The obtained results show that the structural fine-tuning of conjugated polymers is one of the major parameters to achieve the suitable properties essential for high PCE performance, but further efficiency improvements require a combination of other parameters including device architecture and processing. Therefore, more efficient device could be developed to make the OPV a true competitor to the inorganic photovoltaics.

Acknowledgments

Foremost, I would like to express my sincere gratitude to my advisors, Prof. Antonio Papagni and Dr. Abderrahim Yassar. Without their guidance and constant feedback, the results presented in my PhD work would not have been achievable.

My sincere thanks also go to all who have contributed to this thesis, especially Dr. Luciano Miozzo e Dr. Denis Tondellier: you both contributed a lot to this thesis and without your help it would have not been possible to do some important experiments.

I thank my fellow labmates in Milan, Dr. Alberto Gregori, Dr. Paolo Coghi and all the students, with special thanks to Dr. Matteo Parravicini for all the fun we have had in the last three years.

I would like to show my gratitude to all the other members at the Ecolè Polytechnique for their help during my French period. Thanks to Jinwoo Choi for the photovoltaic measurements.

Many of the results describes in this thesis would not have been obtained without a close collaboration with few laboratories: thank you Dr. Riccardo Po, Dr. Andrea Pellegrino, D.ssa Alessandra Tacca, Dr. Riccardo Ruffo, Dr. Matteo Salamone, Dr. Giorgio Patriarca and Dr. Alberto Bianchi for your contribution.

In addition, I have been privileged to collaborate with many other great people who became friends over the last several years. I am indebted to LASMO colleagues for providing a stimulating and fun filled environment during the lunch break.

There are two other friends that I must mention: Dany and Silvia, thank you for your encouragement and support even if often you confessed to not understanding anything of my work.

Of course no acknowledgments would be complete without giving thanks to my parents. Both have instilled many admirable qualities in me and given me a good foundation with which to meet life.

And last, but not least, to Tommy, who shares my passions. Thank you to fire up my dreams.